

Coptation of Innate Immune Cells in Promoting and Combating Infections

by

Mohammad Arifuzzaman

Department of Molecular Genetics and Microbiology
Duke University

Date: _____

Approved:

Soman N. Abraham, Supervisor

J. Andrew Alspaugh

Dennis C. Ko

Margarethe J. Kuehn

Herman F. Staats

Dissertation submitted in partial fulfillment of
the requirements for the degree of Doctor
of Philosophy in the Department of
Molecular Genetics and Microbiology in the Graduate School
of Duke University

2018

ABSTRACT

Cooption of Innate Immune Cells in Promoting and Combating Infections

by

Mohammad Arifuzzaman

Department of Molecular Genetics and Microbiology
Duke University

Date: _____

Approved:

Soman N. Abraham, Supervisor

J. Andrew Alspaugh

Dennis C. Ko

Margarethe J. Kuehn

Herman F. Staats

An abstract of a dissertation submitted in partial
fulfillment of the requirements for the degree
of Doctor of Philosophy in the Department of
Molecular Genetics and Microbiology in the Graduate School of
Duke University

2018

Copyright by
Mohammad Arifuzzaman
2018

Abstract

The key components of innate immune defense to pathogens are various migratory as well as tissue resident innate immune cells, however, their interactions with pathogens as well as their immune-orchestrating roles are often poorly understood. While immune cells encounter pathogens at barrier sites and mount the first line of defense, pathogens are well adapted to bypass, inactivate and even exploit the functions of these cells. Better understanding of the interactions between pathogens and innate immune cells can teach us how pathogens avoid or exploit immune cells and how to overcome these mechanisms of pathogenesis by therapeutic interventions. In this work, we examined two scenarios of pathogen invasion and sought to understand the complex ways of external targeting of innate immunocytes that can either benefit the pathogen or the host.

First, we studied the migratory innate immunocytes in draining lymph nodes upon entry of *Yersinia pestis* via the skin and identified how this plague-causing bacterium coopted host cell death pathways of infiltrated mononuclear phagocytes. By employing time-lapse microscopy and flow cytometry, we demonstrated that within the confines of infected lymph nodes, bacteria-triggered necroptotic cell death resulted in the release of intracellular bacteria into the extracellular environment and attracted neighboring phagocytic cells, promoting their infection by these recently released

bacteria. This expansion of bacteria-bearing immune cells which eventually migrate to secondary lymph nodes, enables large numbers of *Y. pestis* to disseminate from one node to the next via the lymphatic system. We show this mechanism of dissemination being essential for the transition of plague from a bubonic to septicemic stage and demonstrate immunotherapeutic potential of necroptosis inhibitors.

Next, we focused on mast cells, a resident innate immunocyte in the context of skin infection by *Staphylococcus aureus*. We showed that connective tissue mast cells promoted recruitment of neutrophils at the early stage and CD301b⁺ dendritic cells at the later stages of infection, which played critical roles in infection control and repair, respectively. We further demonstrated that exogenous activation of skin mast cells via a mast cell-specific G protein-coupled receptor controlled infection as well as enhanced mobilization of dendritic cells to draining lymph nodes in a mast-cell dependent manner and protected mice from re-infection. Therefore, selective activation of mast cells appears to orchestrate immunomodulation integrating both the innate and adaptive immune arms.

These studies reveal the yin and yang of innate immune cells in two very different infectious settings. They emphasize how different strategies to target these cells at the immune checkpoints can be beneficial for host-directed therapy against bacterial infections.

Dedication

This thesis is dedicated to my father who instilled my love of wisdom (philosophy) and my wife who instilled my wisdom of love.

Contents

Abstract	iv
List of Figures	xii
Acknowledgements	xiv
1. Introduction	1
1.1 Migratory and resident innate immune cells	2
1.2 Dual-checkpoint immune surveillance in the periphery	2
1.3 Phagocytosis in immune surveillance and bacterial clearance	3
1.4 Role of immune modulator secretion in immune surveillance and bacterial clearance	4
1.5 Targeting of immune cells by bacterial pathogens	5
1.6 Targeting of immune cells for host-directed antibacterial therapy	7
1.7 Impetus for this work.....	8
2. Lysis of infected monocytic cells induced by <i>Yersinia pestis</i> promotes bacterial dissemination.....	12
2.1 Introduction.....	12
2.1.1 Role of buboes in plague pathogenesis	12
2.1.2 Role of cell death in bacterial infections.....	13
2.2 Methods	16
2.2.1 Animals.....	16
2.2.2 Bacterial strains and culture conditions	16
2.2.3 Antibodies and reagents.....	16

2.2.4 Bacterial and cell cultures.....	17
2.2.5 <i>In vitro</i> infections	18
2.2.6 Animal infections	18
2.2.7 CFU determination.....	19
2.2.8 Flow cytometry.....	19
2.2.9 Immunofluorescence microscopy	20
2.2.10 Time-lapse microscopy.....	21
2.2.11 Real time quantitative PCR.....	21
2.2.12 Cell death assay	22
2.2.13 Necrostatin treatment	22
2.2.14 Trans-well assay	22
2.2.15 YopJ complementation	23
2.2.16 Statistics	23
2.3 Results.....	25
2.3.1 YopJ is critical for dispersal of <i>Y. pestis</i> through buboes.	25
2.3.2 The primary DLNs is a critical checkpoint for YopJ-dependent dissemination	27
2.3.3 YopJ triggers release of intracellular bacteria.....	30
2.3.4 <i>Y. pestis</i> -induced cell death promotes infection of neighboring cells	32
2.3.5 YopJ mediates early necrosis but not inflammation in buboes.....	35
2.3.6 Virulence of YopJ depends on RIPK1-dependent cell death.....	37
2.3.7 RIPK1 inhibitors protect from lethal infection	40

2.3.8 <i>Y. pestis</i> -triggered cell death involves necroptosis	42
2.3.9 Cell death during <i>Y. pestis</i> infection is delayed.....	45
2.3.10 Macrophage death alters local S1P gradients promoting intra-nodal bacterial spread.....	48
2.4 Discussion.....	53
3. Activation of peripheral mast cells via the MRGPR receptor potentiates bacterial clearance	59
3.1 Introduction.....	59
3.1.1 The role of mast cells in pathogen clearance	59
3.1.2 The role of mast cells in adaptive immunity	60
3.1.3 Targeting of mast cells for anti-bacterial therapy	61
3.2 Methods	63
3.2.1 Study Design.....	63
3.2.2 Mice	63
3.2.3 Cell lines and transfections	64
3.2.4 Bacterial culture and infection.....	64
3.2.5 Peptides and antibiotics.....	65
3.2.6 Topical treatments.....	66
3.2.7 Skin tissue collection.....	66
3.2.8 Enzymatic assays.....	66
3.2.9 CFU determination.....	68
3.2.10 Immunofluorescence microscopy	68
3.2.11 Toluidine blue staining.....	68

3.2.12 Mason’s trichrome staining.....	69
3.2.13 Flow cytometry	69
3.2.14 Western blot	70
3.2.15 MIC assay	71
3.2.16 Luciferase reporter assay.....	71
3.2.17 Cytotoxicity assay.....	72
3.2.18 TLR/NLR ligand screening assay.....	72
3.2.19 Depletion of neutrophils	73
3.2.20 Peptide design for structure-function analysis	73
2.2.21 Statistical analyses.....	75
3.3 Results.....	76
3.3.1 <i>S. aureus</i> dermonecrotic skin infection model.....	76
3.3.2 Connective tissue mast cells control <i>S. aureus</i> skin infection.....	78
3.3.2 MC-mediated infection control is via neutrophil recruitment.....	81
3.3.3 MCA activates CTMC via MRGPRX2 receptor.....	82
3.3.4 CTMC activation by mastoparan recruits neutrophils <i>in vivo</i>	87
3.3.5 Topical application of MCA degranulates skin MCs and recruit neutrophils .	91
3.3.6 MCA -mediated neutrophil recruitment accelerates bacterial clearance in the skin.	94
3.3.7 Therapeutic effect of mastoparan is specific to MC activation.	99
3.3.8 Treatment with MCA promotes regenerative healing	101
3.3.9 CTMCs recruits wound healing CD301b ⁺ cells	103

3.3.10 MCA mobilizes DCs to DLNs.....	105
3.3.11 Treatment with MCA boosts antibody responses and protects from reinfection.....	107
3.4 Discussion.....	109
4. Conclusion	114
4.1 Cooption of innate immune cells in promoting infection.....	114
4.2 Cooption of innate immune cells in combating infection.....	118
4.3 Concluding remarks.....	120
References	121
Biography.....	138

List of Figures

Figure 1: The footpad infection model.....	25
Figure 2: Bubo formation and septicemia.....	26
Figure 3: Bacterial burden at various sites.....	28
Figure 4: Bacterial distribution in primary buboes	29
Figure 5: Monocytes/macrophages are major targets of <i>Y. pestis</i> in buboes.....	30
Figure 6: YopJ-triggered macrophage death promotes infection of neighboring cells.....	32
Figure 7: Cell death promoting infection of neighboring cells.....	33
Figure 8: YopJ-dependent cell death in popliteal lymph nodes.....	35
Figure 9: Cellular infiltration in popliteal lymph nodes.....	36
Figure 10: YopJ-triggered cell death in WT and RIPK1 mutant macrophages	38
Figure 11: Virulence of YopJ depends on RIPK1-mediated programmed cell death	39
Figure 12: RIPK1 inhibitor prevents cell-to-cell spread of <i>Y. pestis</i>	41
Figure 13: RIPK1 inhibitors protect from lethal.....	42
Figure 14: YopJ-triggered cell death is necroptotic	44
Figure 15: FLIP upregulation during <i>Y. pestis</i> infection of macrophages	47
Figure 16: YopJ-triggered cell death results in chemotaxis of uninfected macrophages..	49
Figure 17: S1P upregulation in dying cells.....	51
Figure 18: S1P promotes intra-nodal bacterial spread.....	52
Figure 19: Mouse dermonecrotic model	77
Figure 20: Depletion of CTMCs	79

Figure 21: CTMCs are critical for controlling skin infections	80
Figure 22: CTMCs' control of skin infection is neutrophil-dependent.....	81
Figure 23: MRGPRX2-dependent degranulation by mastoparan	83
Figure 24: Mastoparan activates $G_{\alpha q}$ axis and PLC γ 1	85
Figure 25: Receptor-specificity of mastoparan.....	86
Figure 26: Cytokines released from mast cells upon activation by mastoparan.....	87
Figure 27: Dose-dependent degranulation of mast cells <i>in vivo</i> by mastoparan.....	89
Figure 28: Mastoparan-mediated neutrophil recruitment	90
Figure 29: (A) Penetration of mastoparan into dermis	91
Figure 30: MC degranulation by topical mastoparan	92
Figure 31: Neutrophil recruitment by mastoparan during <i>S. aureus</i> infection	95
Figure 32: Mastoparan treatment accelerates bacterial clearance	97
Figure 33: Efficacy and neutrophil-dependency of mastoparan's antibacterial effect.....	98
Figure 34: Mastoparan's therapeutic effect requires CTMCs	99
Figure 35: Therapeutic effect of mastoparan is specific to MC activation	100
Figure 36: Treatment with MCA promotes regenerative healing	102
Figure 37: CTMCs restores wound healing CD301b ⁺ cells.....	103
Figure 38: MCA mobilizes DCs to DLNs.....	106
Figure 39: Mastoparan boosts adaptive immunity and controls reinfection.....	107
Figure 40: Mechanism of <i>Y. pestis</i> dissemination within buboes.	115
Figure 41: Mechanism for mastoparan's therapeutic effect	119

Acknowledgements

First, I would like to thank Soman Abraham for being an outstanding mentor and tremendously supportive. I appreciate his continuous encouragement as well as the enormous breadth of opportunities and freedom of thinking he has given. I learned every aspect in the process of research and how to think independently. I feel very privileged to have had the experiences to work with a person who I consider truly visionary and whose mentoring focuses on the students' improvement.

Next, I would like to thank my committee members, Andrew Alspaugh, Dennis Ko, Meta Kuehn and Herman Staats. The work was vastly improved by their critical questions. They have all been insightful and encouraging.

I also owe a great deal of gratitude to the former and current lab members. I would like to thank Ashley, Yuvon and Cheryl who initiate me in the lab before they left. I would like to thank fellow students Haewoong and Gladys for training me and for always being helpful and supportive. I would like to thank Phoenix, Jianxuan and Abhay for their advice, Byron and Jason for proofreading. I would also like to thank Jason, Jorn, Jasmine and Laura for their friendship and building rapport.

I also must thank the students that have worked with me, especially Cristina and Zach. I would like to thank my fellow CMB and MGM graduate students, the graduate life would not be any fun without them during the first few years.

Finally, I would like to thank my family, for their countless support throughout my graduate life. In particular, my parents for always believing in me, my brother who took care of my parents when I could not, and last but not the least, my wife, who decided to move with me to Duke and made many sacrifices that have not gone unnoticed. This work would not have been possible without the extensive support I have received from her.

1. Introduction

Innate immune cells are the key structural components of the innate immune system and act as the first line of defense against microbial pathogens. Discoveries in last few decades have revealed at the molecular level how these cells sense pathogens and then transduce signals. Innate immune cells detect invading pathogens through various pattern recognition receptors (PRRs) which recognizes specific pathogen-associated molecular patterns (PAMPs) (1, 2). Upon recognition, intracellular signal transduction occurs and several defense mechanisms, either alone or in combination, may take place, depending on the type of immunocyte, the host and the pathogen. These mechanisms are primarily i) direct killing of the pathogen via phagocytosis or antimicrobials, ii) secretion of pre-stored or de novo synthesized immune mediators which activate and/or recruit additional innate or adaptive immune cells, or iii) processing and presentation of antigens to other immune cells.

The innate immune system is evolutionarily older than the adaptive immune system and many of its components are conserved among invertebrates and vertebrates (1). Apart from protection from pathogens, many innate immune cells play critical beneficial roles in physiological functions such as scavenging, wound healing and generating anti-tumor effects (3-5). Immunotherapy has long been focused on the adaptive immune system, especially due to success of many vaccines but also partially due to skeptic views towards the non-specific nature of innate defense (2, 6). As innate

immune cells do not adapt to the pathogen type, many pathogens have evolved ways to escape or even exploit these cells via diverse mechanisms. Furthermore, non-specific or overreaction of these cells causes inflammatory diseases and hypersensitivity. Better understanding of these mechanisms would allow for therapeutic intervention not only to control pathogens but also to prevent pathologies caused by hyperactive innate immune cells.

1.1 Migratory and resident innate immune cells

Innate immune cells can be resident or migratory. Resident cells, such as macrophages or mast cells, function where they are located. On the other hand, migratory innate immune cells can be located in peripheral organs and then migrate to lymphoid tissues to transport antigens upon exposure to a pathogen. Alternatively, migratory innate immune cells can be stored in lymphoid organs or circulate through blood and lymph. These cells can then get recruited to the site of infection or immunization via chemokine signaling. The migratory cells include monocytes (which can further be converted into macrophages or dendritic cells base on specific chemical cues), neutrophils, dendritic cells and natural killer cells.

1.2 Dual-checkpoint immune surveillance in the periphery

Various immune cell subsets are located close to the anatomical barriers such as skin and mucosa to act as sentinels. These immune cells can either be evenly distributed, such as Langerhans cells in skin epidermis, various dendritic cell subsets, macrophages

and mast cells in dermis. Alternatively, immune cells can be organized into specialized small concentrations of lymphoid tissues such as macrophages, dendritic cells and microfold cells (M-cells) in Payer's patches of intestinal mucosa and NALTs (nasal-associated lymphoid tissue) (7).

Pathogens that escape these checkpoints near the physical barrier are encountered by an additional layer of surveillance throughout the body. The draining lymph nodes (DLNs) serve as filtering stations located throughout the network of lymphatic vessels, through which lymph percolates before they get to the blood. Bacterial and viral pathogens that venture into the lymph are rapidly filtered out by these organs before they can become systemic (8). Critical to this function are macrophages that line the lymph node sinuses to capture pathogens and eliminate them by degrading them within lysosomes (9). Therefore, mammalian innate immune defense is comprised of two layers of immune-checkpoints to prevent systemic invasion of pathogens.

1.3 Phagocytosis in immune surveillance and bacterial clearance

Although many immune and non-immune cells can phagocytose pathogens upon their detection, certain immune cells are specialized for phagocytosis and therefore are called professional phagocytes, such as neutrophils, dendritic cells and macrophages (10, 11). Macrophages survey for pathogens, capture and destroy them, and then process and present antigens to nearby B cells or T cells. Dendritic cells present antigens to local

T cells as well as migrate to transport antigens to T cells at distal lymphoid organs (12). When they fail and there is an acute infection, inflammatory reactions cause recruitment of neutrophils. Neutrophils are primarily found in the bloodstream and they are the first responders and the major phagocytic cells to play a critical role in controlling infection. Upon phagocytosis, pathogens are killed by reactive oxygen species and hydrolytic enzymes secreted into phagosomes. Neutrophils are also capable of killing extracellular pathogens by a process called NETosis in which cells release a web-like structure comprised of DNA and protein called neutrophil- extracellular trap (NET) (13).

1.4 Role of immune modulator secretion in immune surveillance and bacterial clearance

Immune modulators secreted by innate immune cells can be either prestored (eg. various modulators secreted by neutrophils and mast cells) or *de novo* synthesized (eg. modulators secreted by macrophages and dendritic cells). These immunomodulators have a diverse array of functions, from direct killing of pathogens to recruiting additional immune cells (14). Neutrophil contains defensins and cathelicidins which are antimicrobial peptides that kill pathogens by membrane disruption. Mast cells release TNF which recruits neutrophils as well as mobilizes dendritic cells. Macrophages and dendritic cells undergo *de novo* inflammatory signaling initiated by PAMP binding to PRRs, which leads to NF- κ b activation and production of inflammatory cytokines which recruit neutrophils and other immune cells (14, 15).

It is worthwhile to mention that the intracellular components of signal transduction that leads to production of inflammatory cytokines upon pathogen detection often involve the key components for various types of cell death such as apoptosis, pyroptosis or necroptosis. Therefore, secretion of inflammatory signals is often associated with cell death, especially in macrophages.

1.5 Targeting of immune cells by bacterial pathogens

Since the innate immune cells are activated upon direct contact of pathogens, and their detection mechanism is conserved, pathogens have evolved mechanisms to resist innate defense pathways via diverse strategies. First, pathogens can avoid detection by immune cells. For example, flagellin is a bacterial globular protein which is the building block of bacterial motility structures called flagella. Upon bacterial invasion to host cells, flagellin can be detected by the NLR family CARD domain-containing protein 4 (NLRC4), leading to caspase-1 activation and subsequent inflammatory reactions (16). It has been shown that in certain host adapted pathogen such as the enteric bacteria *Salmonella Typhimurium*, the bacteria do not express flagellin *in vivo* so they can remain undetected and ensure intracellular survival and replication (17). Other enteric pathogens express flagellin at 30°C but not at 37°C, the body temperature of mammalian hosts (17), whereas *Y. pestis*, the plague-causing bacteria, has permanently lost the capacity to express flagellin by mutation (18). *Y. pestis* also express a tetra-acetylated form of lipid A (a component of lipopolysaccharides or LPS, the major PAMP of Gram-

negative bacteria) which is poorly detected by the corresponding host PRR Toll-like receptor 4 (TLR4) compared to the normal hexa-acetylated form of lipid A in most other bacteria (19).

Second, many bacterial pathogens also actively prevent recruitment of innate immune cells. For example, *Y. pestis* employs virulence proteins secreted via a Type III secretion system (T3SS) to delay neutrophil recruitment during pneumonic plague (20, 21). A third mechanism is paralyzing the innate immunocytes. It has been shown that *S. Typhimurium* and *Y. pestis* paralyze mast cells function by employing a T3SS protein which blocks Syk phosphorylation and therefore mast cell degranulation (22). On the other hand, several T3SS factors of *Yersinia pseudotuberculosis* have been shown to block phagocytosis by neutrophils (23). Gene expression profiling of *Y. pestis in vivo* suggest that they can generate protective responses to reactive oxygen species such as nitric oxide employed by neutrophils (24).

In addition to avoiding detection or active blocking of immune cell functions, various pathogens have also adapted to actively exploit immune cells. Macrophages have been demonstrated to be the intracellular niche for pathogens like *Mycobacterium tuberculosis* and *Salmonella* species. Furthermore, intracellular mycobacteria have been shown to use the ESX-1/RD1 virulence locus to promote recruitment of more macrophages into granulomas. These macrophages then get infected and travel to another site carrying intracellular bacteria, leading to formation of another granuloma

(25). Additional exploitation mechanisms involve hijacking immune cells for nutrients. For example, inflammation triggered during Salmonella infection can benefit the bacteria as they can utilize a respiratory electron acceptor derived from reactive oxygen species generated by neutrophils and other inflammatory cells which provides them a growth advantage over gut microbiota (26). To summarize, various innate immune cells at either barrier sites (skin or mucosa) or secondary checkpoints (such as lymph nodes) can be targeted by pathogens for their benefits in numerous distinct ways.

1.6 Targeting of immune cells for host-directed antibacterial therapy

It is conceivable that if pathogens can target immune cells for their benefits, we may also be able to utilize them as targets for immunotherapy, either by blocking the pathogen exploitation of host cells or by boosting their innate capacities which would overcome any pathogen-mediated blockades. Various forms of immunotherapy targeting innate or adaptive immune cells has recently provided dramatic breakthroughs against cancer, particularly against tumors that have become resistant to conventional chemotherapy (27). In view of this success, there is great interest in utilizing immunotherapy against infections. So far, the strategy for immunotherapy against infections have focused on cytokines or ligands of pattern recognition receptors (PRRs) activating many different immune cell types (2). Prominent examples include interferon- γ (IFN- γ) for mycobacterial infection (28), IFN- α for hepatitis C (29) and Imiquimod (a TLR7 agonist) for human papillomavirus and molluscum contagiosum

(30). Unfortunately, activation of multiple cell types using agents like these often resulted in a tradeoff between better clearance of infection versus uncontrolled inflammation. Therefore, one of the major conceptual shifts in immune therapy has been the pursuit of agents that specifically affect individual cell types. The specific immune modulation approach has yet to be fully applied to infection, however. Furthermore, which cell type is most effective to target is also an open question; one might expect that targeting neutrophils and macrophages would be best for enhancing innate immune responses, while targeting cell types that move into draining lymph nodes, such as dendritic cells (DCs) and T cells, would be required for enhancing adaptive immunity.

1.7 Impetus for this work

Over the ages, the plague has been characterized by its rapid onset and deadly outcome within the population (31). However, how *Y. pestis*, the etiologic agent, evades the immune system and achieves such widespread dispersal within the host is not fully understood (31-33). Intracellular survival and replication of *Y. pestis* within host phagocytes have been known for decades (34-37). Nonetheless, *Y. pestis* is considered mostly an extracellular blood-borne pathogen (38, 39) since its virulence is linked to its resistance to ingestion by circulating phagocytes, a trait ascribed to its capacity to inject potent paralyzing effector proteins into host cells (40-43). Bubonic plague, the most common form of the disease, is transmitted via bites of infected fleas and characterized by hypertrophic lymph nodes (buboes) (31, 44). Recently, we discovered that *Y. pestis*

deposited in the skin displayed a strong predisposition for trafficking within the lymphatic system to reach draining lymph nodes (DLNs) which they converted into buboes. Interestingly, the trafficking bacteria were largely intracellular while spreading from the site of infection to the primary and then to secondary DLNs (45). The importance of this infection strategy was evident from the observation that it was possible to protect mice against lethal *Y. pestis* infection merely by treating them with drugs that disrupt the signaling circuitry associated with immune cell trafficking within DLNs (45).

However, this capacity to spread within the host while sheltering within immune cells is seemingly incongruent with the capacity of *Y. pestis* to trigger cell death (46), as it would disrupt their intracellular niche. Furthermore, since YopJ-mediated death of host cells has been linked to enhanced local inflammation, it has been proposed that this activity is detrimental to the pathogen (47). Here we sought to investigate how *Y. pestis* coopts innate immune cells to support bacterial spread. In the next chapter, we will reveal our surprising discovery that in the tightly packed confines of the buboes, this bacteria-triggered cell death is a powerful mechanism for the cooption of mononuclear phagocytes by the pathogen for bacterial spread.

While innate immunocytes are often targeted by pathogens for their benefits, we can also target these cells for host-directed therapies. If we enhance the innate immune system, or increase its activation, we can reverse the spread of some pathogens. Over the

past four decades there has been an explosion of antimicrobial-resistant bacteria including the frequent occurrence of so-called 'superbugs' (48). Therefore, there is growing interest in identifying inducers of innate immunity that can safely be employed as an alternative approach to combat infections (49, 50). However, targeting specific immune cell types for optimum efficacy is often difficult, as discussed earlier. We have previously shown the importance of MCs in the innate immune response to infections (51-53), partially through their effect on neutrophils (54). MCs are preferentially found, with high concentrations, at tissue interfaces exposed to the external environment, with estimated abundances of 7,000 to 12,000 per mm³ in skin placing them in an ideal position to be one of the first cells to respond to infection. Furthermore, MCs are remarkable for storing large amounts of inflammatory mediators tightly packed within distinct intracellular granules which can be released almost immediately upon activation (55, 56). Thus, unlike other inflammatory cell types that take hours to de novo synthesize and secrete mediators, MCs react within minutes. In the third chapter, we will reveal the multifaceted role of mast cells during various stages of bacterial skin infection and how these cells can be targeted via a mast-cell specific receptor for host-directed therapy to control and prevent infections.

Preface to Chapter 2

This chapter is a modified version of the following manuscript published in JCI Insight:

Arifuzzaman M, Ang WXC, Choi HW, Nilles ML, St. John AL, Abraham SN.

Necroptosis of infiltrated macrophages drives *Yersinia pestis* dispersal within buboes. JCI Insight. 2018 Sep 20;3(18). pii: 122188. PMID: 30232285

2. Lysis of infected monocytic cells induced by *Yersinia pestis* promotes bacterial dissemination

2.1 Introduction

2.1.1 Role of buboes in plague pathogenesis

Draining lymph nodes (DLNs) are secondary lymphoid organs within which resident macrophages and other immune cells constantly survey the lymph for pathogens (57). *Y. pestis*, evade the macrophage-mediated killing program to successfully colonize the DLN (37). Seemingly in response to this challenge, a large number of phagocytic cells are rapidly recruited into the DLN, resulting in highly enlarged nodes or “buboes”. Recently, we showed that chemokines such as CCL2 and CCL21 are the primary mediators of the recruitment of mononuclear phagocytes into DLNs whereas their subsequent exit from DLNs via efferent lymph vessels is controlled by a signaling sphingolipid called sphingosine 1 phosphate (S1P) (45). Since the large influx of immune cells into buboes is almost exclusively phagocytic cells, it is conceivable that the role of these recently recruited immune cells is to engulf bacteria and limit their spread. However, *Y. pestis* rely on the lymphatic system as a conduit to reach a systemic infection (45, 58, 59) and is unique in its ability to rapidly escape lymph nodes, and how this is achieved is still not fully understood.

Y. pestis infection results in a specific pathology of DLNs, where the normally quiescent structures become massively swollen with substantial burden of intra- and extracellular bacteria, disrupting the native architecture of the DLN (32). We have

previously established that *Y. pestis* disseminating from buboes enter the lymphatics borne within mononuclear phagocytes (45). Interestingly, we also noticed that these infected buboes exhibit a high degree of necrosis, suggesting that a programmed cell death may precede the escape of *Y. pestis*-bearing phagocytes from infected buboes.

2.1.2 Role of cell death in bacterial infections

The contribution of programmed cell death to the host's immune defenses during infection can be either beneficial or detrimental depending on the pathogen, the cell type and mode of cell death involved. For example, pyroptotic death of *S. Typhimurium*-infected macrophages is beneficial to the host as the accompanying inflammation results in vigorous influx of neutrophils which rapidly engulfs the cell corpses, killing the entrapped bacteria (60). On the other hand, apoptosis of *Mycobacterium tuberculosis*-infected macrophages, which is associated with little or no inflammation appears detrimental to the host. This is because when surrounding macrophages engulf bacteria bearing corpses, these host cells become infected as they possess limited bactericidal abilities (25). In case of *Y. pestis* infection, the programmed cell death pathway in macrophages are triggered by a bacterial factor, Yersinia outer protein J (YopJ), an acetyl transferase produced by *Y. pestis* and related Yersinia species (46, 61, 62). The host molecular components of this programmed cell death include caspase 8 and receptor-interacting protein kinase 1 (RIPK1) (47) which are key molecules involved in apoptotic and necroptotic cell death pathways. For *Y. pestis*, the role of YopJ

as a virulence factor is less clear. It has been shown to inhibit innate immune signaling such as NF- κ B activation and TNF secretion, and to induce apoptosis of immune cells. Additionally, it has also been reported to activate inflammasomes, which are powerful recruiters of pathogen-clearing immune cells (62, 63). Since *Y. pestis* target and trigger death of phagocytic immune cells, especially monocytes and macrophages, we hypothesize that a highly effective pathogen such as *Y. pestis* might have successfully co-evolved with the host to encode virulence factors that are beneficial for the bacteria; and studying the characteristics of *Y. pestis*-triggered cell death might reveal how it impacts the pathogen and the host.

Apoptosis has been considered as the primary mode of programmed cell death until recent expansion of our understanding of various non-apoptotic programmed cell death (64). Necroptosis, a form of regulated necrosis has been shown to be induced by various PAMPs (pathogen-associated molecular pattern) but also negatively regulated by prosurvival factors at various steps of the signaling pathway (65). Interestingly, the necroptotic pathway is tightly linked with apoptosis and therefore a given death stimulus may lead to either form of cell death and inhibition of one form may lead to activation of the other (65-67), blurring interpretation of cell death programs involved. However, the recent discoveries of the necrosome as an integral necroptosis-inducing signaling complex and the pore-forming protein MLKL (mixed lineage kinase domain-

like) as the executor of necroptosis, have now provided specific molecular markers to pinpoint necroptosis (68, 69).

Here, we describe that YopJ-triggered necroptosis is consequential to the spread and escape of *Y. pestis* from buboes. Targeting immune cells and triggering their death is a way to not merely suppress antimicrobial activities, but also systematically expand intracellular infection. Unlike non-bubo forming infections by other *Yersinia* species, when this pathway is triggered in *Y. pestis*-infected buboes, it has the effect of allowing bacterial release from monocytic cells (monocytes/macrophages) and massively amplifying the numbers of bacteria within buboes and their potential to infect new cellular targets. Furthermore, we identified that the signaling program induced by *Y. pestis* within dying cells involves sphingosine 1-phosphate (S1P) production, which brings new uninfected cellular targets proximal to the necroptotic host cells, further augmenting infection. This novel mechanism of bacterial spread explains how *Y. pestis* exploits the host immune response that is generated in the lymph node to achieve successful infection.

2.2 Methods

2.2.1 Animals

Six- to eight-week old C57BL/6J mice were purchased from Jackson Laboratory. The *Cx3cr1-Cre* mice (Jackson stock no. 025524) and *S1pr1^{loxP}* mice (Jackson stock no. 019141) were purchased from Jackson laboratory and then bred in the Duke University Vivarium to generate *Cx3cr1-Cre S1pr1^{fl/fl}* mice (45). *Ripk1^{D138N/D138N}* mice were provided by Vishva M. Dixit, Genentech, San Francisco. All animal studies were carried out at Duke University and approved by the Duke University Institutional Animal Care and Use Committee.

2.2.2 Bacterial strains and culture conditions

The Kim5 strain was selected for this study and regarded as wild type as its growth rate was slow, due to the absence of a pigmentation (*pgm*) locus associated with iron acquisition, allowing for a slower and more tractable progression of pathogenesis (70). The Kim5-OFP strain was generated previously (45) and $\Delta yopJ$, $\Delta yopJ$ pYopJ and $\Delta yopJ$ -OFP strains in Kim5 background were generated in this study.

2.2.3 Antibodies and reagents

For western blot, immunofluorescence staining or flow cytometry, the following antibodies were used: Rabbit anti-RIPK1 (Cell Signaling 3493), Rabbit anti-RIPK3 (Cell Signaling 15828), Rabbit anti-Caspase-8 (Cell Signaling 4927), Rabbit anti-MLKL (Cell Signaling 37705), Rabbit anti-phospho-MLKL (Ser345) (Cell Signaling 62233), Rabbit

anti- FLIP_{S/L} (Santa Cruz 8347), Mouse anti- β -actin (Sigma A5441), Rabbit anti-SphK1 (Abcam 71700), Goat anti-rabbit IgG-HRP (Bio-Rad 170-6515), Goat anti-mouse IgG-HRP (Bio-Rad 170-6516), Donkey anti-rabbit IgG-FITC (Jackson 711-095-152), Anti-CD45 APC/Cy7 (Biolegend 103115), Anti-CD11b-PE (eBioscience 12-0112-81), Anti-CD11b-APC (eBioscience 17-0112-81), Anti-CD11b-PerCP-Cy5.5 (BD 561114), Anti-F4/80-FITC (eBioscience 11-4801-82), Anti-Ly-6C-AF700 (clone AL-21) (BD 561237), Anti-Ly-6G-PE (clone 1A8) (BD 561104), Anti-Ly-6G and Ly-6C-PerCP Cy5.5 (clone RB6-8C5) (BD 552093), Anti-CD3-APC (eBioscience 17-0032-82), Anti-B220-FITC (eBioscience 11-0452-85). Other reagents include Phalloidin-AF647 (Life Technologies A22287), SYTO9 green fluorescent nucleic acid stain (Life Technologies S34854), Propidium iodide (Life Technologies P21493), LIVE/DEAD fixable green dead cell stain kit (Life Technologies L23101), Zombie Violet fixable viability kit (Biolegend 423113), CytoTox 96 non-radioactive cytotoxicity assay kit (Promega G1780), Necrostatin-1 (Abcam 141053), Nec-1s (7-Cl-O-Nec-1) (Millipore 5.04297.0001), SAHA (Sigma SML0061).

2.2.4 Bacterial and cell cultures

All cultures of *Y. pestis* strains were grown in brain heart infusion (BHI) broth (Beckton Dickinson, BD) under shaking conditions. To mimic the infectious state of bacteria that are regurgitated by fleas into the host, cultures were grown at 25°C (room temperature, RT) for 48–72 hours. The monocyte/macrophage cell line J774A.1 (ATCC TIB-67) was cultured in DMEM containing glucose, glutamine and sodium pyruvate

(Life Technologies) and 10% fetal bovine serum (FBS, HyClone) and incubated at 37°C with 5% CO₂ and humidification. Bone marrow derived macrophages (BMDMs) from WT or *Ripk1*^{D138N/D138N} mice were cultured in RPMI 1640 (Life Technologies) supplemented with glutamine, 10% FBS and M-CSF (Biolegend) following standard protocol (71).

2.2.5 *In vitro* infections

Macrophages (J774.A1 or BMDM) were infected with bacteria in DMEM at a multiplicity of infection (MOI) of 10. Culture plates were centrifuged at 55 × g for 2 min to settle down the bacteria and then incubated at 37°C. Two hours post infection, cells were washed and treated with 10 µg/ml gentamicin (Life Technologies) for an hour, washed again and concentration of gentamicin was reduced to 2 µg/ml. A higher concentration of gentamicin (50 µg/ml) was used to treat infected cells when they were harvested to transfer into wells containing uninfected cells for cell-to-cell spread experiments.

2.2.6 Animal infections

For mouse infections, 10⁵ CFUs of bacteria in a 20 µl volume of sterile PBS were injected intradermally into a single rear footpad. For survival curves, 2 × 10⁵ CFUs of log-phase bacteria were used and infected animals were monitored every 24 hours for death or humane endpoints (interference with a vital physiological function such as

respiration, mastication, swallowing, urination, defecation or locomotion, hunched abnormal posture > 48 hours, self-mutilation etc.).

2.2.7 CFU determination

To determine CFU in organs, infected mice were euthanized at the noted time points after infection and organs were harvested. Organs were then homogenized in sterile water using zirconia silica beads for 2 cycles of 60 sec each using an automatic homogenizer. Homogenates were serially diluted on BHI plates and the colonies were counted after 48-72 hours incubation at RT. CFU in blood were determined by collecting peripheral blood at indicated time points and plating on BHI plates upon dilution in PBS. The limit of detection was 5 CFU. To determine intracellular CFUs, infected cells were treated with 10 or 50 µg/ml gentamicin for an hour, washed with PBS and lysed by incubation with sterile water for 10 min. The lysates were then diluted and plated on BHI agar to count CFU.

2.2.8 Flow cytometry

Lymph nodes were isolated from mice at the time points indicated, minced in DMEM containing 10% FBS and 100 U/ml of Collagenase A (Sigma), and incubated for 30 min. Single cell suspensions were produced by straining the disrupted lymph nodes through a 70 µm cell straining filter (BD Biosciences). Cells were then washed in PBS with 10 mM EDTA and 1% BSA, blocked with rat/mouse normal serums and Fc receptor block (eBioscience) and stained with fluorochrome-tagged antibodies. Number of cells

was counted using a hemacytometer. Dead cells were detected using LIVE/DEAD fixable Green dead cell stain kit or Zombie Violet fixable viability kit. Uninfected cells and cells stained with a single antibody were used as compensation controls. Stained cells were analyzed by BD FACSCalibur or FACSCanto IIs flow cytometer and FlowJo software version 10.1.

2.2.9 Immunofluorescence microscopy

For tissue sectioning, isolated tissues were flash frozen in optimal cutting temperature (OCT) compound (TissueTek), then sectioned (12 μm) on a microtome-cryostat. For propidium iodide staining, tissue sections on slides were stained for 1 minute with 1:10000 dilution of propidium iodide, followed by washing with PBS and mounting. For all immunostaining, tissue sections were fixed with acetone for 15 min at 4°C. Tissue sections were rehydrated in PBS and blocked with 1% BSA in PBS for 20 min, followed by staining with antibodies, as indicated in the figure legends. A Nikon ECLIPSE TE200 confocal microscope was used to capture immunofluorescent images.

To image J774A.1 macrophages, cells were grown on glass coverslips and infected with OFP-labeled bacteria (MOI 10) for 30 min and then treated with gentamicin for an hour, as described previously. Cells were fixed 6 hours post infection with 4% PFA, blocked and permeabilized with 1% gelatin and 0.5% saponin in PBS and incubated overnight with anti-SphK1 polyclonal antibody. The cells were then stained with anti-rabbit-FITC and Phalloidin-AF647 to detect SphK1 and actin (background

staining), respectively and mounted on a glass slide using Prolong Gold (Life Technologies).

2.2.10 Time-lapse microscopy

For *in vitro* live imaging, J774A.1 cells were grown on chambered #1.0 borosilicate coverglass system (Lab-Tek, Nunc). Additional cells were grown on 24-well plates and infected with GFP-labeled bacteria. To follow cell death, cells were pre-labeled with SYTO9 green fluorescent nucleic acid stain prior to infection with unlabeled Kim5 bacteria. After gentamicin treatment for an hour and washing, infected cells were harvested and transferred into Lab-Tek chambers pre-seeded with uninfected cells. The chambers were then placed in the live cell station and maintained at 37°C and 5% CO₂ with humidification. Propidium iodide was applied to the culture medium to visualize cell death. Zeiss Axio Observer microscope with Metamorph software was used to capture live moments.

2.2.11 Real time quantitative PCR

RNA was purified from cells using the RNeasy Mini Kit (Qiagen), cDNA was synthesized using the iScript cDNA Synthesis kit (BioRad) and real time PCR was performed using SYBR Green and the StepOnePlus™ Real-Time PCR System (Applied Biosystems), with normalization to actin expression. Primers were obtained from Integrated DNA Technologies for β -actin: 5' – TGA GAG GGA AAT CGT GCG TGA CAT, 5' – ACC GCT CAT TGA CGA TAG TGA TGA; FLIP: 5' –GGC TTC GCT CCC

AAA ATT GAG T, 5' –TTG GCT CTT TAC TTC GCC CA; SphK1: 5' – CCT GCT CAT
CAA CTG CAC AC, 5' – AGG TCC ACG TCA GCA ACA AA; SphK2: 5' – GTC CCT
CAA TGG TGG TGG T, 5' – AGC TGT TTT GAG AGC GTT GG.

2.2.12 Cell death assay

Lactose dehydrogenase (LDH) release from 2×10^4 cells was determined using the CytoTox 96® Non-Radioactive Cytotoxicity Assay kit according to manufacturer's protocol. The spontaneous LDH release by cells incubated with media alone was subtracted from other data.

2.2.13 Necrostatin treatment

For *in vitro* studies, cells were pre-incubated 2 hours prior to infection and maintained during infection with 30 μ M Necrostatin-1 (Nec-1). For *in vivo* studies, mice were treated with a metabolically stable analog of Nec-1 with improved specificity (Nec-1s) (72). Mice were treated with 2 mg/kg Nec-1s or vehicle (6% 2-Hydroxypropyl- β -cyclodextrin in PBS), distributed into footpad and intraperitoneal (i.p.) injections 15 min before bacterial infection. Additional doses were given at 6, 12, 24, 48 and 72 h.p.i. (i.p. only).

2.2.14 Trans-well assay

Upon bacterial infection for 2 hours and gentamicin treatment (20 μ g/ml for 1 hour), J774.A1 cells in a 24-well plate (Falcon) were maintained in serum-free migration buffer (DMEM with 0.1% BSA) and low concentration of gentamicin (2 μ g/ml). A cell

culture insert with 8 µm pore size filter (Falcon) was seeded with uninfected J774A.1 cells in serum-free migration buffer and placed on the well containing infected cells. After 14 hours incubation at 37°C, the cells remaining in the upper chambers were removed with a cotton tip applicator. Migrated cells attaching to the lower surface of the filters were fixed with 75% ethanol for 10 min, allowed to dry and then stained with 0.2% crystal violet for 10 min. The filters were then removed from cell culture inserts, placed on a glass slide and mounted with a coverslip. The number of cells migrated across the filter was counted under microscope using ImageJ software (73).

2.2.15 YopJ complementation

YopJ was amplified from Kim5 strain by PCR using primers 5' – CGC GAA TTC GAT GAT CGG ACC AAT ATC ACA AAT AA and 5' – CCC CTC GAG TTA TAC TTT GAG AAG TGT TTT ATA T, inserted into a low copy expression plasmid pWSK29 (74) which was then electroporated into electrocompetent *ΔyopJ* bacteria. Colonies were screened by PCR using pWSK29-specific flanking region primers 5' – GTC ACG ACG TTG TAA AAC GAC GGC CAG and 5' – GTG GAA TTG TGA GCG GAT AAC AAT TTC and confirmed by sequencing using M13 primers (5' – GTA AAA CGA CGG CCA GT and 5' – CAG GAA ACA GCT ATG AC).

2.2.16 Statistics

Statistical significance was determined by unpaired two-tailed Student's t tests where only two groups existed, or by one-way ANOVA with Tukey's post test, as

appropriate. Significance for Kaplan-Meier curves was determined by the log-rank test. Differences between groups were considered significant at $p < 0.05$. All error bars indicate SEM. * $p < 0.05$, ** $p < 0.01$, *** $p < 0.001$. ns, not significant. Analyses were performed using GraphPad Prism 5.0 and Microsoft Excel 2010 software.

2.3 Results

2.3.1 YopJ is critical for dispersal of *Y. pestis* through buboes.

To address the question of whether YopJ influences bacterial dissemination through buboes, we undertook a mouse challenge study where the pathogen was inoculated into rear footpads to mimic the natural intradermal route of infection. This site is drained by a single lymph node, the popliteal node (PN), which in turn is drained by the iliac nodes (INs) (Figure 1).

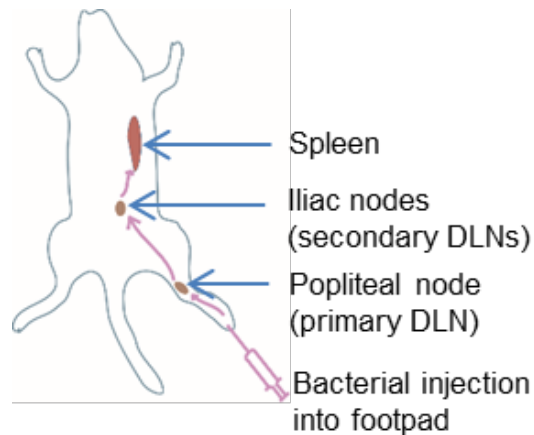


Figure 1: The footpad infection model. Bacteria injected in a rear footpad encounter a single sentinel draining node (popliteal node, PN) before reaching secondary nodes (iliac nodes, INs) and beyond.

We initially confirmed that footpad infection of mice with *Y. pestis* led to bubo formation and infection of the node, followed by septicemia, consistent with prior studies (32, 45). As shown in Figure 2A, formation of bubo, characterized by massive influx of CD11b⁺ leukocytes in the DLN, was observed as early as 6 hours post infection (h.p.i.); and by 24 hours, the normal architecture of lymph nodes (distinct B cell and T

cell zones) were destroyed. While bacterial burden in buboes was high by 24 hours, no bacteria could be detected in blood until 48 hours (Figure 2B).

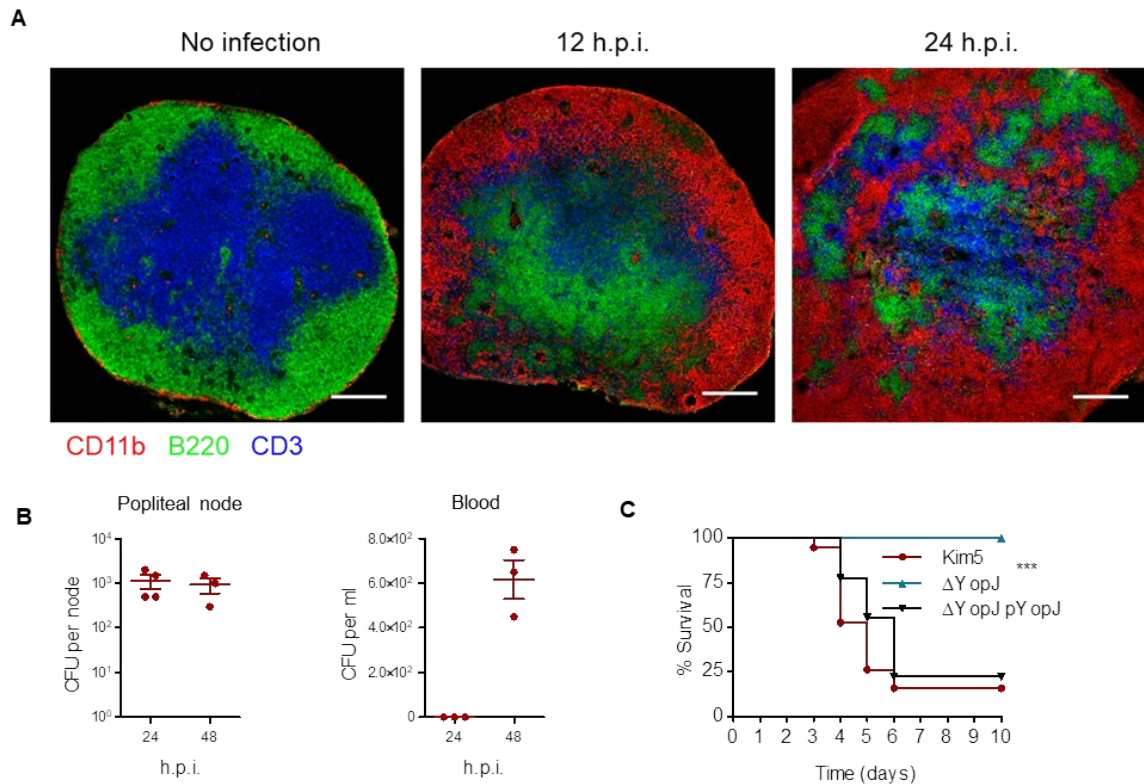


Figure 2: Bubo formation and septicemia. (A) PN tissue sections harvested from mice injected in footpad with saline, Kim5 or $\Delta yopJ$ bacteria; and stained for B cells (B220, green), T cells (CD3, blue) and CD11b⁺ cells (red); scale bar, 200 μ m. (B) Count of viable bacteria from PNs and blood at indicated time points post footpad infection (n = 3-4). (C) Survival of mice challenged with bacteria instilled into a single rear footpad. Data are combined from two independent experiments, n = 9-10.

When we instilled a lethal dose of wild type (WT) *Y. pestis* Kim5 strain or a comparable bacterial dose of the isogenic $\Delta yopJ$ mutant, most of the Kim5-infected mice died by day 7 whereas all mice infected with $\Delta yopJ$ strain survived (Figure 2C). The survival rate of mice infected with a $\Delta yopJ$ strain complemented with *yopJ* encoded in a

low-copy expression vector was comparable to that of mice infected with the WT Kim5 strain (Figure 2C), confirming that YopJ is a potent virulence factor promoting the pathogenesis of *Y. pestis*.

2.3.2 The primary DLNs is a critical checkpoint for YopJ-dependent dissemination

To examine if the YopJ-mediated lethality coincided with enhanced bacterial dissemination, we compared bacterial numbers in the blood 48 hours post infection (h.p.i.), which is when bacterial infection becomes systemic (Figure 2B). We found that the numbers of $\Delta yopJ$ mutant bacteria were significantly lower than Kim5 bacteria in the blood (Figure 3A). A similar difference in bacterial numbers was also observed in the spleen 72 h.p.i. (Figure 3B) suggesting that YopJ promotes bacterial dissemination. Next, we compared bacterial numbers in the PNs and INs, the primary and secondary lymph nodes encountered early in the infectious process, respectively. We found that by 24 h.p.i., both Kim5 and $\Delta yopJ$ bacteria induced the formation of large buboes (Figure 3C). Consistent with our data from spleen and blood, we observed a significant difference between Kim5 and $\Delta yopJ$ bacteria in the INs (Figure 3D) but remarkably; we did not observe any such difference between the two strains in the PNs (Figure 3E). This suggested that *Y. pestis* lacking YopJ have no defects in survival and entry into the lymphatic system, but subsequent stages of infection within or beyond the primary lymph node are affected.

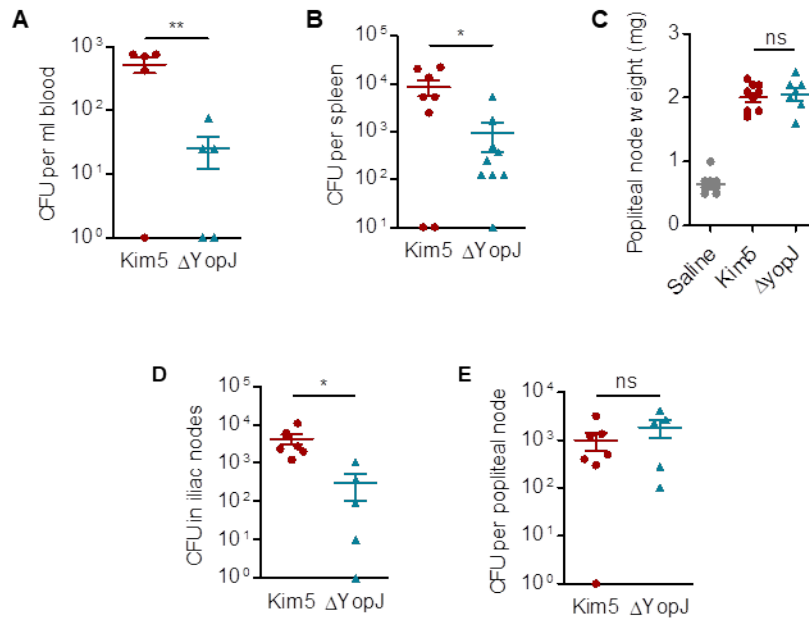


Figure 3: Bacterial burden at various sites. (A) Bacterial numbers (CFU) in the blood, 48 h post footpad infection with Kim5 or $\Delta yopJ$ strain (n = 5). (B) Bacterial numbers in spleen, 72 h.p.i. (hours post infection) (n = 8-9). (C) Weight of the PNs harvested 24 h.p.i. (n = 7-10). (D and E) Bacterial numbers in (D) iliac nodes (INs) and (E) popliteal nodes (PNs), 24 h.p.i. (n = 5-7). Data are representative of three independent experiments.

To investigate bacterial distribution and compartmentalization within nodes further, we infected mice with OFP (orange fluorescent protein)-labeled bacteria and then examined cross-sections of the primary PN 24 h.p.i. for the bacilli. Knowing that phagocytic cells, particularly of the monocyte/macrophage lineages, are the primary targets for *Y. pestis* infection and that they aid in the trafficking of bacteria between nodes, we examined whether *Y. pestis* could infect those cells efficiently in the absence of YopJ. Surprisingly, although both Kim5 and $\Delta yopJ$ strains appeared to be within CD11b⁺ phagocytic cells, $\Delta yopJ$ bacteria were found to be restricted in large pockets that were

relatively few in number. In contrast, Kim5 *Y. pestis* appeared well dispersed throughout the node (Figure 4A), suggesting YopJ is important for bacterial spread within a bubo.

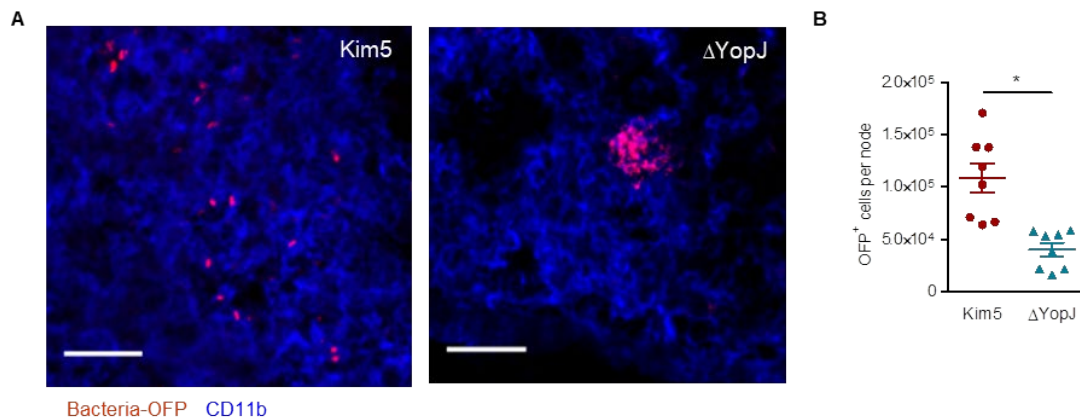


Figure 4: Bacterial distribution in primary buboes. (A) Immunofluorescence staining of PN cross-sections 24 h after footpad infection with GFP-labeled Kim5 or $\Delta yopJ$ bacteria. The images are representative of two independent experiments, Scale bar, 25 μm . (B) Quantification of GFP⁺ cells in PNs 24 h.p.i by flow cytometry. Data are combined from two independent experiments, each with 4 mice per group.

Indeed, flow cytometry of single cell suspensions from PNs confirmed that the numbers of bacteria-harboring cells in Kim5-infected buboes were significantly higher than in $\Delta yopJ$ -infected buboes (Figure 4B), even though the total numbers of bacteria in Kim5 and $\Delta yopJ$ infected PNs were comparable (Figure 3E). These data show that YopJ is a potent virulence factor that promotes bacterial dissemination in the primary DLN.

2.3.3 YopJ triggers release of intracellular bacteria

Since we noted significantly higher numbers of Kim5-bearing macrophages compared to the $\Delta yopJ$ -bearing macrophages within the PNs (Figure 4), we hypothesized that YopJ-dependent cell death initiated bacterial spread within the DLN.

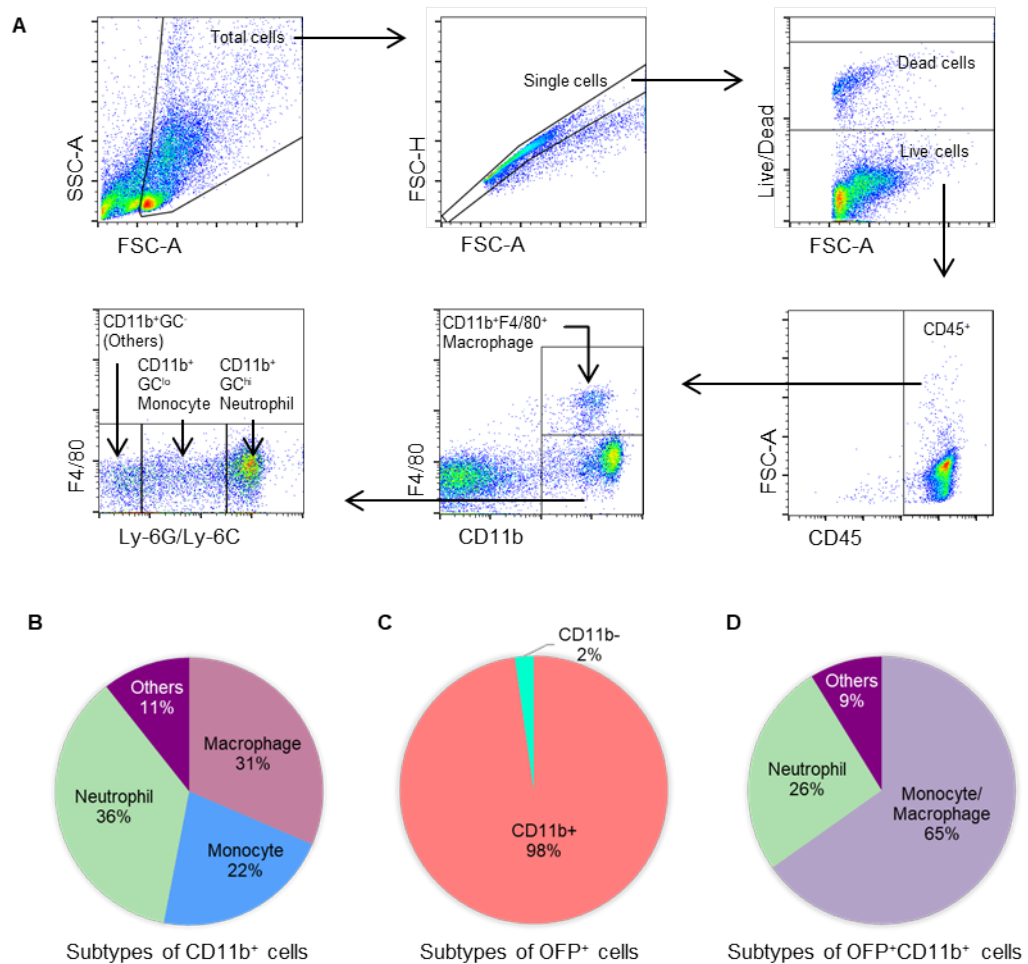


Figure 5: Monocytes/macrophages are major targets of *Y. pestis* in buboes. (A) Flow cytometry gating strategy. Ly-6GC^{hi} cells detected by an anti-Ly-6G and Ly-6C antibody (Clone RB6-8C5) were defined as neutrophils (further verified as Ly6G^{hi} using anti-Ly-6G antibody clone 1A8, data not shown) and Ly-6GC^{lo} cells as monocytes (further verified as Ly6C^{hi} using anti-Ly-6C antibody clone AL-21, data not shown). ‘Others’ indicate residual CD11b⁺ cells, which include mostly NK cells and dendritic cells, were not subtyped in these samples. (B) Mean percentage of major phagocytic cell

types as a proportion of total CD11b⁺ cells in PNs 24 h.p.i. with *Y. pestis* Kim5 (n = 9). (C) Mean percentage of CD11b⁺ cells as a proportion of total OFP⁺ cells in PNs (n = 4). (D) Mean percentage of major phagocytic cell types as a proportion of total OFP⁺ cells in PNs (n = 4).

When phenotyped by flow cytometry, we observed that major phagocytic cells infiltrated into buboes at 24 h.p.i. were macrophages, monocytes and neutrophils (Figure 5, A-B), consistent with previous reports (32, 45). We also observed that monocytes and macrophages were the major targets of *Y. pestis* in buboes (Figure 5, C-D). Based on the role of monocytes and macrophages in *Y. pestis* trafficking between nodes (45) and our observations here, we utilized J774A.1 cells, which display similar phenotype to the target cell population in buboes, as an *in vitro* model system to test whether YopJ-dependent cell death could trigger bacterial release from cells. Cells were infected with OFP-labeled *Y. pestis* at an MOI of 10:1, exposed to gentamycin to kill extracellular bacteria and transferred onto a monolayer of uninfected macrophages at a ratio of 1:10 (infected: uninfected). The dissemination of infection was then tracked by time-lapse fluorescence microscopy. Upon addition of Kim5-OFP-infected cells onto uninfected cells, we observed exteriorization of bacteria from the infected cells followed by infection of multiple neighboring cells (Figure 6A, top panels). In contrast, addition of cells bearing $\Delta yopJ$ -OFP bacteria did not result in infection of neighboring cells (Figure 6A, bottom panels). Indeed, these $\Delta yopJ$ -OFP bacteria could not escape their host cell, even though they multiplied intracellularly at similar rate to Kim5-OFP (Figure 6B). These data suggest a contribution of YopJ to bacterial escape from infected

macrophages.

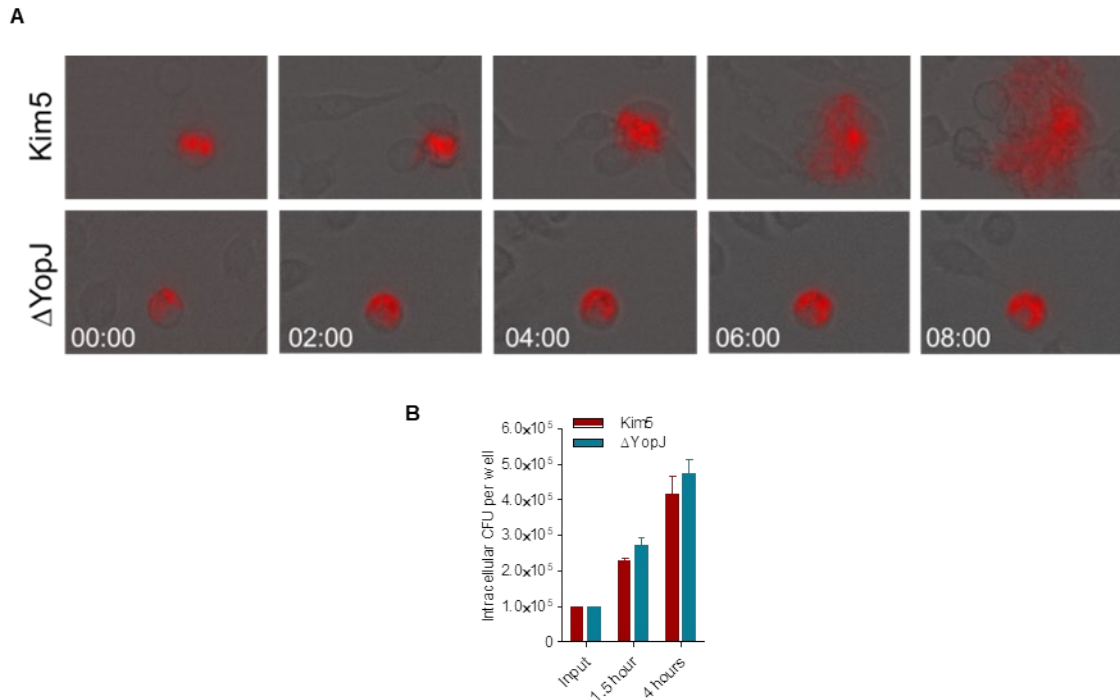


Figure 6: YopJ-triggered macrophage death promotes infection of neighboring cells. (A) Time-lapse images showing intracellular OFP⁺ bacteria (red) and their release from J774A.1 macrophages (magnification 200x). Time 00:00 (hh:mm) indicates 4 h post initial infection. (B) Number of intracellular bacteria per well at 1.5 h and 4 h post infection of 2×10^4 J774A.1 cells for 30 min ($n = 3$). Input indicates CFU count at 0 min from the bacterial suspension added to each well.

2.3.4 *Y. pestis*-induced cell death promotes infection of neighboring cells

If *Y. pestis* were to exploit macrophages as a reservoir followed by a burst of bacterial release due to cell death, we expect a close association between cytolysis and bacterial exteriorization. To visualize cytolysis during infection, we labeled macrophages with a green fluorescent dye and infected them with Kim5 bacteria followed by gentamycin treatment to kill extracellular bacteria. These labeled and

infected macrophages were then placed on a monolayer of unlabeled and uninfected macrophages. Propidium iodide was added to the extracellular medium so that cells losing membrane integrity could be readily visualized by time-lapse microscopy.

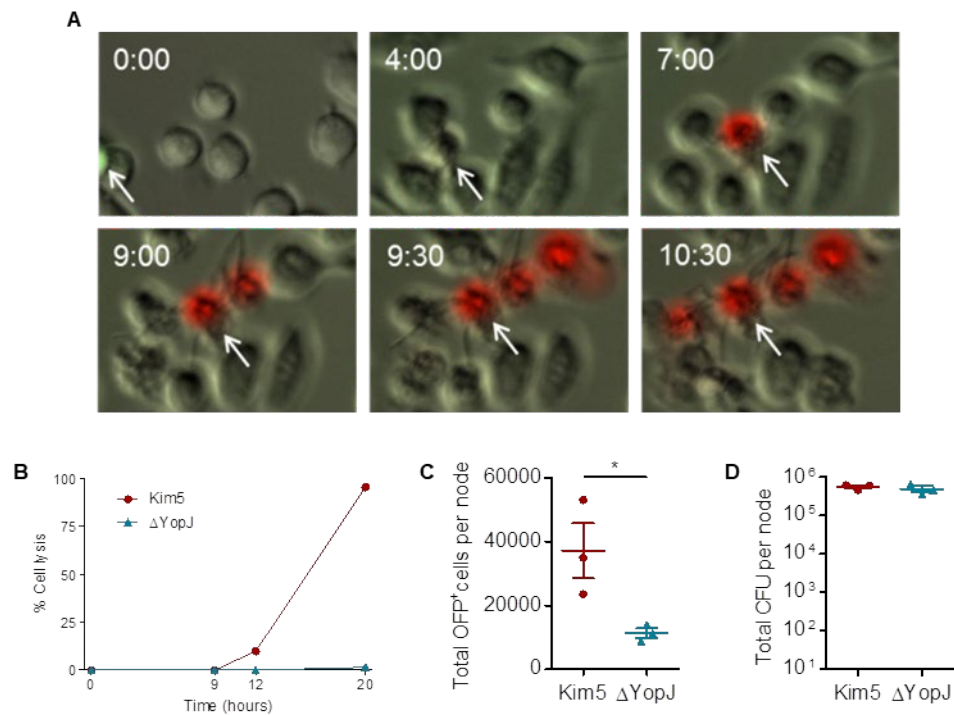


Figure 7: Cell death promoting infection of neighboring cells. (A) Cytolysis visualized by the entry of propidium iodide (red) into J774A.1 macrophages (magnification 200x). Time 00:00 (hh:mm) indicates 4 h post initial infection. The arrow in each panel indicates the initially infected cell. Ratio of infected:uninfected cells = 1:10. (B) Percent cell lysis representing death of initially and newly infected cells combined at various time points post initial infection. Ratio of initially infected:uninfected cells = 1:10. Data are represented as the mean of duplicate for each time point. (C and D) Total GFP⁺ cells (C) and bacterial count (D) in PNs 9 h after footpad injection with J774.1A cells bearing Kim5-OFP or Δ yopJ-OFP (n = 3).

We observed that lysis of an originally infected macrophage was followed sequentially by lysis of neighboring macrophages (Figure 7A). Since YopJ is a type III secretion protein which triggers cell death only upon its active injection by bacteria into

host cytosol (42), the lysis of neighboring macrophages must have been preceded by their infection by live bacteria released from the originally infected cell. We also incubated Kim5-infected cells with uninfected cells and quantitated the rate of cell lysis over a 20-hour period by LDH assay. We detected lysis of only 10% of total cells by 12 hours, which presumably were the originally infected cells, however, the remaining cells lost their viability by 20 hours (Figure 7B). As expected, no detectable cell death was observed during a similar experiment with $\Delta yopJ$ bacteria (Figure 7B). These observations indicate that the lysis of the primary infected cell allows infection of neighboring cells which are also lysed subsequently after uptake of bacteria.

Finally, to demonstrate cell-to-cell bacterial spread *in vivo*, we infected 10,000 J774A.1 cells with either GFP-labeled Kim5 or mutant bacteria and then injected these cells into the mouse footpad. We observed significantly higher numbers of infected cells after 9 hours in the PNs of mice injected with Kim5-infected macrophages compared to mice injected with $\Delta yopJ$ -infected macrophages (Figure 7C) but total number of viable bacteria was still comparable (Figure 7D). Altogether our data show that the initial burst of bacteria in the primary DLN is due to death of infected macrophages, which results in the spread of *Y. pestis* within DLN. Mechanistically this occurs through the *Y. pestis* virulence factor YopJ.

2.3.5 YopJ mediates early necrosis but not inflammation in buboes

Having identified that monocyte/macrophage lysis is a key step in *Y. pestis* reaching new cellular targets within DLNs, we questioned whether reduced cell death would be observed in $\Delta yopJ$ -infected DLNs.

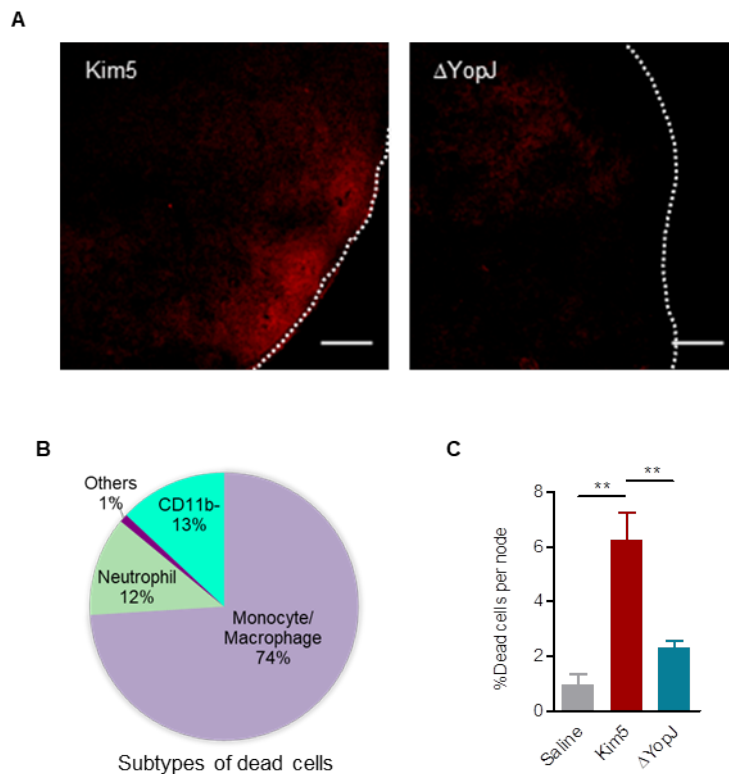


Figure 8: YopJ-dependent cell death in popliteal lymph nodes. (A) Representative images showing degree of necrosis in PNs revealed by propidium iodide staining 24 hours post infection with Kim5 or $\Delta yopJ$ strains ($n = 2$); scale bar 100 μm . (B) Percentage of various cell types as a proportion of total dead cells in single cell suspensions prepared from PNs 24 hours post footpad infection with Kim5 bacteria. (C) Quantification of dead cells in the PNs by flow cytometry ($n = 3-4$). Data are representative of two independent experiments.

Even as early as 24 h.p.i., distinct signs of cell death in Kim5-infected PNs could be observed after propidium iodide staining to visualize dead cells, but this was

strikingly reduced in $\Delta yopJ$ -infected nodes (Figure 8A). Dead cells were quantified in single cell preparations from each of the nodes by flow cytometry, which identified majority of the dead cells as monocyte/macrophages (Figure 8B) and supported a significant reduction in dead cells in $\Delta yopJ$ -infected compared to Kim5-infected PNs (Figure 8C).

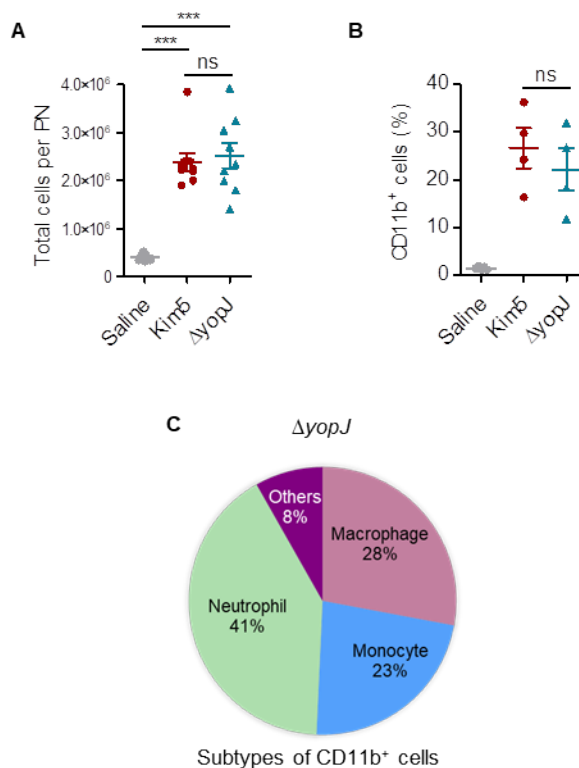


Figure 9: Cellular infiltration in popliteal lymph nodes. (A and B) Total number of cells (A) and percentage of CD11b⁺ cells (B) in PNs, 24 h.p.i. (n = 7-9). (C) Mean percentage of major phagocytic cell types as a proportion of total CD11b⁺ cells in PNs 24 h.p.i. with $\Delta yopJ$ strain (n = 9).

Interestingly, in spite of the cell death occurring in Kim5 *Y. pestis*-infected PNs, their cellularity remained comparable to that observed in $\Delta yopJ$ mutant-infected PNs

(Figure 9, A-B). There was also no appreciable difference in the infiltrated phagocytic cell subtypes between Kim5 and $\Delta yopJ$ mutant-infected PNs (Figures 5D and 9C). These results support the association of cell death *in vivo* with YopJ-induced virulence.

2.3.6 Virulence of YopJ depends on RIPK1-dependent cell death

Since deficiency of receptor-interacting protein kinase 1 (RIPK1) has previously been shown to protect against *Y. pestis*-induced cell death (47), we investigated whether RIPK1 is involved in YopJ-dependent pathogenesis. RIPK1 has a kinase-independent scaffolding activity critical for neonatal development, therefore, RIPK1 deficiency is perinatally lethal (75). However, viable knock-in mice have been described which express a kinase-inactive mutant RIPK1 (*Ripk1*^{D138N/D138N}) that is unable to execute cell death (66). If the YopJ-dependent cell death involves RIPK1, macrophages from *Ripk1*^{D138N/D138N} mice should resist death when infected by Kim5 *Y. pestis*. Shown in Figure 10A is the viability of bone-marrow derived macrophages (BMDMs) from wild type (WT) and mutant *Ripk1*^{D138N/D138N} mice following infection with Kim5 or $\Delta yopJ$ *Y. pestis*. Although the WT and mutant macrophages were comparably infected (Figure 10B), *Ripk1*^{D138N/D138N} BMDMs were resistant to *Y. pestis*-induced cell death (Figure 10A), confirming that *Y. pestis* YopJ-triggered cell death is dependent on RIPK1 kinase activity.

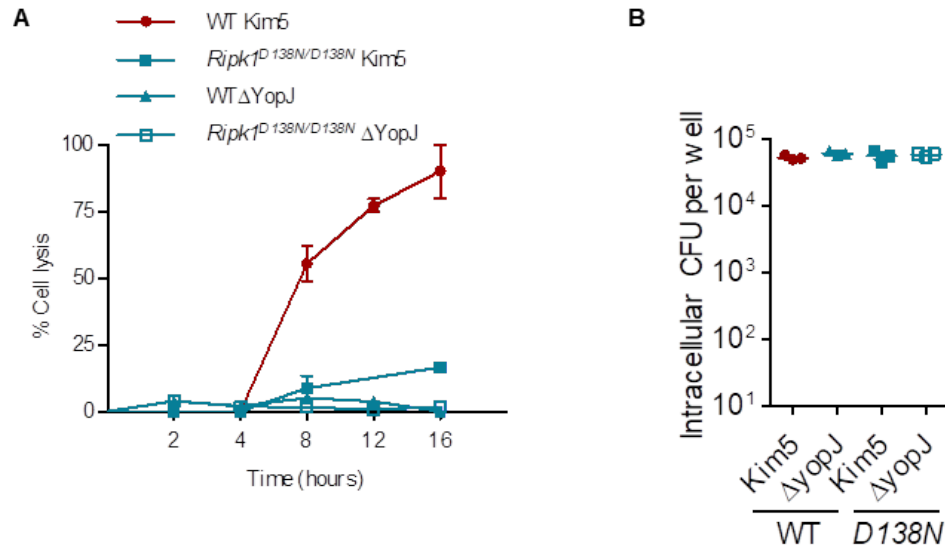


Figure 10: YopJ-triggered cell death in WT and RIPK1 mutant macrophages.

(A) Lysis of BMDMs isolated from WT or *RipK1*^{D138N/D138N} mice following *in vitro* infection with Kim5 or $\Delta yopJ$ (MOI 10). Data are representative of three independent experiments. (B) Number of intracellular bacteria per well as determined by CFU counts. 2×10^4 BMDMs from WT or *Ripk1*^{D138N/D138N} mice were infected with bacteria at MOI 10 for 2 hours, treated with gentamicin for an hour, then washed, lysed and plated (n = 3).

Upon confirming *in vitro* that YopJ-triggered cell death requires RIPK1 kinase activity, we reasoned that if YopJ-triggered cell death promoted lymphatic

dissemination of *Y. pestis*, bacterial dissemination from popliteal nodes to iliac nodes

should be compromised in *Ripk1*^{D138N/D138N} mice. Indeed, we observed that bacterial

numbers in INs relative to that in respective PNs were much lower in *Ripk1*^{D138N/D138N}

mice compared to that of WT mice (Figure 11A) suggesting that RIPK1-dependent cell

death is important for the amplification of infection within primary DLNs, leading to

increased spread of bacteria from the primary DLN to the secondary DLNs.

Consequently, compared to WT mice, *Ripk1*^{D138N/D138N} mice were significantly resistant to

lethal Kim5 *Y. pestis* challenge (Figure 11B). It is noteworthy that *Ripk1*^{D138N/D138N} mice had normal sized PNs and the size of buboes formed following Kim5 *Y. pestis* infection was also comparable to that seen with WT mice (Figures 11C and 3C), indicating that there was no intrinsic defect in the recruitment of immune cells in mutant mice and that RIPK1 kinase activity does not substantially influence cellular recruitment into *Y. pestis*-infected DLNs.

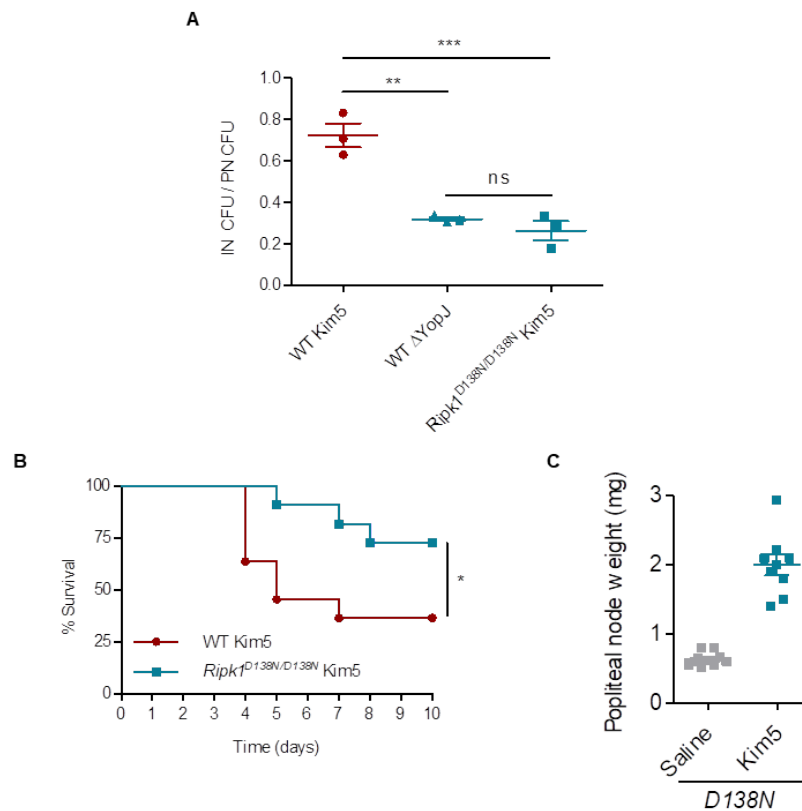


Figure 11: Virulence of YopJ depends on RIPK1-mediated programmed cell death. (A) Bacterial counts in INs relative to bacterial counts in PNs 24 hours post footpad infection (n = 3). (B) Survival of WT and *Ripk1*^{D138N/D138N} mice following footpad challenge with Kim5 bacteria. Data are combined from two independent experiments, each with 5-6 mice per group. (C) PN weights of *Ripk1*^{D138N/D138N} mice 24 hours post footpad injection with saline or Kim5 bacteria (n = 9-10).

2.3.7 RIPK1 inhibitors protect from lethal infection

Since RIPK1-dependent cell death is preventable by necrostatin-1 (Nec-1), an inhibitor of RIPK1 kinase activity (76), we investigated if this inhibitory agent could also block *Y. pestis* YopJ-triggered death of infected macrophages *in vitro*. We observed that Nec-1 was a potent inhibitor of *Y. pestis*-induced death of J774A.1 macrophages (Figure 12A). Nec-1 itself neither had any direct bactericidal effects nor affected bacterial invasion (Figure 12, B-C). Furthermore, when *Y. pestis*-infected macrophages were incubated together with uninfected macrophages, Nec-1 inhibited cell-to-cell bacterial spread (Figure 12D).

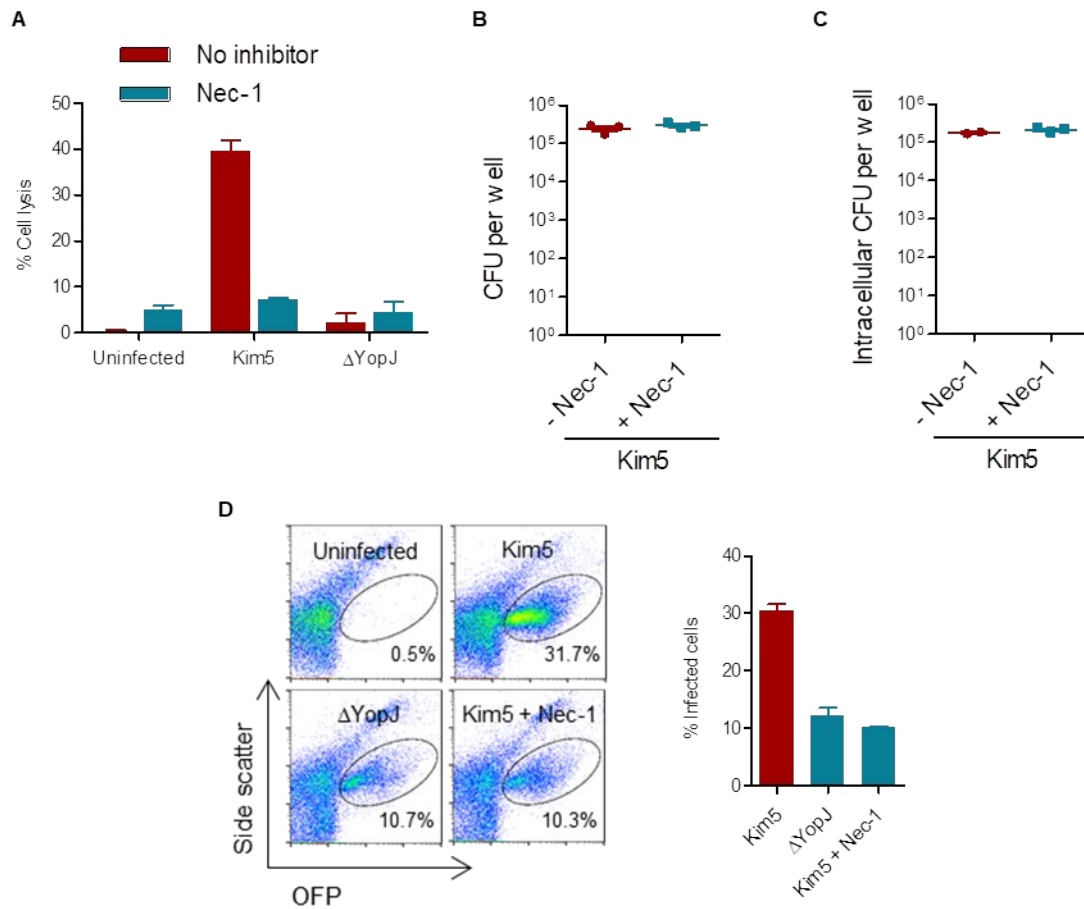


Figure 12: RIPK1 inhibitor prevents cell-to-cell spread of *Y. pestis*. (A) Lysis of J774A.1 macrophages at 8 h.p.i. during Kim5 or $\Delta yopJ$ infections in the presence or absence of Necrostatin-1 (Nec-1, 30 μ M) (n = 3). (B) Number of viable bacteria per well determined by agar plating. 2×10^5 bacteria were incubated for 2 hours with media alone or media containing Nec-1 and then plated for CFU count. Number of viable bacteria per well determined by agar plating. 2×10^5 bacteria were incubated for 2 hours with media alone or media containing Nec-1 and then plated for CFU count (n = 3). (C) Number of intracellular bacteria per well. 2×10^5 macrophages were pre-incubated with or without Nec-1 for 2 hours, infected with bacteria (MOI 10) for 30 min and treated with gentamicin for an hour in presence or absence of Nec-1, then washed, lysed and plated for CFU count (n = 2-3). (D) Flow cytometry plots and percentage graph showing infection of neighboring macrophages from Kim5-OFP or $\Delta yopJ$ -OFP infected macrophages in the presence or absence of Nec-1, 10 hours post initial infection (n = 3). Data are representative of two independent experiments.

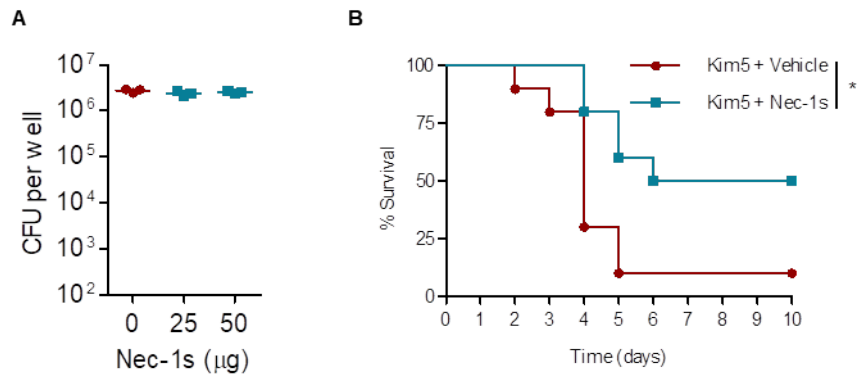


Figure 13: RIPK1 inhibitors protect from lethal. (A) Number of viable bacteria per well determined by agar plating. 10^5 bacteria were incubated for 24 h with media alone or media containing indicated amount of Nec-1s and then plated for CFU count ($n = 3$). (B) Survival of Kim5-infected mice with or without Nec-1s treatment. Data are combined from two independent experiments, $n = 5$ in each experiment.

We, therefore, employed Nec-1s, a metabolically stable variant of this agent which also did not have any direct antibacterial activity (Figure 13A), to demonstrate the importance of YopJ-triggered cell death in the pathogenesis of *Y. pestis*. We found that treatment of mice with Nec-1s was sufficient to significantly protect these animals from lethal *Y. pestis* infection (Figure 13B). Taken together, YopJ triggered a RIPK1-dependent cell death program within buboes that was essential for the virulence of *Y. pestis*. Furthermore, RIPK1 is a therapeutic target for limiting *Y. pestis* dissemination.

2.3.8 *Y. pestis*-triggered cell death involves necroptosis

Programmed cell death can be defined as apoptosis, autosis or various types of regulated necrosis such as pyroptosis and necroptosis, each triggered by distinct but often interconnected signaling programs (65). Having established the importance of *Y.*

pestis-induced cell death to bacterial dissemination in vivo, we sought to further characterize the type of cell death that was induced. While RIPK1-mediated cell death programs can result in either apoptosis or necroptosis (65), our finding that bacterial exteriorization occurs from dying macrophages (Figure 6A) strongly suggests necroptotic mode of cell death. In contrast to apoptosis where the cellular membrane is intact, necroptosis results in membrane disruption (77), which would allow bacteria to be released extracellularly. To validate if YopJ triggers macrophage necroptosis through a RIPK1-dependent mechanism, we performed immunoprecipitation studies on BMDMs from WT or RIPK1-inactive mutant (*Ripk1*^{D138N/D138N}) mice. Necroptosis is initiated when RIPK1, upon its interaction with caspase-8, becomes bound to RIPK3 to form a high molecular weight detergent-insoluble complex called necrosome (64, 68).

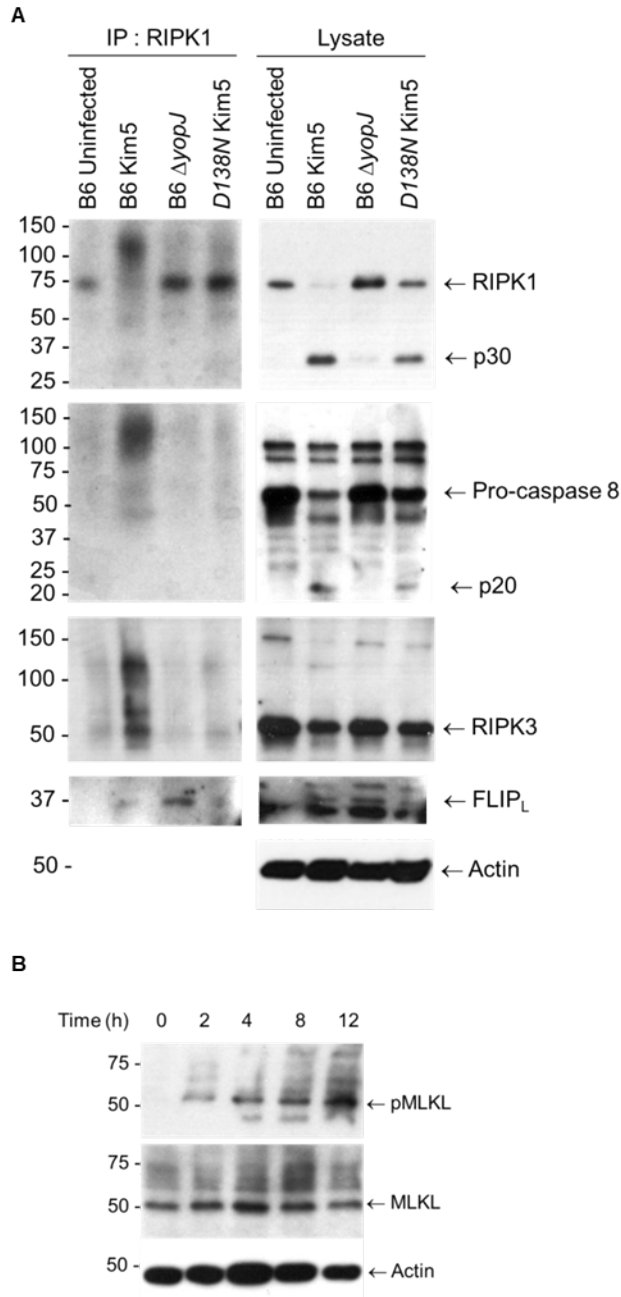


Figure 14: YopJ-triggered cell death is necroptotic. (A) RIPK1 immunoprecipitated from WT (B6) or RIPK1 mutant (*D138N*) BMDMs 3 h.p.i. and the presence of RIPK1, Caspase-8, RIPK3 and FLIP detected by immunoblotting. Total lysates were also assayed for these proteins and β -actin. p30 and p20 indicate cleavage products of corresponding proteins. (B) Immunoblot analysis of lysates prepared from Kim5-infected BMDMs at indicated time points and probed for MLKL, phospho-MLKL

and β -actin. Intensity measurements relative to actin were shown under corresponding bands.

Therefore, we attempted to pulldown this protein complex from *Y. pestis*-infected BMDMs using a RIPK1-specific antibody. We found that while the high molecular weight complex was detectable in macrophages infected with YopJ-expressing bacteria, it failed to form in the absence of YopJ (Figure 14A). As expected, no complex was also formed in macrophages derived from RIPK1 inactive mutant mice (*Ripk1*^{D138N/D138N}) upon Kim5 *Y. pestis* infection (Figure 14A). Further confirmation of the necroptotic mode of cell death comes from the observation that mixed lineage kinase domain-like (MLKL) protein, the executor of necroptosis (78), became progressively more phosphorylated (Figure 14B), which is the key step for the polymerization of MLKL and subsequent formation of membrane disrupting pores. Thus, a significant portion of *Y. pestis*-infected cells undergo necroptosis.

2.3.9 Cell death during *Y. pestis* infection is delayed

We noted that macrophage lysis occurred only after a lag phase of at least 4 hours *in vitro* (Figure 10A), which provided sufficient time for *Y. pestis* to replicate intracellularly (Figure 6B). We, therefore, questioned whether the necrosome formation was delayed to provide this lag period. Since the RIPK1-mediated cell death program is highly sensitive to prosurvival factors produced by host cells, we investigated if there was a link between the delay in cell death and expression of one or more prosurvival factors. The fas-associated death domain (FADD)-like interleukin-1- β converting enzyme

(FLICE/Caspase-8)-like inhibitory protein (FLIP) is a prosurvival factor which physically prevents the assembly of the cell death-signaling protein complex containing RIPK1, FADD and caspase-8, by competitively binding one of more partners in the complex (79, 80). Indeed, we observed that FLIP was bound to the cell death signaling complex more in the absence of YopJ, indicating that it plays a role in *Y. pestis*-induced cell death (Figure 14A). This observation led us to hypothesize that upon *Y. pestis* infection, any activation of the RIPK1-mediated cell death pathway in macrophages is abrogated by FLIP. YopJ interferes with this inhibitory activity and eventually cell death is initiated. Support for this hypothesis comes from the finding that a significant increase of expression levels of FLIP_L and FLIP_S (long and short isoforms) was observed in *Y. pestis*-infected macrophages as early as 30 min after infection (Figure 15A). Amounts of FLIP_L and FLIP_S in Kim5-infected cells were lower compared to $\Delta yopJ$ -infected cells and FLIP_S also appeared to diminish with time (short exposure in Figure 15A). Furthermore, FLIP mRNA expression levels were lower in Kim5-infected cells compared to $\Delta yopJ$ -infected cells, indicating that YopJ was influencing mRNA levels (Figure 15B). When we infected BMDMs in presence of suberanilohydroxamic acid (SAHA), which targets FLIP for proteosomal degradation (81), we observed significant induction of early cell lysis by 4 hours irrespective of the presence of YopJ (Figure 15C).

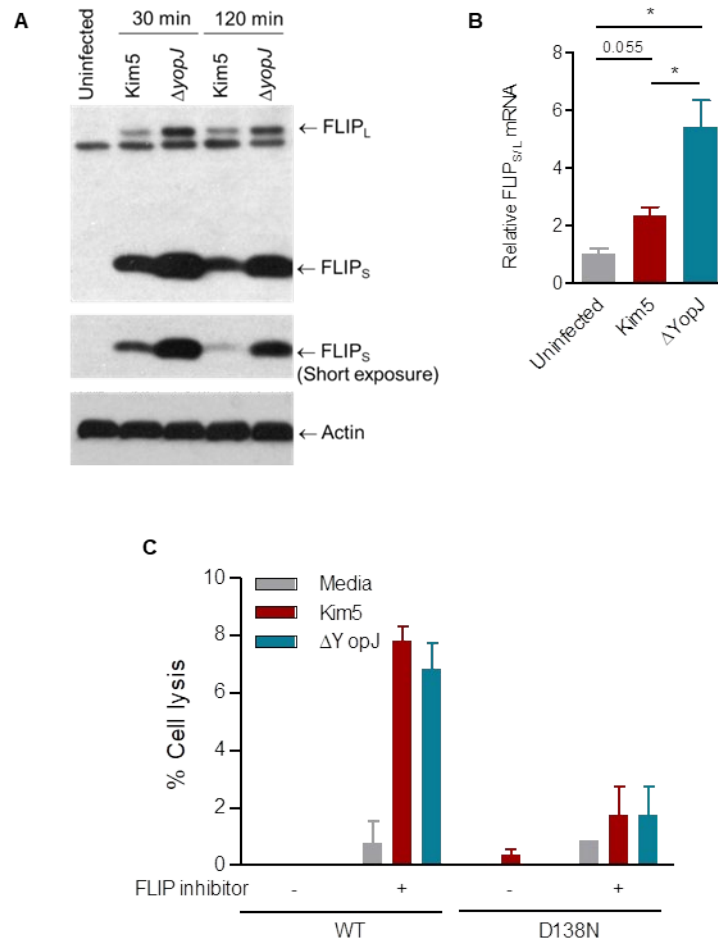


Figure 15: FLIP upregulation during *Y. pestis* infection of macrophages. (A) Immunoblot analysis of lysates prepared from uninfected macrophages, or macrophages collected at indicated time points after infection with Kim5 or $\Delta yopJ$ strain. Immunoblots were probed with anti-FLIP_{S/L} and anti- β -actin. Band intensities relative to actin were shown for the short exposure panel. (B) Fold change of FLIP mRNA 2 h.p.i relative to expression in uninfected macrophages (n = 3). (C) Lysis of WT or *Ripk1*^{D138N/D138N} BMDMs 4 h post infection with *Y. pestis* Kim5 or $\Delta yopJ$ strain in presence or absence of 10 μ M SAHA, a FLIP inhibitor (n = 3-4). Data are representative of two independent experiments.

These observations cumulatively suggest *Y. pestis*-induced cell death is delayed, at least in part, due to interference by prosurvival factors activated in macrophages resulting in a window of time that allows for intracellular bacterial replication.

2.3.10 Macrophage death alters local S1P gradients promoting intra-nodal bacterial spread

A remarkable observation we made in the time-lapse videos tracking the spread of *Y. pestis* from infected macrophages to neighboring macrophages was the large number of surrounding cells actively moving towards the Kim5-infected macrophage (Figure 6A, top panels). This directional movement of neighboring macrophages, which appeared to promote bacterial infection of a greater number of surrounding cells, was absent with $\Delta yopJ$ -infected cells (Figure 6A, bottom panels), suggesting that potential chemotactic signals were emanating from necroptotic cells. To verify this observation, we undertook a trans-well migration assay where we observed much greater numbers of uninfected macrophages migrating across the membrane barrier towards Kim5-infected cells compared to $\Delta yopJ$ -infected cells (Figure 16).

Sphingosine 1-phosphate (S1P) has been implicated as a putative 'find-me' signal secreted by dying cells to attract phagocytes to promote their clearance (82, 83). This chemoattractant is especially relevant here as it is also a major chemoattractant regulating movement of immune cells within and out of DLNs including during *Y. pestis* infection (45, 84, 85). To determine if S1P production might be enhanced in macrophages during *Y. pestis* infection *in vitro*, we assessed the expression of sphingosine kinase 1

(SphK1), the specific sphingosine-phosphorylating enzyme involved in S1P generation (86).

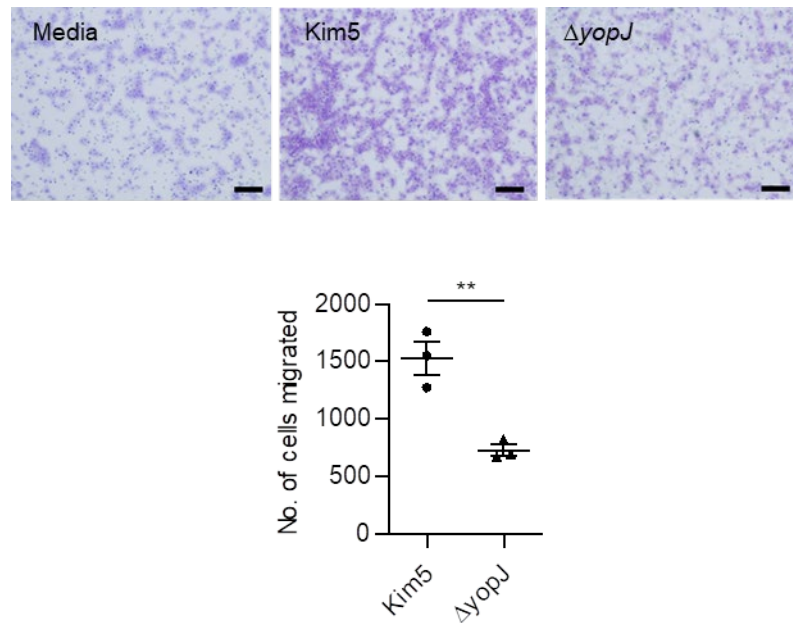


Figure 16: YopJ-triggered cell death results in chemotaxis of uninfected macrophages. Representative images of trans-well migration of J774A.1 cells towards uninfected, Kim5-infected or $\Delta yopJ$ -infected cells. Images of the filter membranes were taken after fixation and staining of cells migrated across the membrane (purple in color) as described in the methods. Scale bar, 200 μm . Pores of the membranes are also visible in the images as the numerous small, round dots. Graph shows quantification of migrated cells ($n = 3$).

We observed robust upregulation of *Sphk1* mRNA expression in Kim5-infected cells preceding cell lysis, but not in $\Delta yopJ$ -infected cells or in presence of Nec-1 (Figure 17A). Similar effect of Nec-1 was also observed in mRNA expression of sphingosine kinase 2 (SphK2), an alternate S1P-generating enzyme (Figure 17B). Microscopic observation of infected macrophages also corroborated the RIPK1-dependent increase of

SphK1 protein levels (Figure 17C), suggesting that these macrophages have the potential of producing S1P during necroptosis resulting in the recruitment of surrounding macrophages.

If S1P production by infected and dying monocytes/macrophages is also contributing to bacterial spread in infected PNs, we predicted that the deletion of S1PR1, the corresponding receptor would markedly impact the distribution of bacteria within PNs. To test this hypothesis, we employed a previously generated *Cx3cr1-Cre S1pr1^{fl/fl}* mice in which S1PR1 is deleted only in mononuclear phagocytes and this conditional deletion does not alter the cellularity of the lymph nodes (45). We used Kim5-OFP *Y. pestis* for infection to investigate the distribution of bacteria in the PNs of *Cx3cr1-Cre S1pr1^{fl/fl}* mice compared to that in PNs of littermate controls (*Cx3cr1-Cre S1pr1^{+/+}*). We found that the bacteria in the PNs of *Cx3cr1-Cre S1pr1^{fl/fl}* mice was limited to the peripheral region (proximal to subcapsular sinus), which is in marked contrast to the littermate controls where the dispersal of bacteria was observed throughout the node (Figure 18, A-B). However, there was no difference between the two genotypes in the total number of bacteria found in the PNs (Figure 18C).

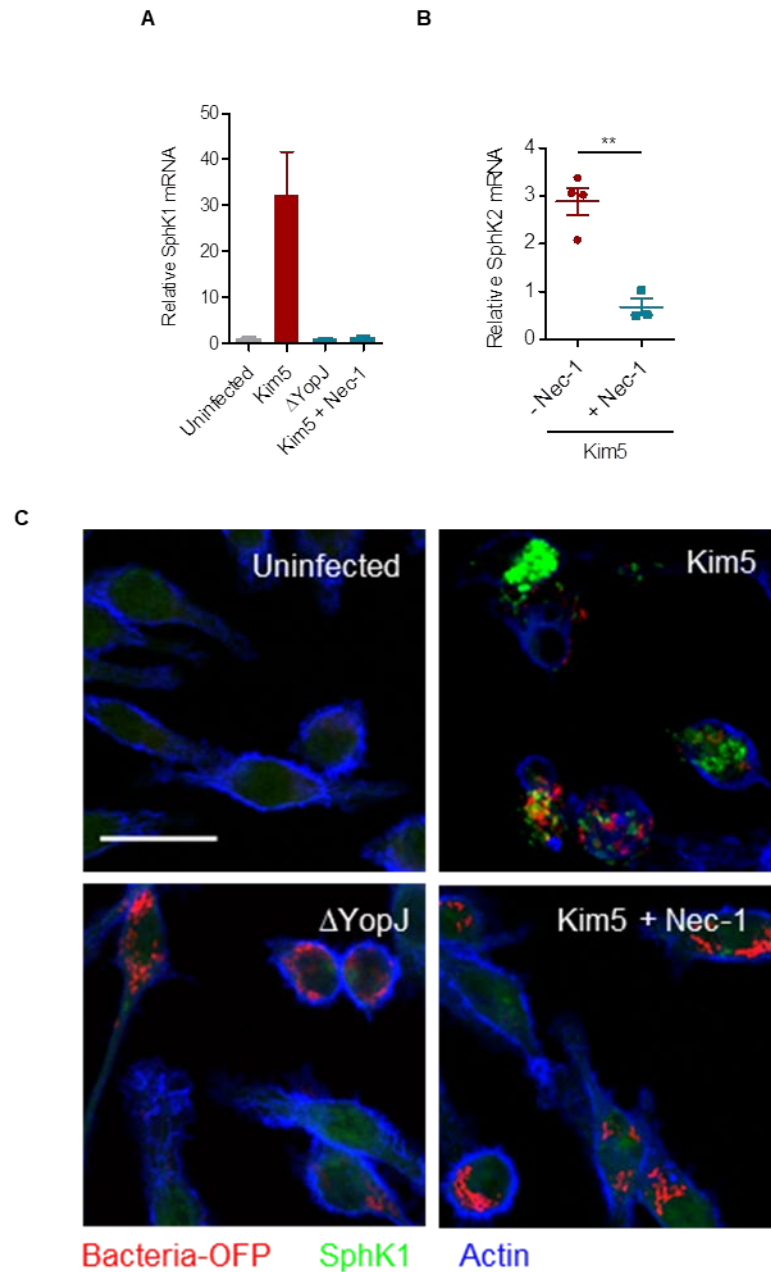


Figure 17: S1P upregulation in dying cells. (A and B) Fold change of (A) *Sphk1* and (B) *Sphk2* mRNA in J774A.1 macrophages at 8 h.p.i. relative to uninfected controls (n = 3-4). (C) Immunofluorescence staining for SphK1 (green) in uninfected, Kim5-OFP-infected or in Δ yopJ-infected macrophages. Scale bar, 25 μ m.

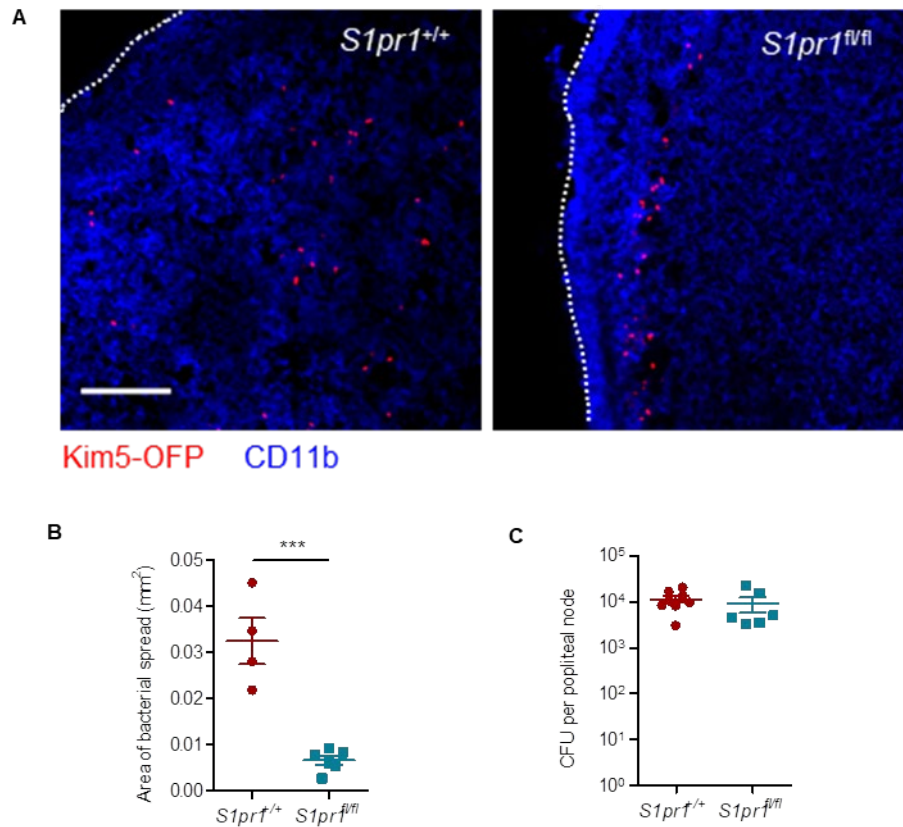


Figure 18: S1P promotes intra-nodal bacterial spread. (A) Immunofluorescence staining of PNs from mice whose mononuclear phagocytes were S1PR1-sufficient (*Cx3cr1-Cre S1pr1*^{+/+}) or deficient (*Cx3cr1-Cre S1pr1*^{fl/fl}), 24 hours after footpad infection with Kim5-OFP bacteria. Scale bar, 50 μ m. (B) Area of bacterial spread measured from the PN images (n = 4-6). (C) Bacterial numbers in PNs of *Cx3cr1-Cre S1pr1*^{+/+} or *Cx3cr1-Cre S1pr1*^{fl/fl} mice, 24 hours following footpad infection with Kim5 *Y. pestis* (n = 6).

These observations suggest that in addition to enhanced bacterial spread mediated by the necroptotic death and extracellular release of bacteria, S1P released by dying cells were attracting neighboring cells, further enhancing the spread of bacteria.

2.4 Discussion

Following intradermal inoculation by a flea bite, *Y. pestis* sequentially infects lymph nodes along the lymphatic system, converting each of them into swollen buboes (31, 32). The pathogen even coopts the massive influx of phagocytic cells that the host has mobilized into the node to contain the pathogen by converting these cells into powerful vehicles for bacterial dispersal (45). Our studies reveal the crucial role of necroptotic cell death in amplifying the number of bacteria-bearing monocytic phagocytes within buboes, and its subsequent impact on bacterial dissemination. We observed that early bubo necrosis was caused by the *Y. pestis* YopJ protein, which initiates a RIPK1-dependent necroptotic form of death in infected cells. Aside from the protection offered against host factors such as complement and antibodies, the intracellular stage of *Y. pestis* is important for its dispersal through the lymphatic system since it hitchhikes within mononuclear phagocytes to reach systemic infection (45). We also show that replication of bacteria occurs during this critical intracellular stage of infection. However, lysis of a *Y. pestis*-infected cell and exteriorization of bacteria can lead to the simultaneous infection of multiple cells and amplification of the infection in surrounding macrophages, which may then traffic to secondary nodes and spread the infection systemically. Thus, both the intra- and extracellular stages of the *Y. pestis* life cycle are critical to its virulence and, importantly, we have identified a trigger regulating the switch between these two stages. It is remarkable that the bubo sizes and bacterial

numbers in primary buboes were comparable between Kim5 and YopJ mutant- infected mice, as it indicated that in spite of the significant cell death, neither the recruitment of immune cells into buboes nor bacterial growth was affected at this early stage of infection. Indeed, only the cell death-mediated difference in the number and distribution of bacteria-bearing macrophages within each node was found to be critical in determining bacterial dispersal and ultimately, host survival.

The *in vivo* contribution of *Y. pestis*-mediated cell death to bacterial virulence was evident not only from studies with the YopJ mutant bacteria, but also from parallel studies using RIPK1 mutant (Ripk1D138N/D138N) mice or RIPK1 inhibitor-treated animals infected by Kim5 *Y. pestis*. From these studies, we have identified several distinct features of YopJ-RIPK1-mediated cell death that greatly favor bacterial spread within the buboes, which subsequently impacts their systemic dissemination. Firstly, the type of cell death that is triggered is necroptosis, which, unlike apoptosis, involves physical rupture of lysosomal and plasma membranes (77). Membrane rupture during necroptosis is more extensive than that in pyroptosis since the cells flatten during pyroptosis but swell and burst during necroptosis (87). Disintegration of the membranes of infected cells allows for the unrestricted release of intracellular bacteria into the extracellular space, promoting expedient infection of neighboring cells. Unlike necrosis, which was traditionally assumed to be the type of cell death induced in *Y. pestis*-infected buboes, the process of necroptosis that we have now identified is regulated by specific

signals within the host cell. Secondly, the cell death occurs after a period of lag (in excess of 4 hours) since the infected macrophages produce high levels of the prosurvival factor FLIP immediately upon infection. Presumably, the macrophages attempted to block RIPK1-dependent cell death programs induced by PAMPs to prevent release of intracellular bacteria. However, through the actions of YopJ, the level of FLIP is diminished in a time dependent fashion to allow necroptosis to occur. The downregulation of FLIP by YopJ could be via YopJ-mediated suppression of NF- κ B, an inducer of FLIP (88). Interestingly, this delay in cell death in *Y. pestis*-infected macrophages could be useful for the bacteria in multiple ways. For example, this period allows for intracellular bacterial replication, which would enhance the magnitude of bacterial spread when the cell membrane is disrupted. This lag period between infection and cell death would also provide sufficient time for a newly infected cell to travel from the site of infection to primary DLNs or from the primary DLN to secondary DLNs. Therefore, it is possible that *Y. pestis* YopJ has evolved to be less potent in triggering cell death compared to the homologous protein YopP in ancestor species *Y. enterocolitica* (89). Our findings also distinguish the role of YopJ in *Y. pestis* compared to the homologous protein in the parent species *Y. pseudotuberculosis*. In the context of *Y. pseudotuberculosis* infection, RIPK1-mediated apoptosis was beneficial to pathogen clearance by the host (90). Our results contrast with this, showing that *Y. pestis* YopJ leads to necroptosis which is more similar to observations with lytic viruses, allowing a

regulated release of the pathogen from cellular hosts. The mechanism of choosing necroptosis over other cell death types is unclear, which could be due to differences in the potency of YopJ isoforms (63) as well as differences in cell death-inducing PAMPs (18, 91) among various *Yersinia* species.

Y. pestis-mediated cell death attracts surrounding cells towards dying infected macrophages promoting cell-cell contact and fostering further infection in buboes. Massive upregulation of the chemoattractant S1P was associated with the movement of cells towards Kim5-infected cells. This chemoattractant has previously been implicated as a 'find-me' signal produced by dying cells to promote their elimination by phagocytes (82). Interestingly, there is growing evidence that the movement of immune cells within the node is susceptible to local S1P gradients. For example, natural killer cells are recruited and strategically positioned in the medulla of lymph nodes in response to the enhanced extracellular presence of S1P at these sites (85). From the study of *Y. pestis* infections in mice where the S1P receptor 1 is lacking in mononuclear phagocytes, we deduced that S1P was a key contributor to bacterial dispersal within the buboes, in addition to its previously described role in permitting the egress of infected cells from buboes (45). Thus, the sharp increase in the population of bacteria-bearing macrophages in Kim5-infected buboes compared to YopJ mutant-infected buboes is attributable to the complementary actions of cell lysis and secretion of S1P which greatly facilitate infection of surrounding macrophages. Although it has been known for more than a decade that

YopJ-mediated cell death is associated with *Y. pestis* infection (46), its significance has largely remained elusive. This study extends our understanding of *Y. pestis* pathogenesis by revealing how YopJ directs a delayed necroptotic cell death program to amplify bacterial infectivity within buboes. By greatly expanding the number of bacteria-bearing cells in primary buboes, the pathogen improves its chances of successfully infecting secondary lymph nodes and reaching the circulating system in enough numbers to overcome host defenses.

Our study reveals that abrogating this pathogen-initiated cell death program by therapeutically targeting RIPK1 is potentially a powerful approach to combating *Y. pestis* infection as it would prevent bacterial dissemination while still protecting the lymph nodes from destruction. This latter aspect could be important as it will preserve the host's ability to develop protective immunity against future infections. Since this treatment does not directly target *Y. pestis*, it is also unlikely that any resistance will be developed by the pathogen. Recent findings of a series of RIPK1 inhibitors with improved potency and pharmacokinetics (92) is highly encouraging as they could be even more effective against this pathogen.

Preface to Chapter 3

This chapter is a modified version of the following manuscript accepted for publication in Science Advances:

Arifuzzaman M, Mobley YR, Choi HW, Bist P, Salinas CA, Brown ZD, Chen SL, Staats HF, Abraham SN. MRGPR-mediated activation of local mast cells clears cutaneous bacterial infection and protects against reinfection. Science Advances (in press)

3. Activation of peripheral mast cells via the MRGPR receptor potentiates bacterial clearance

3.1 Introduction

3.1.1 The role of mast cells in pathogen clearance

Although best known as mediators of allergy, mast cells (MCs) are increasingly becoming recognized as key players in mobilizing innate and adaptive immune responses against various pathogens. There is a growing consensus that these cells play a critical role in immune surveillance and significantly contribute to the early immune responses to bacterial, viral and parasitic infections (93). These cells are especially adept at this role because of their critical location at the host-environment interface as well as their capacity to rapidly release key immunostimulatory mediators that are prestored in granules.

Being an immune-surveillance cell type at the barrier sites such as skin and mucosa, MCs are equipped at their cell surface with a wide range of pattern recognition receptors (PRRs) that can directly recognize pathogen associated molecular patterns (PAMPs) found on pathogens or their products. These cells are also equipped with various receptors specific to host-generated antimicrobial peptides, complement components and danger signals such as ATP (93, 94). The mediators that MCs release upon pathogen recognition include proteases (tryptases and chymases), chemokines and cytokines. Tumor necrosis factor, one of these mediators, when acting in concert can promote large scale recruitment of neutrophils and natural killer cells from circulation

into the tissue resulting in early clearance of various bacteria and viruses (53, 95).

Furthermore, degranulation of activated mast cells is followed by *de novo* synthesis and secretion of a wide range of proinflammatory mediators such as leukotrienes and various additional cytokines and chemokines (such as various interleukins) (93). Studies in various MC knockout mouse models have revealed that the ability of the host to clear various pathogens is severely compromised in the absence of MCs (53, 95-98).

3.1.2 The role of mast cells in adaptive immunity

During infection, resident MCs secrete TNF which can promote the recruitment of antigen-presenting dendritic cells (DCs) to the site of infection, which eventually migrate to the draining lymph nodes (DLNs) (99). At the DLNs, dendritic cells initiate development of adaptive immune responses through antigen presentation to T cells (100-102). In addition to recruiting DCs at the site of MC activation, MC activation can also promote mobilization of dendritic cells to the DLNs. We previously demonstrated that a portion of granules released from activated mast cells at the peripheral sites such as skin was drained into lymph nodes where the granules released immunomodulators such as TNF (103). The result was a sharp upregulation of chemoattractant CCL21 expression in the nodes (99), which enhanced coordinate trafficking of antigen presenting DCs from the site of MC activation into the lymph node (104) as well as T cells from circulation (102). Therefore, when small-molecule mast cell activators (MCAs) were co-administered with vaccine antigens in skin or nasal mucosa, this synchronous

recruitment of critical immune cells resulted in a highly enhanced antibody response to antigen (104). Therefore, MCAs could function as highly effective adjuvants boosting adaptive immune responses when co-administered with subunit vaccine antigens at mucosal surfaces or the skin.

3.1.3 Targeting of mast cells for anti-bacterial therapy

Local and selective activation of a single immunoregulatory cell type such as MCs may be more efficient and less harmful than targeting various immune cells via common PRR ligands, as these cells have their own controlled program to release different immunomodulators with different time courses (93). Furthermore, MCs coordinate both innate and adaptive immunity, therefore, may help improve the ability to clear and existing infection while also improve protection from future reinfections. MCs can be activated by various endogenous cationic peptides naturally occurring in our body such as substance P, cathelicidin and β -defensin (93). The receptor for these MC secretagogues is a Mas-related G protein-coupled receptor called MRGPRX2 (105, 106). The orthologue of this receptor in mice has recently been identified in mice as *Mrgprb2* which is found exclusively on a subset of mast cells called connective tissue mast cells (CTMCs) (107). Therefore, activation of MCs via this receptor would be specific, providing a more controlled immune response. Furthermore, the nature of MRGPRX2-mediated activation of MCs is distinct from that by cross linking of the IgE receptor, Fc ϵ RI, during allergy. Recent studies revealed that the inflammatory responses

evoked by MCs following activation of MRGPRX2 are transient and markedly more tempered, unlike the sustained inflammatory reactions mediated by the IgE receptor (108). We reasoned that a more tempered and transient activation of local MCs could be sufficient to evoke inflammatory responses necessary to combat infections with minimal side effects.

Skin and soft tissue infections which range from simple folliculitis to severe necrotic wounds, are a major therapeutic challenge (109). These infections are generally caused by both Gram positive and negative skin bacteria, including *Staphylococcus aureus*, coagulase-negative *Staphylococcus*, *Enterococcus* spp, and *Escherichia coli*. We chose *S. aureus* as our model pathogen since this bacterial species is responsible for most skin infections (110, 111). Here, we first investigated the role of mast cells in antibacterial defense using a mouse dermonecrotic *Staphylococcus aureus* infection model and then tested exogenous mast cell-activating peptides to identify therapeutic potential of mast cells in treating skin infections as well as key immunomodulatory pathways behind them.

3.2 Methods

3.2.1 Study Design

The major objective of this study was to examine whether treatment with mast cell activators expedites resolution of bacterial infections and mechanism of their function. Infected mice were randomly divided into treatment or control groups. Blinding was not deemed necessary, and all animals were used. Power analyses were performed to determine minimum numbers of animals per group needed to attain significance of $p < 0.05$ with a 90% or 95% probability. At least ten mice per group were used for lesion size measurement upon mastoparan treatment and 5-7 mice for most other experiments. End points to assess different parameters of resolution of infection were designed based on various established assays. All histomorphometric analyses were performed by a blinded observer.

3.2.2 Mice

Eight-to ten-week old C57BL/6 mice were obtained from Jackson Laboratory or National Cancer Institute Animal Production Area. *Mcpt5-Cre⁺iDTR⁺* mice were generated by crossing between *Mcpt5-Cre* mice (a gift from Axel Roers, University of Technology, Dresden) and *iDTR* mice. To achieve and maintain depletion of CTMCs, *Mcpt5-Cre⁺iDTR⁺* mice or littermates were treated every 72 hours with 20 ng diphtheria toxin (DT)/g bodyweight divided into intraperitoneal and subcutaneous injections. All

animal studies were carried out at Duke University and approved by the Duke University Institutional Animal Care and Use Committee.

3.2.3 Cell lines and transfections

The mouse mast cell line MC/9 (ATCC CRL-8306) was maintained in DMEM (Gibco) containing 10% fetal bovine serum (HyClone) at 37°C with 5% CO₂. RBL-2H3 (ATCC CRL-2256) cells were maintained in MEM with Earle's salts, L-glutamine, 1 mM sodium pyruvate and 15% heat-inactivated FBS. The ROSA and LAD2 cell lines were maintained in IMDM and StemPro™-34 SFM media, respectively. For transfections, human MRGPRX2 was amplified from LAD2 cells, and cloned in pCMV-Flag-tagged plasmid (Takara), termed Flag-MRGPRX2. RBL-2H3 cells were transfected with empty plasmid or plasmid encoding Flag-MRGPRX2 using P2 primary solution and program DN-100 in 4D-Nucleofector (Lonza). Cells were assayed 36 hours after transfection. HEK293 cells were co-transfected with renilla luciferase plasmid (Promega), Flag-MRGPRX2 or empty plasmid and one of the following plasmid: NFAT (pGL4 [NFAT-RE/ minP/luc2P]), CRE (pGL4 [CRE/minP/luc2P]), or SRE (pGL4 [luc2/Hygro] SRE) (Promega), using JetPrime reagent (Polyplus). All transfections were verified by western blot.

3.2.4 Bacterial culture and infection

A clinical strain of *S. aureus* (strain ID 10201) was used for all experiments in this study. Bacteria were grown in Luria-Bertani broth (BD) overnight at 37°C with shaking,

then diluted 1:10000 and allowed to reach log phase. The mouse dermonecrotic model was modified from skin infection models described previously (112, 113). Briefly, eight- to ten-week old mice were anesthetized by ketamine and xylazine and hair was removed from dorsal area using clipper and hair removal cream (Veet, Reckitt Benckiser) two days prior to infection. To induce dermonecrotic infection, mice were injected intradermally using a 25-gauge needle with 10^8 log-phase bacteria in 100 μ l phosphate buffered saline (PBS) complexed with dextran microbeads (Cytodex, Sigma) as carriers. The microbeads were used to ensure localized and uniform lesions for all dermonecrotic infections except for reinfection studies where lesion sizes were expected to be indicators of protective immunity development. The lesions were measured every other day beginning on day 1 by digital planimetry in which margins of a lesion were traced using acetate transparency films (Staples) and surface area was calculated using ImageJ upon digital rendering of the traces.

3.2.5 Peptides and antibiotics

Mastoparan (MW: 1479.9), originally isolated from the venom of social wasp *Vespula lewisii* (114), and mastoparan 17 (INLKAKAALAKKLL-NH₂, MW: 1494.9) (115) were obtained commercially at >90% purity from CPC Scientific (Sunnyvale, CA). Mastoparan 6I (MW: 1480) and Duke Mast F (MW: 2504.87) were custom-made by CPC scientific for us. The number of molecules used for all other peptides were adjusted to equimolar quantities to that of mastoparan. For the triple antibiotic cocktail, 100 units of

Polymyxin B, 8 units of Bacitracin and 100 µg of Neomycin (all from Sigma) were dissolved into 10 µl vehicle, based on the concentrations of active ingredients in Neosporin, an OTC antibiotic ointment.

3.2.6 Topical treatments

All topical treatments were applied with a pipette, using the pipette tip to facilitate spreading. Olive oil (10%) and DMSO were used to enable the active component(s) to stay in place and facilitate transdermal migration, respectively. In case of uninfected skins, the area of application was fixed to 2 cm² and marked with a surgical skin marker (Covidien) for observation or tissue collection.

3.2.7 Skin tissue collection

For CFU determination, whole infected area of the skin was harvested. For MPO assays and flow cytometry, skin tissues were harvested using a 8 mm biopsy punch (Miltex). For some assays with infected tissues, the diameter of the biopsy punch was aligned to the border of infection so that the harvested tissue includes equal portions of infected area and adjacent uninfected skin.

3.2.8 Enzymatic assays

For β-hexosaminidase assays, 2 x 10⁴ cells seeded in a 96-well plate were incubated in Tyrode's buffer (5.5 mM glucose, 0.5% BSA, 135 mM NaCl, 5mM KCl, 1 mM MgCl₂, 1.3 mM CaCl₂, pH 7.4) in presence of various concentrations of mastoparan or its analogs for 30 min at 37°C. Then, β-hexosaminidase activity in the supernatants

was measured as described previously (95). Briefly, supernatants or cell lysates (lysed by 0.1% Triton X-100) were incubated with the substrate p-nitrophenyl-N-acetyl- β -D-glucosaminide in 0.1 M sodium citrate (pH 4.5) for 1 hour at 37 °C. Then 0.1 M carbonate buffer (pH 10.0) was added and the product 4-p-nitrophenol was quantitated by measuring change in absorbance at 405 nm. The percentage degranulation was calculated from total β -hexosaminidase quantitated from cell lysates.

To determine skin myeloperoxidase (MPO) levels, skin tissues were collected in 500 μ l of potassium phosphate buffer (50 mM, pH 6.5) with 0.5% hexadecyltrimethylammonium bromide (HTAB), then homogenized using zirconia silica beads and an automatic homogenizer and lysed by multiple freeze-thaw cycles. To determine peritoneal MPO levels, mouse peritoneums were lavages using 5 ml PBS with 10 μ M EDTA. Cells from 1-2 ml lavage was then centrifuged and resuspended in 200 μ l HTAB buffer and lysed by multiple freeze thaw cycles. Then 20 μ l of the lysate supernatants were transferred in triplicate to a 96-well plate and 200 μ L of 50 mM potassium phosphate buffer (pH 6.0) with 0.167 mg/mL o-dianisidine dihydrochloride and 0.0005% H₂O₂ was added. The MPO activity was measured during 1 min interval three times at 450nm. MPO content was calculated as units per gram tissue or units per peritoneum using a standard curve, which was established using a recombinant MPO standard.

3.2.9 CFU determination

Infected skin tissues were harvested and homogenized in 0.1% Triton X-100 using zirconia silica beads for 3 cycles of 1.5 min each using an automatic homogenizer. Homogenates were serially diluted and plated on LB agar plates and the colonies were counted after overnight incubation at 37°C. The limit of detection was 25 CFU.

3.2.10 Immunofluorescence microscopy

Uninfected or infected skin tissues were fixed with 4% PFA and blocked and permeabilized with 0.3% triton X-100 in 1% BSA-PBS with 5% goat serum. Then the tissue samples were stained with anti-Ly-6G (1A8) and anti-CD31 antibodies at 4°C overnight, followed by incubation with AF647- and AF488-conjugated secondary antibodies and avidin-TRITC for 2 hours at room temperature. Stained whole skins were then mounted on a glass slide using prolog gold antifade mounting agent. Confocal images were taken by a Nikon ECLIPSE TE200 microscope.

3.2.11 Toluidine blue staining

To visualize granulated peritoneal MCs, peritoneal lavages were performed using 5 ml of PBS with 10 μ M EDTA. Cells from 200 μ l lavage was cytospun on glass slide, fixed with Carnoy's fixative, stained with 5 % toluidine blue, mounted on a glass slide and viewed under a bright-field microscope. Fully or partially granulated cells were scored as granulated MCs (22, 102). Ten random fields were counted for granulated MCs and averaged to determine granulated MCs per field for each

peritoneum. To visualize granulated MCs in skin tissues, skins from dorsum or ear pinnae were removed and fixed with Carnoy's fixative, stained with 5% toluidine blue, washed and whole skin mounted on a glass slide for visualization and counting under microscope.

3.2.12 Mason's trichrome staining

Skin tissues with scars were harvested 28 days post infection and flash-frozen in OCT compound. Fifteen micrometer sections were prepared from the frozen tissues and stained using a trichrome staining kit (Abcam) as per manufacturer's protocol. Scarred area was defined primarily by absence of hair follicles along with increased collagen density (116).

3.2.13 Flow cytometry

To quantitate peritoneal neutrophils by flow cytometry, cells from one ml lavage were washed with 1% bovine serum albumin (BSA) in PBS, incubated with normal serums and Fc receptor block (eBioscience) and stained with anti-Ly-6G-PE (clone 1A8) (BD) and anti-CD11b-APC (eBioscience) antibodies. To phenotype dendritic cells, skin tissues or popliteal lymph nodes were minced and incubated for 30 min in 100 U/ml of Collagenase A (Sigma) in HBSS containing FBS and DNase I. Single cell suspensions were prepared by straining the digested tissues through a 70 μ m cell straining filter (BD Biosciences). Cells were then washed with 1% BSA in PBS supplemented with FBS and 10 mM EDTA, blocked, and stained with fluorochrome-tagged antibodies to CD45,

CD64, IA/IE, CD11b, CD11c, CD207, CD301b and CD103. Dead cells were detected using Zombie Violet fixable viability kit. Cells stained with a single antibody and isotype controls were used as needed. To detect neutrophils in circulation, peripheral blood was collected in heparin tubes, stained with antibodies and RBCs were lysed using FACS lysing solution (BD). Upon fixation with PFA, stained cells were analyzed by BD FACSCalibur or FACSCanto II flow cytometer and FlowJo software version 10.1. Total cells in peritoneal lavages or lymph nodes were counted using a hemocytometer.

3.2.14 Western blot

Cells were lysed with Western lysis buffer (150 mM NaCl, 0.1% NP-40, 0.5% Sodium deoxycholate, 50 mM Tris, pH 8.0) supplemented with complete protease inhibitor cocktail (Roche) and total protein concentrations were determined by Bradford's assay. Cell lysates were immediately processed for analysis. 75 µg lysate was separated on 4–15% mini-PROTEAN® TGX™ precast gel and transferred to a nitrocellulose membrane in a semi-dry electrophoretic transfer cell (Bio-Rad). The membrane was blocked with 5% skimmed milk in TBST (50 mM Tris pH 8, 150 mM NaCl, 0.05% Tween 20) and incubated with primary antibody in the same blocking solution for 15 h at 4°C, followed by four washes in TBST. The membrane was then incubated with secondary antibody conjugated to horse radish peroxidase for 1 h at room temperature followed by washing in TBST. The protein bands were detected with ECL-prime luminol reagent (Pierce™, ThermoFisher Scientific) in a gel documentation

system (Chemi-Doc, BioRad). Antibody dilutions were: rabbit-anti-phospho PLC γ 1, anti-PLC γ 1, Flag (Cell signaling) and mouse-anti rabbit-HRP (Roche) at 1:1000; and anti-GAPDH-HRP (Proteintech) at 1:10,000.

3.2.15 MIC assay

The minimum inhibitory concentration (MIC) was assayed by the broth microdilution method according to procedures outlined by the Clinical and Laboratory Standards Institute (CLSI M07, 2012). Bacteria were grown in Mueller Hinton Broth (MHB, Becton Dickinson) to log phase. The initial inoculum was then adjusted to obtain 5×10^5 colony forming units (CFU) per ml and incubated in a microtiter plate with a two-fold serial dilution of the antimicrobial agent ranging from 2 mg/ml - 4 μ g/ml in a 100 μ l volume. Each concentration was tested in triplicate and the microtiter plate was incubated at 37°C overnight. The MIC was taken as the lowest concentration of the antibacterial agent that completely inhibits visible bacterial growth.

3.2.16 Luciferase reporter assay

After 36 hours post transfection, HEK293 cells were stimulated with mastoparan (0.25 and 0.5 μ g/ml) or left unstimulated for 4-6 hours. The cell lysates were measured for firefly luciferase activities specific to GPCR response elements and constitutive renilla luciferase activity using Dual-Glo luciferase assay kits (Promega) according to the manufacturer's instructions. The total fold induction was calculated as fold of induction = firefly RLU_{induced} / renilla firefly RLU.

3.2.17 Cytotoxicity assay

Cytotoxicity of mastoparan and related peptides was determined using the CytoTox 96® Non-Radioactive Cytotoxicity Assay kit (Promega) according to manufacturer's protocol. Briefly, 2×10^4 L929 fibroblast cells (ATCC® CCL-1™) were incubated with a test peptide for 4 hours and release of lactose dehydrogenase (LDH) in culture supernatant was measured. The LDH released spontaneously by cells incubated with media alone was subtracted from all data.

3.2.18 TLR/NLR ligand screening assay

Stimulation of Toll-Like Receptor (TLR) and NOD-Like Receptor (NLR) was tested using a PRR screening service provided by Invivogen (San Diego, CA). In this assay, PRR activation was determined by assessing NF- κ B activation in HEK293 reporter cells expressing a given TLR or NLR. NF- κ B activity was assessed by measurement of NF- κ B-dependent secreted embryonic alkaline phosphatase (SEAP) at 650nm. A mastoparan peptide was tested at 50 μ g/ml concentration on seven different mouse TLRs (TLR2, 3, 4, 5, 7, 8 and 9) and mouse NOD1 and NOD2. Following ligands were used as positive controls for corresponding receptors; TLR2: HKLM (heat-killed *Listeria monocytogenes*) at 10^8 cells/ml; TLR3: Poly(I:C) at 1 μ g/ml; TLR4: *E. coli* K12 LPS at 100 ng/ml; TLR5: *S. Typhimurium* flagellin at 100 ng/ml; TLR7: CL097 at 1 μ g/ml; TLR8: CL075 at 10 μ g/ml + Poly(dT) 10 μ M; TLR9: CpG ODN 1826 at 100 ng/ml; NOD1: C12-iE-DAP at 1 μ g/ml; NOD2: L18-MDP at 100 ng/ml.

3.2.19 Depletion of neutrophils

Mice were treated intraperitoneally with 500 µg of anti-Ly6G (1A8) or control antibodies (2A3) in 100 µl volume 24 hours post infection with *S. aureus*. Peripheral blood was collected 48 hours post injection of the antibodies to confirm depletion of neutrophils. Neutrophils were also quantitated in infected or uninfected skin by an MPO assay as described above.

3.2.20 Peptide design for structure-function analysis

Mastoparan 17 is a known analog of mastoparan which has neither MC-degranulating (115) nor antimicrobial activity (MIC against *S. aureus* >2000 µg/ml). Since Mastoparan 17 has substitutions at position 6 and 13 (INLKAKAAALAKKLL-NH₂), we first generated analogs with one substitution (either position 6 or position 13) attempted to determine which position is more critical. While MP-13L peptide (leucine in place of isoleucine at position 13) retained both antimicrobial and MC-degranulating activities, MP-6K (lysine in place of leucine at position 13) completely lost them (data not shown). Finding position 6 to be critical, we then synthesized a series of mastoparan analogs with various single amino acid substitutions at this position with an aim to obtain a peptide with no degranulating but comparable antimicrobial activity. When the degranulating capacities of these peptide analogs were compared to mastoparan, MP-6W (tryptophan at position 6) was slightly better (data not shown), degranulation by MP-6I (isoleucine at position 6) was significantly reduced but still detectable; and most

others had no detectable activity (data not shown). On the other hand, when the analogs were tested for MIC against *S. aureus*, only MP-6I retained antimicrobial activity similar to mastoparan. Other substitutions tested either reduced or completely lost antimicrobial activity (data not shown). Therefore MP-6I was chosen as the mastoparan analog with no degranulating but similar antimicrobial activity. Single amino acid substitutions did not yield to the alternate mastoparan analog which has no antimicrobial activity but similar MC-degranulating activity. Therefore, we took another strategy to generate a series of completely unrelated MCA peptides which were rich in tryptophans and arginines and devoid of any antimicrobial activity. It has previously been demonstrated that while lysines are critical to antimicrobial capacity pertaining to membrane disruption, arginines facilitate interaction with membranes but do not disrupt them (117, 118). In *Vespula* mastoparan there is no arginine, however, there are single or multiple arginines present in human cationic peptide MCAs such as kallidin, LL-37 or substance P. Therefore, we developed multiple mastoparan-inspired peptides where lysines were replaced with arginines to nullify the membrane disrupting activity. The asparagine at position 2 was also replaced with arginine to increase cationic property of the peptide. Other amino acids were replaced with tryptophans to provide ample motifs close to tetrahydroisoquinoline (THIQ) (which has recently been speculated to be the motif critical for MRGPRX2 activation (107)) as well as to increase hydrophobicity. These modifications resulted in various novel peptides including Duke

Mast F (Mastoparan, INLKALAALAKKIL→ INLRALAALARRIL→ IRLRALAALARRIL→ WRWRWWWWWWRRWW). Once tested for MC-degranulating and antimicrobial properties, Duke Mast F was selected as the peptide with similar degranulating but no antimicrobial activity.

3.2.21 Statistical analyses

Statistical significance was determined by unpaired two-tailed Student's t tests where only two groups existed, or by one-way ANOVA with Dunnett's or Tukey's post test. Differences between groups were considered significant at $p < 0.05$. Analyses were performed using GraphPad Prism 5.0 and Microsoft Excel 2010.

3.3 Results

3.3.1 *S. aureus* dermonecrotic skin infection model

Although MCs have been reported to mediate the clearance of various pathogenic bacteria (93), their role in *S. aureus*-mediated skin infections is not known. For our studies, we chose a clinical isolate of *S. aureus* (strain ID 10201) and utilized a dermonecrosis model of infection as the progression of infection and associated healing process in this model takes place over a period of days, allowing us to readily assess the kinetics of bacterial clearance, immune cell recruitment and the healing process (112, 113). We determined that the infectious dose of *S. aureus* 10201 when complexed with cytodex beads required to consistently cause stable and localized dermal infection was 10^8 CFU. Upon injection of this dose into the lower back dermis of control wild type (WT) mice, the site becomes inflamed (swells and turns whitish, forming abscesses) within hours which mimics closed cutaneous infection (Figure 19A).

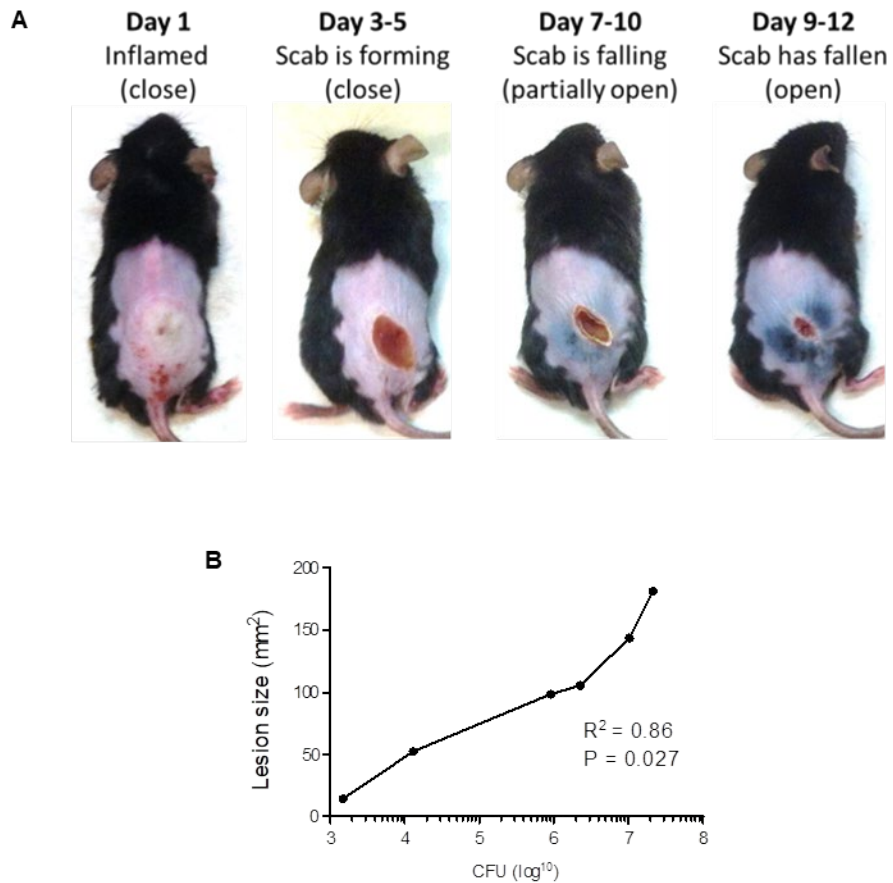


Figure 19: Mouse dermonecrotic model. (A) Progression of infection. (B) Correlation between CFU and lesion size. Skin samples were collected at various days post infection. R indicates the Person's correlation coefficient.

After 24 h the abscess reduces in size but due to the action of staphylococcal toxin A and other virulence factors, the abscess become necrotic. Around day 3, the necrotic region begins to turn into a scab. It is noteworthy that at this stage, the contraction apparatus of the skin is highly active, reducing the area of infection. Thereafter, the scab starts to detach from the surrounding skin, resembling a semi-open lesion often seen in surgical site infections. As the scab completely detaches from the

lesion after a week, the lesion resembles an infected open wound such as a laceration. A new scab soon forms and covers the wound and this cycle of scabbing and wound healing continues until the infection finally resolves. Depending on the initial lesion size, the time of resolution of the infected wound can be as early as 14 days and as late as day 20. There is a significant amount of residual scar tissue at the original site of infection where no fur grows. Over the course of infection, the lesion sizes correlate highly with bacterial burden (Figure 19B).

3.3.2 Connective tissue mast cells control *S. aureus* skin infection

To determine the innate role of MCs during skin *S. aureus* infections, we employed a MC-deficient mouse model (*Mcpt5-Cre⁺iDTR⁺* mice) in which CTMCs, the MC type that populates skin, could selectively be depleted (119) (Figure 20). We induced a localized dermonecrotic infection by intradermal injection of 10^8 bacteria into the dorso-caudal area and observed that MC-depleted mice had significantly more bacterial burden by 24 hours post infection compared to MC-sufficient littermate controls (Figure 21A). The lesion sizes were also two-fold larger in MC-depleted mice, as measured on day 1 post infection (Figure 21B). As expected, the larger initial lesions in absence of MCs resulted in a much slower resolution of infection (Figure 21B).

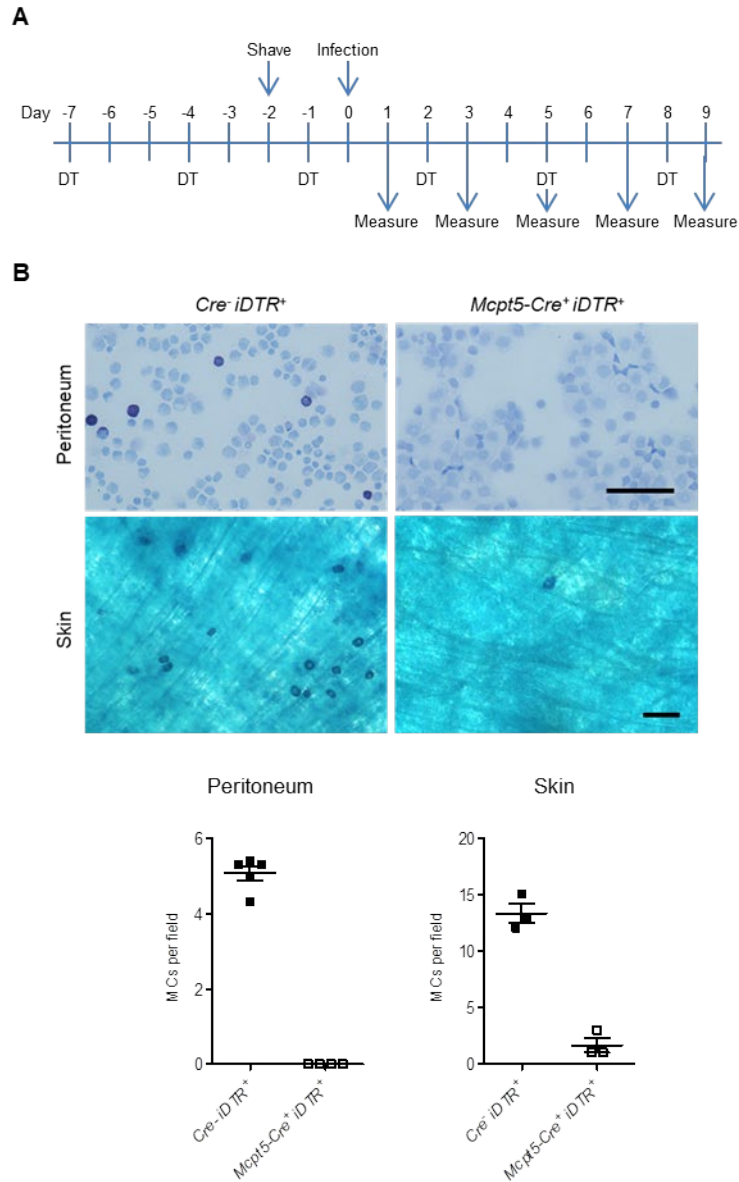


Figure 20: Depletion of CTMCs. (A) Schematic plan for CTMC depletion, dermonecrotic infection and lesion measurement. Depletion of CTMCs was achieved by treating *Mcpt5-Cre⁺iDTR⁺* mice or littermate controls (*Cre-iDTR⁺*) intraperitoneally and subcutaneously with diphtheria toxin (DT) every 3rd day for seven days. (B) Representative images of granulated mast cells stained with toluidine blue in peritoneal lavage or dorsal skin whole mount 24 hours after 3rd dose of DT. Scale bar 10 μ m. Graphs at the bottom show depletion of MCs in *Mcpt5-Cre⁺iDTR⁺* mice compared to control (*Cre-iDTR⁺*) mice.

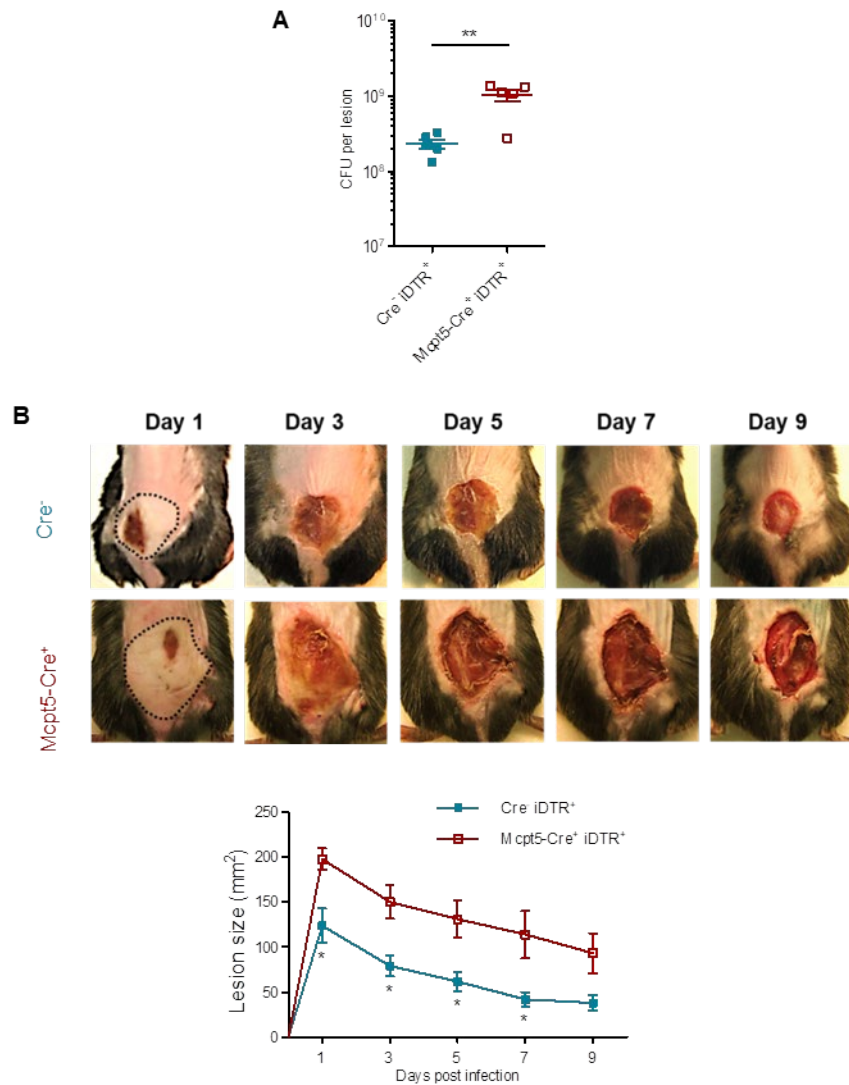


Figure 21: CTMCs are critical for controlling skin infections. (A) Quantification of bacteria in the infected skin tissues at 24 hours post infection (n = 5). Colony forming units (CFUs) were determined by plating on LB agar. (B) Representative images of skin lesions taken on indicated days post infection. Black lines delineate area of infection on day 1. The graph at the bottom represents size of skin lesions in different mouse groups measured on indicated days and area calculated using ImageJ (n = 5).

3.3.2 MC-mediated infection control is via neutrophil recruitment

Since neutrophils are the first responders during bacterial infections at barrier sites, we asked whether MC-dependent infection control is linked neutrophil influx. We observed that MC-depleted mice had significantly less neutrophil influx at 4 hours post infection (Figure 22A).

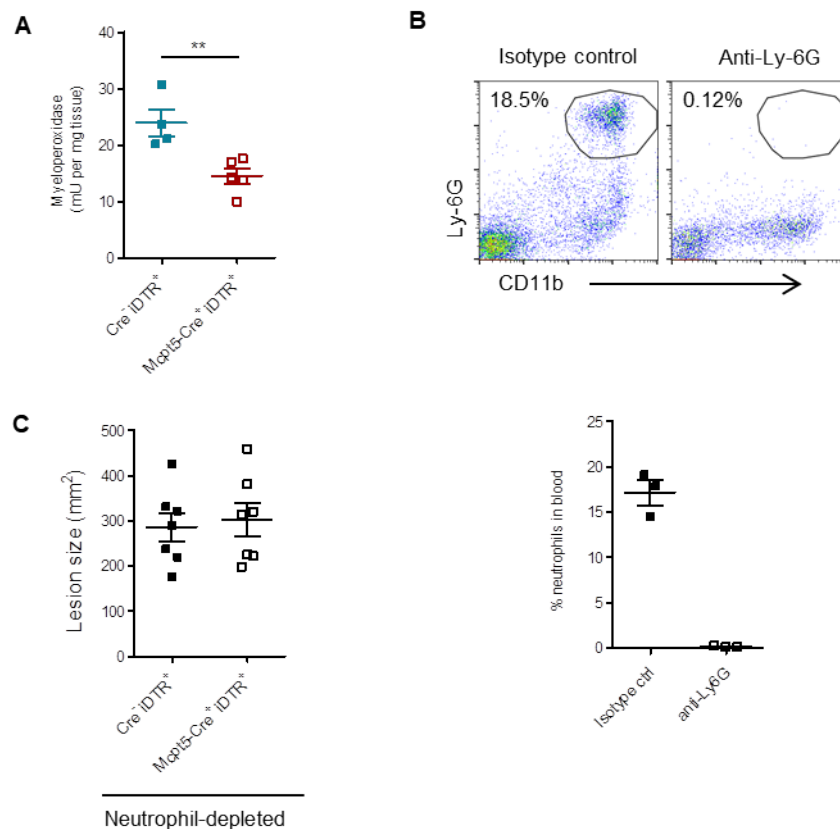


Figure 22: CTMCs' control of skin infection is neutrophil-dependent. (A) Neutrophil recruitment at 4 hours post intradermal infection of MC-sufficient (*Cre*⁻) or MC-deficient (*Cre*⁺) mice with 10⁸ *S. aureus*, assessed by myeloperoxidase assay (n = 4-5). (B) Representative flow cytometry plot and graph (at the bottom) showing almost complete depletion of CD11b⁺Ly6G⁺ neutrophils in blood 48 hours post intraperitoneal injection with 500 μg anti-ly6G antibody. (C) Initial lesion sizes in neutrophil-depleted MC-sufficient (*Cre*⁻) or neutrophil-depleted MC-deficient (*Cre*⁺) mice, measured 24 hours post infection with *S. aureus* (n = 7). Note that initial lesions in neutrophil-depleted

mice were larger compared to those in neutrophil-sufficient mice shown in Figure 21B. Data are representative of two independent experiments.

To further confirm the importance of neutrophils, we depleted both MC-sufficient and -deficient mice of neutrophils prior to infection (Figure 22B). Interestingly, the increase of lesion size in MC-depleted mice was no longer observed in absence of neutrophils (Figure 22C), indicating that the protective role of CTMCs were primarily via neutrophils. Cumulatively, these data demonstrate that CTMCs play a major role in neutrophil recruitment at the very early stage of skin infection which is crucial in limiting the infection.

3.3.3 MCA activates CTMC via MRGPRX2 receptor

Following the identification of CTMCs as a critical recruiter of neutrophils during skin infections, we next sought to establish if receptor-specific activation of these cells by an MCA would also result in local neutrophil recruitment, even in the absence of an infection. However, before undertaking this study, it was important to establish the receptor-binding specificity and distinct MC-signaling activity of the MCA employed. Mastoparan is an MCA, originally isolated from wasp venom (114) and reported to activate both human and murine MCs via the MRGPRX2 receptor (107). We examined the *in vitro* capacity of mastoparan to mediate degranulation of human and murine MC lines (ROSA and MC/9, respectively) by measuring extracellular release of β -hexosaminidase, a component of MC granules. Mastoparan evoked degranulation in a dose-dependent manner in both human and murine MC lines (Figure 23A). As a

negative control, we exposed mastoparan to another well-known MC line rat basophilic leukemia cell line (RBL-2H3) which, however, does not to express MRGPRX2 receptors (120).

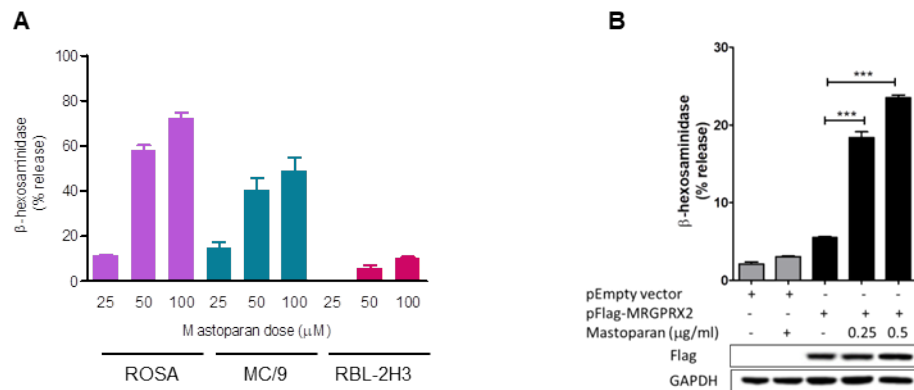


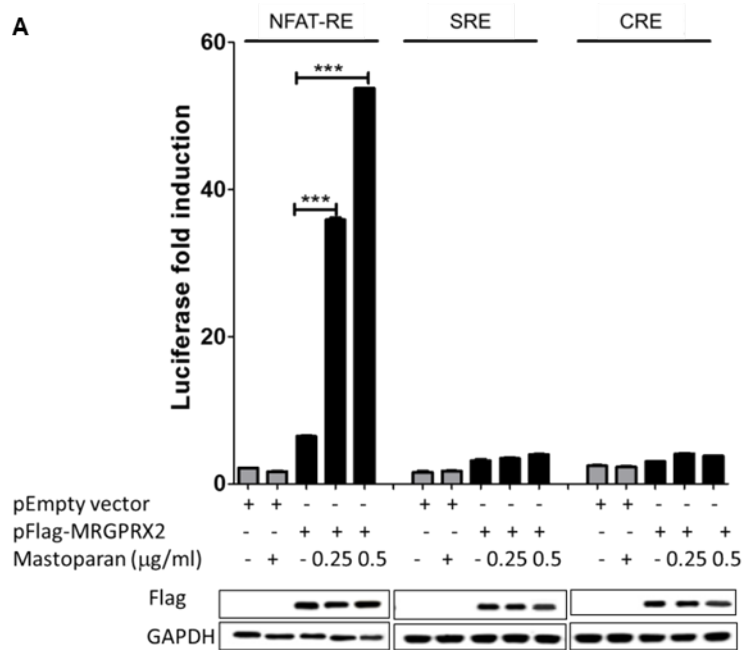
Figure 23: MRGPRX2-dependent degranulation by mastoparan. (A)

Degranulation of a human MC line (ROSA), a murine CTMC line (MC/9) and a rat MC-like cell line (RBL-2H3) *in vitro* expressed as β -hexosaminidase release by increasing concentrations of mastoparan. (B) Degranulation of RBL-2H3 cells transfected with expression construct encoding MRGPRX2 or empty vector followed by mastoparan stimulation. Immunoblots show the introduction of MRGPRX2 in the cells and GAPDH as a loading control.

As expected, the degranulation responses evoked by mastoparan in RBL-2H3 cells were minimal even at high dosages (Figure 23A). To further establish the receptor specificity of mastoparan, we transfected the RBL-2H3 cells with human MRGPRX2 receptor and examined their degranulation response to the MCA. Indeed, we observed significant degranulation responses even at very low concentrations (0.25 μ g/ml or 0.17 μ M) but not in the mock-transfected cells (Figure 23B).

Since little regarding the downstream G protein signaling pathways triggered by mastoparan-mediated activation of MRGPRX2 on MCs is known, we investigated this

question. Depending on the activating ligand, G protein-coupled receptors (GPCRs) such as MRGPRX2, can interact with multiple G_{α} subunits, to initiate distinct signaling pathways (121-123). To identify which specific G_{α} pathways are activated by mastoparan, we employed a reporter gene assay involving HEK293 cells which do not endogenously express MRGPRX2 but possess a full complement of G protein-directed signaling components. We transfected these cells with empty plasmids or plasmids encoding human MRGPRX2 along with plasmids encoding a luciferase-conjugated response element (RE) known to be activated by a particular G_{α} subunit: cAMP response element (CRE) for G_{α_s} , nuclear factor of activated T cell response element (NFAT-RE) for G_{α_q} , or serum response element (SRE) for $G_{i/o}$. Upon incubation with mastoparan, we observed specific activation of NFAT-RE but not SRE-RE or CRE (Figure 24A), indicating that mastoparan specifically activates G_{α_q} , the subunit known to activate phospholipase C (PLC). Indeed, we detected MRGPRX2-specific phosphorylation of PLC γ 1 (Figure 24B), which in turn results in inositol triphosphate (IP3) production, the critical second messenger that mobilizes Ca^{2+} required for MC degranulation (124).



B

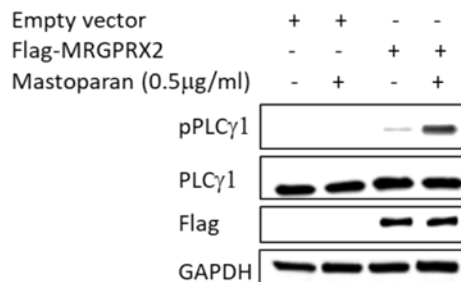


Figure 24: Mastoparan activates $G_{\alpha q}$ axis and PLC γ 1. (A) Luciferase reporter activities triggered by mastoparan in mock- or MRGPRX2-transfected HEK293 cells coexpressing NFAT-RE, SRE or CRE (representing $G_{\alpha q}$, $G_{i/o}$ or $G_{\alpha s}$ pathway, respectively). Immunoblots show the MRGPRX2 expression and loading control GAPDH. (B) Immunoblot analysis of lysates prepared from RBL-2H3 cells (mock- or MRGPRX2-transfected) stimulated with mastoparan for 5 min and probed for phospho- PLC γ 1, PLC γ 1, Flag and GAPDH. Data are presented as the mean of triplicate values in one experiment, representative of at least two independent experiments.

Collectively, these data indicate that mastoparan activates a single pathway downstream to MRGPRX2 which specifically triggers MC degranulation. To investigate if mastoparan could activate other receptors, especially PRRs such as Toll-like receptors (TLRs) or NOD-like receptors (NLRs) commonly found in both immunocytes (including MCs) and non-immune cells, we conducted a commercial TLR/NLR screening assay (see Methods). We observed that mastoparan did not activate any of the tested TLRs or NLRs (Figure 25). So far, our data indicate that mastoparan's action is highly restricted to a single MC-specific receptor and downstream pathway, indicating the potential of MCAs as selective immune-modulators.

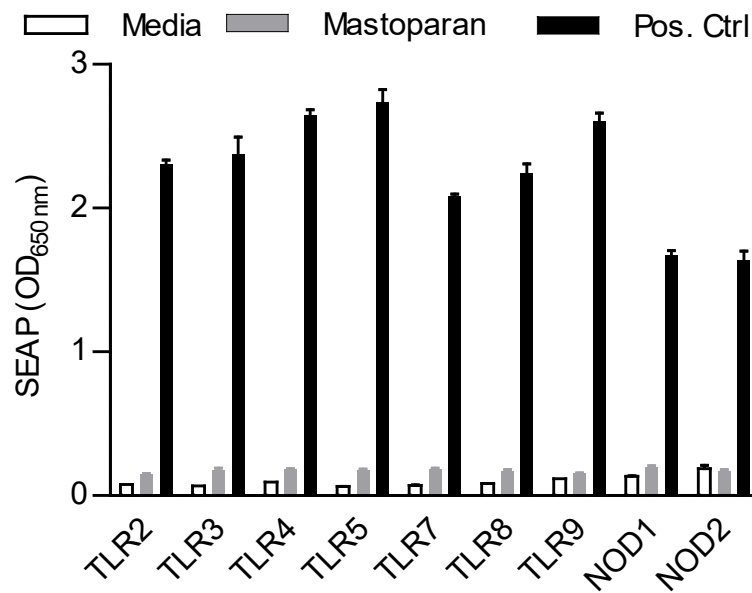


Figure 25: Receptor-specificity of mastoparan. Quantification of activation of TLRs or NLRs by mastoparan (500 μ g/ml) or positive controls specific to each receptor.

3.3.4 CTMC activation by mastoparan recruits neutrophils *in vivo*

To investigate if mastoparan-triggered activation of MCs were associated with the release of immune-mediators known to influence neutrophil recruitment, we examined various cytokines in human MC line LAD2 by a multiplex assay.

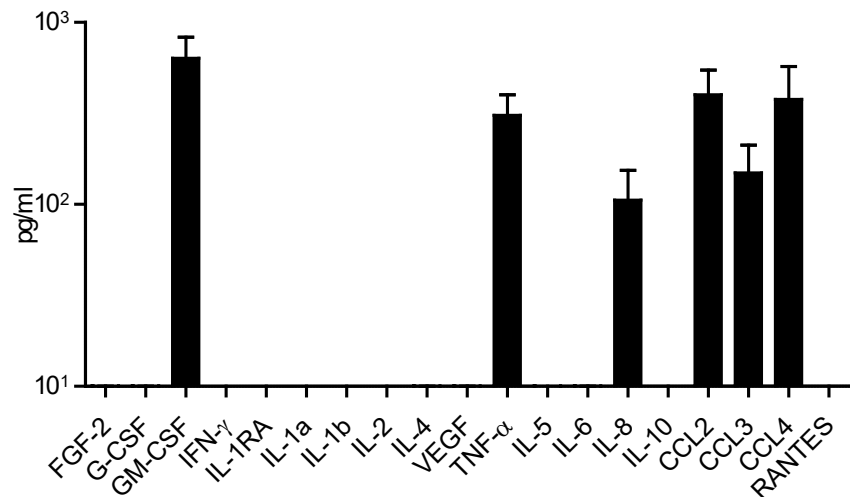


Figure 26: Cytokines released from mast cells upon activation by mastoparan. Cytokines (prestored or *de novo* synthesized) secreted by a human MC line (LAD2) upon stimulation with mastoparan (25 μ M) for 20 hours, measured by a Luminex multiplex fluorescent immunoassay. Data represent mean of triplicate values in a single experiment.

The cytokines that released from human MCs specifically upon mastoparan treatment include TNF, GM-CSF, IL-8 and CCL2 (MCP-1) (Figure 26). While TNF has been shown to mediate MC-dependent neutrophil recruitment following infection (53, 98), the other mediators are known to play critical roles in both recruitment and activation of neutrophils in different inflammatory states (125-129).

Upon determining the capacity of mastoparan to trigger release of neutrophil-recruiting cytokines *in vitro*, we investigated mastoparan's capacity to activate MCs and mediate neutrophil recruitment *in vivo*. Since the mouse peritoneum is rich in CTMCs and relatively easy to assess for MC degranulation and leukocyte recruitment, we injected increasing doses of mastoparan into the peritoneal cavities of mice to determine the minimum concentration of mastoparan required for maximum MC degranulation. Using toluidine blue which metachromatically binds to heparin in MC granules, we could distinguish granulated MCs from other cells in peritoneal lavage employing brightfield microscopy and were able to readily ascertain their degree of degranulation (22, 102) (Figure 27A). Upon administration of concentrations ranging from 0.2 mg to 8 mg per kg body weight, we observed dose-dependent degranulation until the 2 mg/kg dose when maximum degranulation was attained (Figure 27B). When we examined the effect of Mastoparan 17, an inactive analog of mastoparan (115), we did not detect any degranulation at a dose equimolar to 2 mg/kg mastoparan.

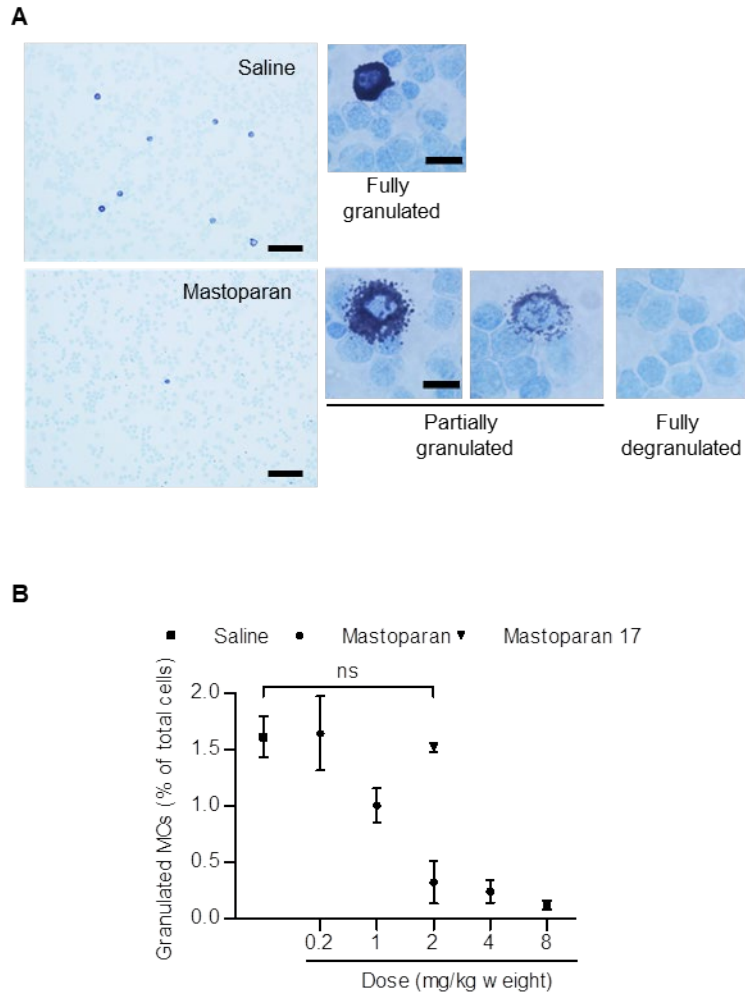


Figure 27: Dose-dependent degranulation of mast cells *in vivo* by mastoparan.

(A) Detection of granulated MCs by toluidine blue staining. Representative images of toluidine blue stained mouse peritoneal cells collected 30 min after intraperitoneal injection of mastoparan (2 mg/kg) or saline. Scale bar 50 μ m. Panels on the right depict higher magnification of MCs, scale bar 10 μ m. Note that in MCA-treated mice, MCs in various stages of degranulation can be detected. (B) Quantification of granulated MCs in the peritoneal lavage of mice 30 min after intraperitoneal (i.p.) injection with various doses of mastoparan (0.2 – 8 mg/kg bodyweight; n = 3) or controls.

Next, we investigated if mastoparan-mediated MC activation in the peritoneum was accompanied by a neutrophil influx. We treated mice intraperitoneally with 2

mg/kg of mastoparan and 2 hours thereafter, collected the peritoneal lavage. Assessment of the lavages by flow cytometry revealed substantial recruitment of neutrophils into the peritoneal cavity following administration of mastoparan but not its inactive counterpart (Figure 28A).

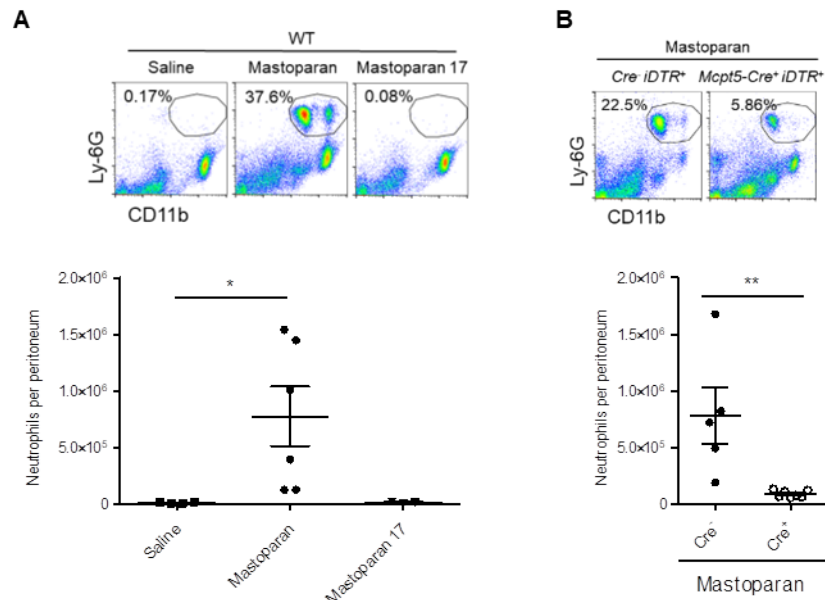


Figure 28: Mastoparan-mediated neutrophil recruitment. (A) Numbers of neutrophils per peritoneum 2 hours post i.p. injection with saline or 2 mg/kg bodyweight of mastoparan. Data represent two independent experiments (n = 3-6). Flow cytometry plots represent percentages of CD11b⁺Ly6G⁺ neutrophils in peritoneum of each group of mice. (B) Numbers of neutrophils per peritoneum 2 hours post i.p. injection 2 mg/kg bodyweight of mastoparan. Flow cytometry plots represent percentages of neutrophils in peritoneum of MC-sufficient or MC-deficient mice. Data represent two independent experiments (n = 5-6).

To confirm that the neutrophil recruitment by mastoparan was dependent on presence of MCs and not by its effect on some other cell type, we assessed neutrophil recruitment in CTMC-depleted mice. In contrast to *Cre*⁻*iDTR*⁺ control mice, neutrophil

influx upon mastoparan injection was minimal in MC-depleted *Mcpt5-Cre⁺iDTR⁺* mice (Figure 28B). Cumulatively, these data show that mastoparan specifically activates MCs via the MRGPRX2 receptor and that this results in MC degranulation which, *in vivo*, can result in significant neutrophil recruitment even in the absence of infection.

3.3.5 Topical application of MCA degranulates skin MCs and recruit neutrophils

We found that it was necessary to dissolve mastoparan in a skin permeating cocktail (vehicle) comprising of dimethyl sulfoxide (DMSO) and olive oil in order to achieve penetrance of the *stratum corneum* with adequate amounts of mastoparan. Examination of high-magnification images of mouse skin cross-sections upon topical application of mastoparan-FITC revealed that the peptide would readily penetrate the epidermis and reach the dermis (Figure 29), where skin MCs reside.

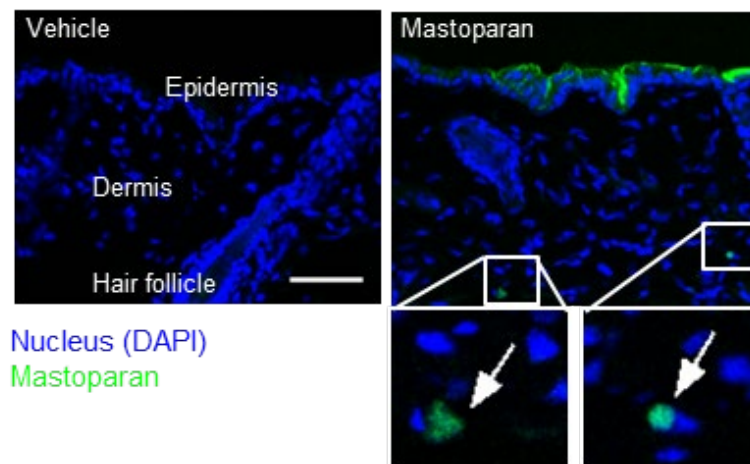


Figure 29: (A) Penetration of mastoparan into dermis. Representative images of mouse dorsal skin cross sections collected at 2 hours post topical application of 10 μ g mastoparan-FITC or vehicle, n = 2-3. Arrows point to the fluorescent peptide detected within dermis. Scale bar 50 μ m.

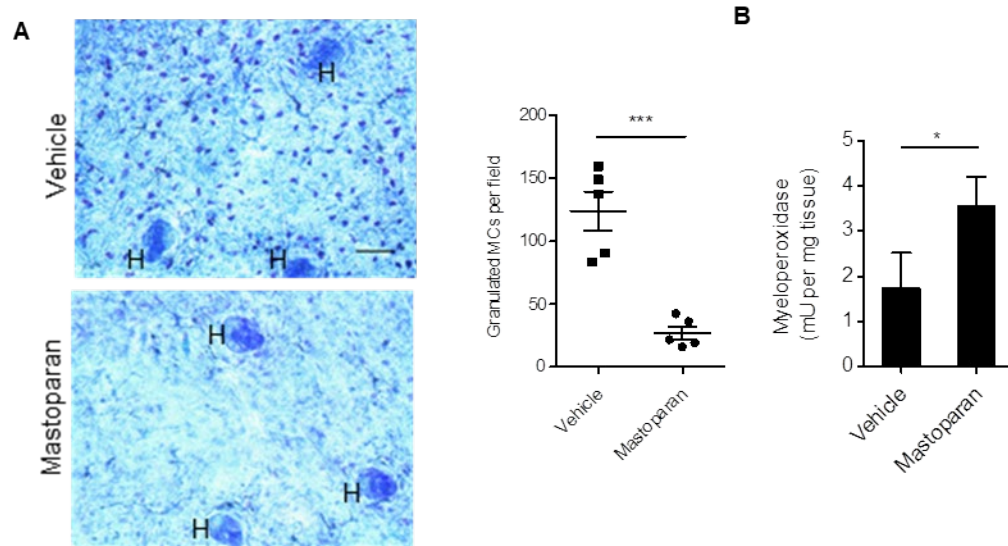


Figure 30: MC degranulation by topical mastoparan. (A) Representative whole mount images showing granulated MCs in vehicle- and mastoparan-treated ear tissue, 2 hours post treatment. 'H' indicates hair follicle. Scale bar 50 μm . Graph shows quantification of granulated MCs in each treatment group, $n = 5$. (B) Quantification of neutrophils in dorsal skin of each treatment group employing myeloperoxidase assay, 6 hours post treatment ($n = 3$).

The numbers of granulated MCs were significantly reduced in the skin treated with 10 μl of 675 μM mastoparan (equal to 10 μg) compared to the skin treated with vehicle (Figure 30A), suggesting that topical application of mastoparan results in activation of skin MCs. The recruitment of neutrophils into the dermis upon topical application of mastoparan was detectable but minimal (Figure 30B), presumably in absence of additional cues from an infection or injury, most of the recruited neutrophils immediately left the skin by reverse migration (130). Mice were monitored for local adverse events such as irritation, inflammation or mutilation of the treatment site after repeated daily treatments of the skin by mastoparan. Signs for systemic adverse events

were also monitored by observing for any changes in body temperature as well as behavior (e.g., distress, discomfort, and activity level). We did not observe any local or systemic adverse effects in the mice, indicating that the topical application of low-dose MCA does not cause any significant local or systemic adverse effects.

3.3.6 MCA -mediated neutrophil recruitment accelerates bacterial clearance in the skin.

Next, we proceeded to investigate the impact of mastoparan treatment in our dermonecrotic model of *S. aureus* skin infection. Beginning 12 hours post infection when a palpable swelling at the site of infection had formed, mice were treated on and around the infected site with mastoparan or vehicle every 12 hours for two weeks. To visualize MC degranulation and neutrophil recruitment into the dermis adjacent to the lesion, we sacrificed a subset of mice on day 5 post infection. Since avidin binds to heparin, we employed avidin conjugated with a fluorochrome to specifically visualize mast cell granules by confocal microscopy of whole skin mounts. We observed that many MCs remained granulated during the course of infection in the vehicle-treated mice and there was a limited recruitment of neutrophils (Figure 31, bottom left). On the other hand, in mastoparan-treated mice almost no granulated mast cells were detected whereas numerous neutrophils were readily detectable (Figure 31, bottom right).

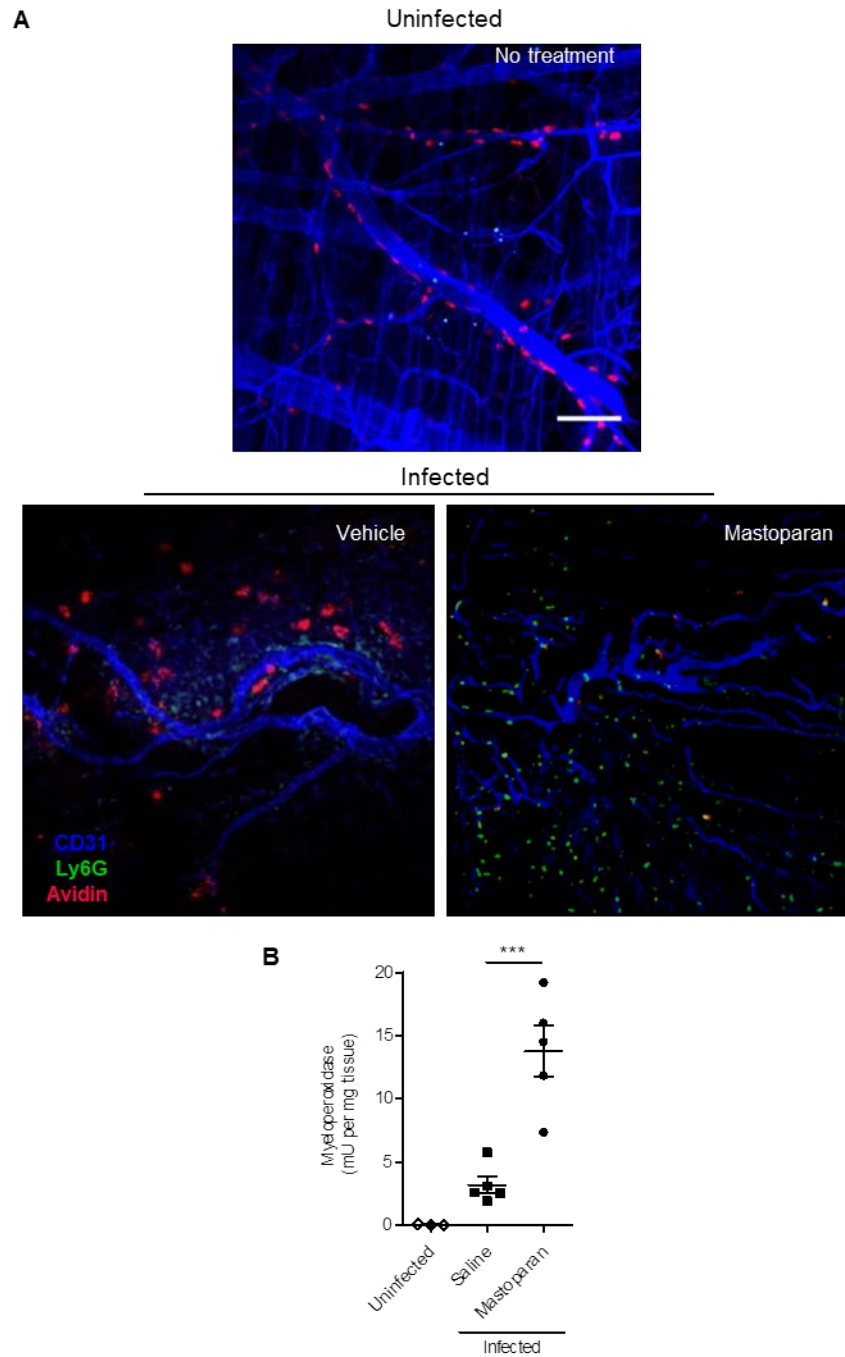


Figure 31: Neutrophil recruitment by mastoparan during *S. aureus* infection.
 (A) Representative whole mount of the dorsal skin following no infection or treatment (top panel), intradermal infection (10^8 *S. aureus*) and topical treatment with vehicle (bottom left panel) or mastoparan (bottom right panel). The infected mice were treated

twice daily and sacrificed 4 hours post treatment on day 5, skin tissues adjacent to scabs were stained for avidin (red), Ly6G (green) and CD31 (blue). Notice that in the mastoparan-treated tissue, MCs are not visible because they are degranulated and numerous neutrophils appear in the image. Scale bar 100 μm . (B) Quantification of neutrophils (myeloperoxidase) in the skin of each group of mice 4 hours post treatment on day 7 (n = 3-5).

To quantitate neutrophil influx, another subset of mice was sacrificed on day 7, approximately halfway to the resolution of infection. Using myeloperoxidase (MPO) assay, we observed a significant increase of neutrophil recruitment in infected mice treated with mastoparan compared to vehicle (Figure 31B). These data indicated that exogenous activation of local MCs by mastoparan recruited additional neutrophils throughout the course of infection. As a result, the bacterial burden in mastoparan-treated mice was trending lower than that in vehicle-treated mice by day 5 and became significantly lower by day 10 and continued to remain so till end of the study period (Figure 32A). In parallel with the reduced bacterial number, the lesion size of the mastoparan-treated animals was significantly smaller than the other group beginning from day 5 (Figure 32B). We included an additional control group of mice which was infected and then treated with 10 μl of a cocktail of three over-the-counter antibiotics commonly used for topical treatment of skin infections (Neomycin/polymyxin B/bacitracin). The rate of healing induced by mastoparan was very similar to that mediated by the antibiotics (Figure 33A). Notably, mastoparan-mediated control in lesion size and bacterial burden was completely abolished in neutrophil-depleted mice

(Figure 33, B-C), indicating that mastoparan's therapeutic effects were indeed neutrophil-dependent.

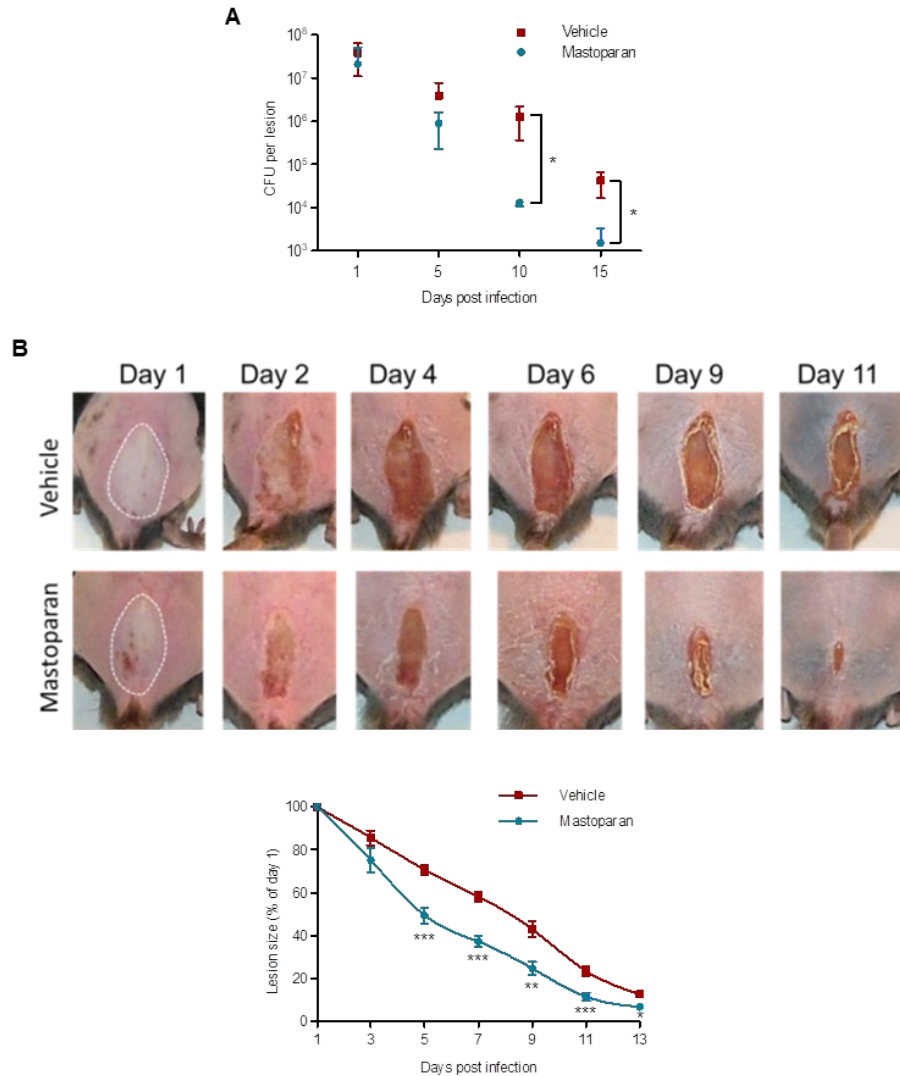


Figure 32: Mastoparan treatment accelerates bacterial clearance. (A) Quantification of bacteria in the infected skin tissues at different time points post infection (n = 4-5). (B) Representative images of skin lesions taken on indicated days post infection and treatment. White lines delineate area of infection on day 1. Graph at the bottom represents size of skin lesions in different treatment groups measured on indicated days and area calculated using ImageJ (n = 10). Data are representative of at least two independent experiments.

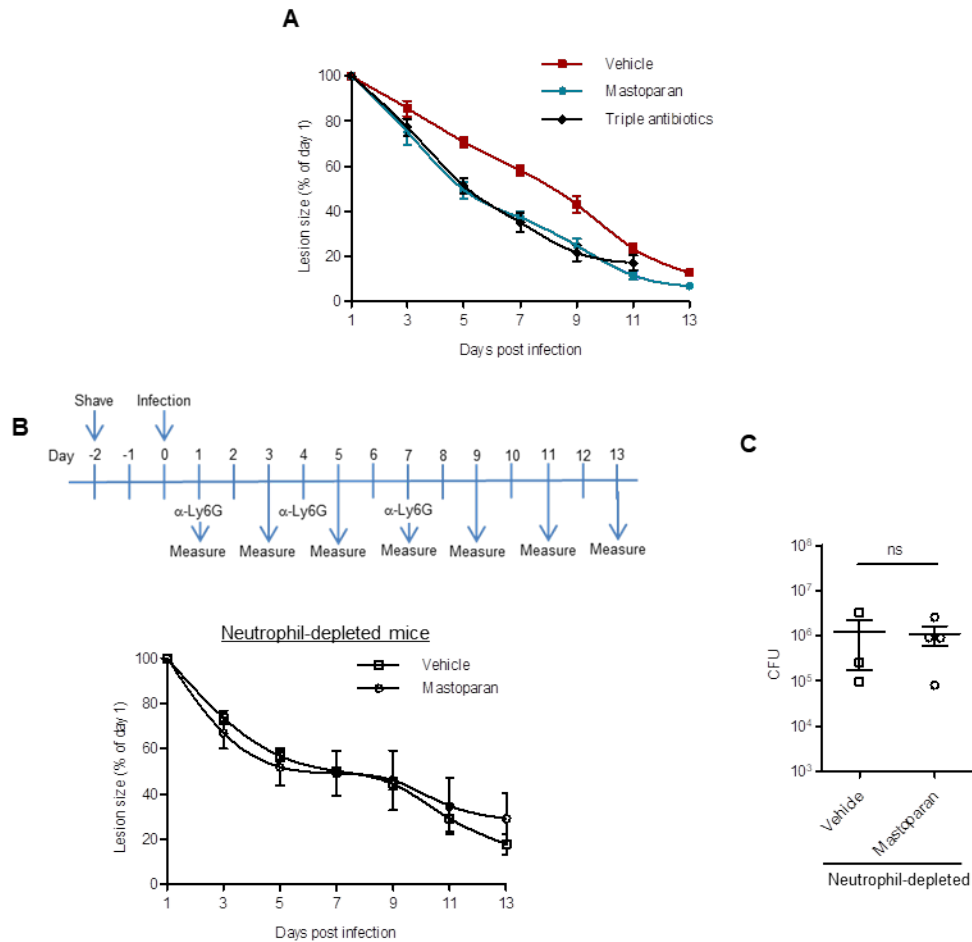


Figure 33: Efficacy and neutrophil-dependency of mastoparan's antibacterial effect. (A) Lesion size of mice infected with *S. aureus* and treated with triple antibiotic (n = 18). Data of mastoparan and vehicle treatment from Fig. 3G were superimposed for comparison. (B) Schematic showing experimental plan and graph depicting mean lesion size at indicated time points post infection of neutrophil-depleted mice and treatment with vehicle or mastoparan (n = 5). (C) bacterial numbers (CFUs) in the infected skin tissues day 15 post infection.

To summarize, topical treatment with mastoparan significantly accelerated bacterial clearance and reduction of lesion size by enhancing neutrophil recruitment, indicating its strong therapeutic effect on resolution of local infection.

3.3.7 Therapeutic effect of mastoparan is specific to MC activation.

Next, we investigated the specificity of MCA-mediated therapeutic effects by multiple approaches. First, employing the previously described CTMC-depletion model, we asked if these cells are essential for the therapeutic effect observed during skin infection. When we treated MC-depleted mice with mastoparan, it failed to improve healing (Figure 34) compared to vehicle treatment, indicating that the therapeutic effects of mastoparan require CTMCs.

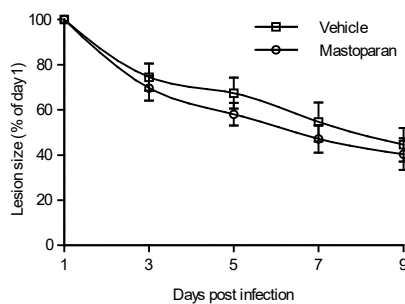


Figure 34: Mastoparan's therapeutic effect requires CTMCs. Quantification of lesion sizes at indicated days post infection of MC-depleted mice with vehicle or mastoparan treatment (n = 6-7). Note that healing rates in MC-depleted mice were slower than that in MC-sufficient mice due to larger initial lesions. Data represent two independent experiments.

A common feature of many peptide and non-peptide MCAs is the direct antimicrobial capacity, attributed to their cationic amphiphilic nature which allows the MCA to bind and disrupt negatively charged bacterial membranes (131-133). Since being a cationic peptide, mastoparan can also lyse bacterial membrane, we attempted to ascertain if part of the therapeutic effects of mastoparan was related to its direct antibacterial activity. We made various alterations to the amino acids of mastoparan to

generate a mastoparan derivative that retained its antimicrobial activities but lost its MC-degranulating capacity.

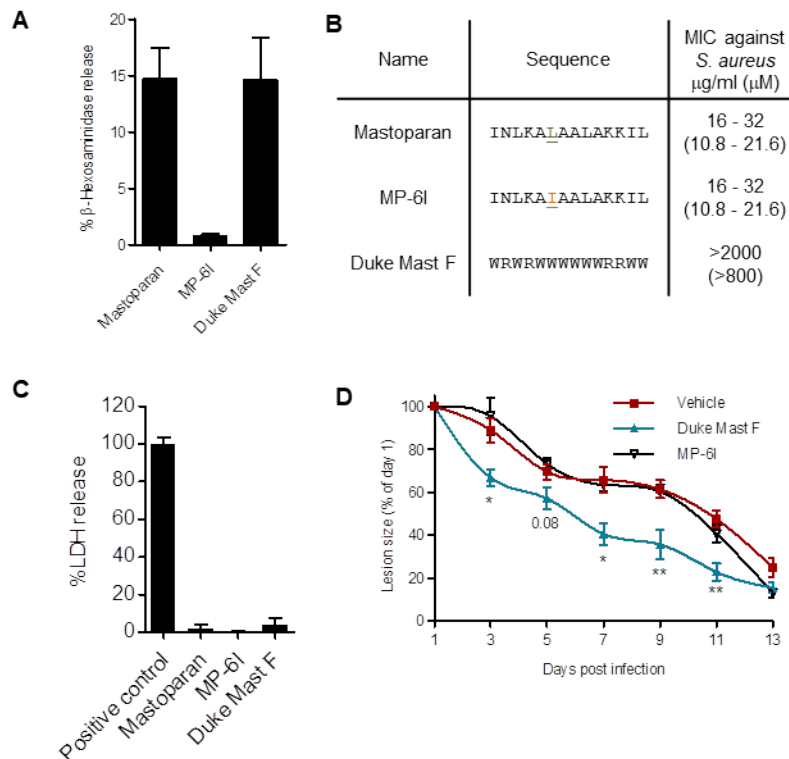


Figure 35: Therapeutic effect of mastoparan is specific to MC activation. (A) Amino acid sequence and MIC (minimum inhibitory concentration) for mastoparan or its analogs each mastoparan analog. (B) Degranulation of MC/9 cells expressed as β -hexosaminidase release by 25 μM mastoparan, MP-6I and Duke Mast F. (C) Cytotoxicity of mastoparan or its analogs measured by LDH assay 4 hours post incubation of L929 cells at a concentration of 50 μM . (D) Quantification of lesion sizes in each treatment group (n = 5).

By systematic substitutions of single amino acids on mastoparan peptide, we identified such a derivative 'MP-6I' (see Methods) in which leucine at position 6 was substituted with isoleucine. This single change was enough to cause complete loss in MC-degranulating activity while retaining comparable antibacterial activity against *S.*

aureus (Figure 35, A-B). However, identifying a mastoparan derivative that retained its MC degranulating property while lost its antibacterial activity was much more challenging. We therefore developed a tryptophan-rich 14-mer peptide named 'Duke Mast F' (see Methods) whose amino acid sequence is unrelated to mastoparan but possess comparable MC-degranulating capacity without any antibacterial activity (Figure 35, A-B). Having selected mastoparan derivatives that exhibited either MC-degranulating activity or antibacterial activity without any significant toxicity (Figure 35C), we investigated their ability to resolve *S. aureus* skin infections at quantities equimolar to native mastoparan. To our surprise, we found that MP-6I, despite its inherent antibacterial activity *in vitro* did not significantly reduce lesion size compared to vehicle treatment following *S. aureus* infections (Figure 35D). Conversely, when we examined the therapeutic ability of Duke Mast F, we found that it was significantly better than the vehicle in reduction of lesion size (Figure 35D). Cumulatively, these initial structure-activity relationship studies on mastoparan suggest that its therapeutic effects are dependent on its MC-activating capacity rather than on direct antibacterial properties and attributable to other MC-activating peptides.

3.3.8 Treatment with MCA promotes regenerative healing.

The lesions in dermonecrotic infections mimic wounds that arise upon loss of the scab and reduction of lesion size involves proliferation and reepithelialization similar to that occurring in wound healing. Since persistence of bacteria at wound sites can

significantly delay natural wound healing and increase scarring (134, 135), we speculated that mastoparan-mediated acceleration in bacterial clearance could result in not only faster but also more regenerative healing of skin lesions i. e. less scarring.

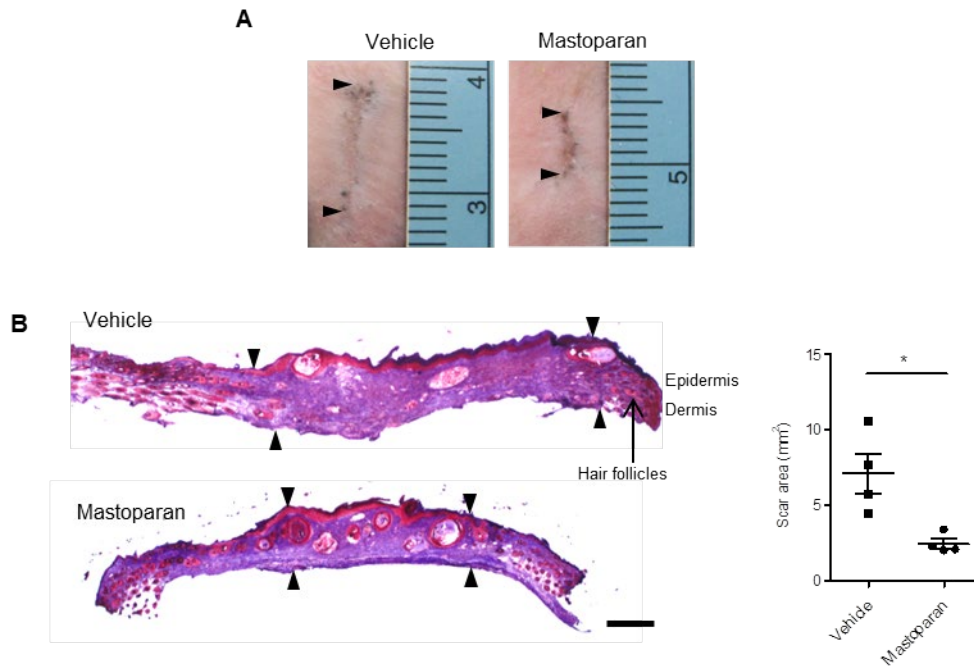


Figure 36: Treatment with MCA promotes regenerative healing. (A) Representative images of skin scars from different mouse groups taken on day 28 post infection. Arrowheads indicate the length of scars. (B) Representative cryosections from scarred regions. The sections taken were perpendicular to the long axis of the scar. Arrowheads define the area of scar regions devoid of hair follicles. Scale bar 500 μ m. The graph on the right represents area of the scar in each group measured using ImageJ (n = 4).

To investigate that, we allowed the lesions in various groups of mice to close completely (which typically takes 2-3 weeks post infection), then waited an additional two weeks to allow all the proliferative processes in the skin to reach steady state levels. Then the scars along with surrounding skins were harvested and the levels of scarring at

each of the infection sites were visualized by trichrome staining of the cross-sections.

Indeed, the scar area was significantly smaller in the mastoparan-treated mice compared to controls (Figure 36).

3.3.9 CTMCs recruits wound healing CD301b⁺ cells

The reduced scarring could be primarily due to accelerated bacterial clearance by mastoparan, nonetheless, we investigated if MCs had any additional role in healing of these infectious wounds other than promoting bacterial clearance. We have recently identified critical roles for dermal CD301b⁺ cells in promoting reepithelialization of sterile wounds (136).

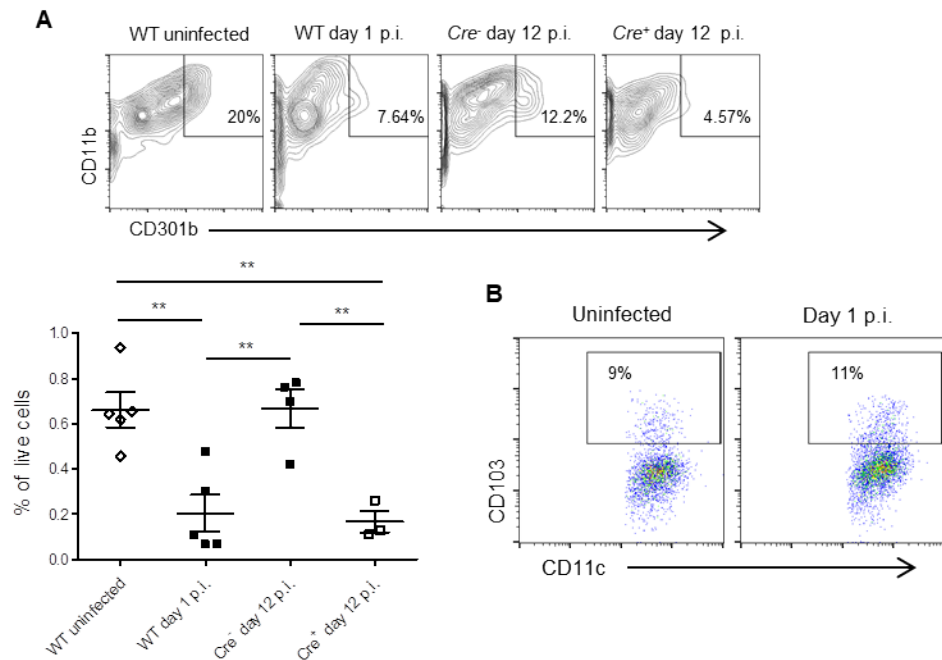


Figure 37: CTMCs restores wound healing CD301b⁺ cells. (A) Representative flow cytometry plots depicting CD11b⁺CD301b⁺ DDC population in skin of mice of indicated groups. Cells within the CD45⁺CD64^{lo}CD11c⁺ gate are shown. Graph at the

bottom shows skin CD301b⁺ DDCs as percentage of total live cells (n = 3-5). Data are representative of two independent experiments. (B) Representative flow cytometry plots depicting CD103⁺ DDCs in the skin with or without infection (gated from CD45⁺CD64^{lo}CD11c⁺CD301b⁻ cells).

Interestingly, in our current study we observed that the CD301b⁺ dermal dendritic cell (DDC) population significantly decreased in the infected skin area by 24 hours post infection, however, the population was restored at the later stage of infection when bacterial burden was minimal (Figure 37A). This phenomenon could be unique to CD301b⁺ cells, as we did not observe a similar reduction in case of the other major DDC population (CD103⁺ cells) by 24 hours (Figure 37B). Since we previously identified that MCs could recruit CD11b⁺ DCs early during *E. coli* skin infection (99) and CD301b⁺ DCs were shown to be a major subset of CD11b⁺ DDCs (137, 138), we asked if MCs had a role in repopulation of these cells during the healing stage of infection. Depletion of CTMC results in higher bacterial burden which may also contribute to reduction of CD301b⁺ cells in the dermis. Therefore, we adjusted the bacterial inoculum to obtain similar lesions in MC-sufficient and MC-depleted mice. We observed that the number of CD301b⁺ DCs on day 12 was significantly lower in absence of MCs (Figure 37A), indicating that MCs contributed to restoring the skin CD301b⁺ DC population to homeostatic levels. Note that absence of MCs did not affect the CD301b⁺ cells population in uninfected skin area (data not shown). To summarize, MCs contribute to healing of infectious wounds not only by clearing bacteria via neutrophil recruitment but also by promoting reepithelialization via restoration of CD301b⁺ DC population.

3.3.10 MCA mobilizes DCs to DLNs

Concurrent with recruiting innate immune cells to clear pathogens at the site of infection, MC mediators also modulate the trafficking of key immune cells involved in antigen presentation, the critical immune activity responsible for initiating adaptive immunity (93). Recent studies have revealed that MCs are responsible for recruiting antigen presenting dendritic cells (DCs) to the site of infection and promoting their migration from the inflamed site to the DLNs, the epicenter of the adaptive immune response (99-101). In this study, we observed that mastoparan triggered release of several cytokines from the human LAD2 MCs such as TNF, CCL2, CCL3 and CCL4 (Figure 2E) which had previously been implicated to be involved in either MC-dependent or MC-independent mobilization of DCs (99, 139-142). To determine whether mastoparan can mobilize DCs to DLNs, we injected mastoparan or its inactive counterpart (mastoparan 17) intradermally into rear footpads of mice since this site is drained by a single DLN, the popliteal node (PN). We observed that by 24 hours, mastoparan elicited lymph node hypertrophy (Figure 38A) in a CTMC-dependent manner. We detected significant levels of various migratory skin DC subsets recruited specifically by mastoparan into PNs which include CD103⁺CD207[±] dermal DCs as well as CD207⁺CD103⁻ Langerhans cells (LCs) (Figure 38B) (143).

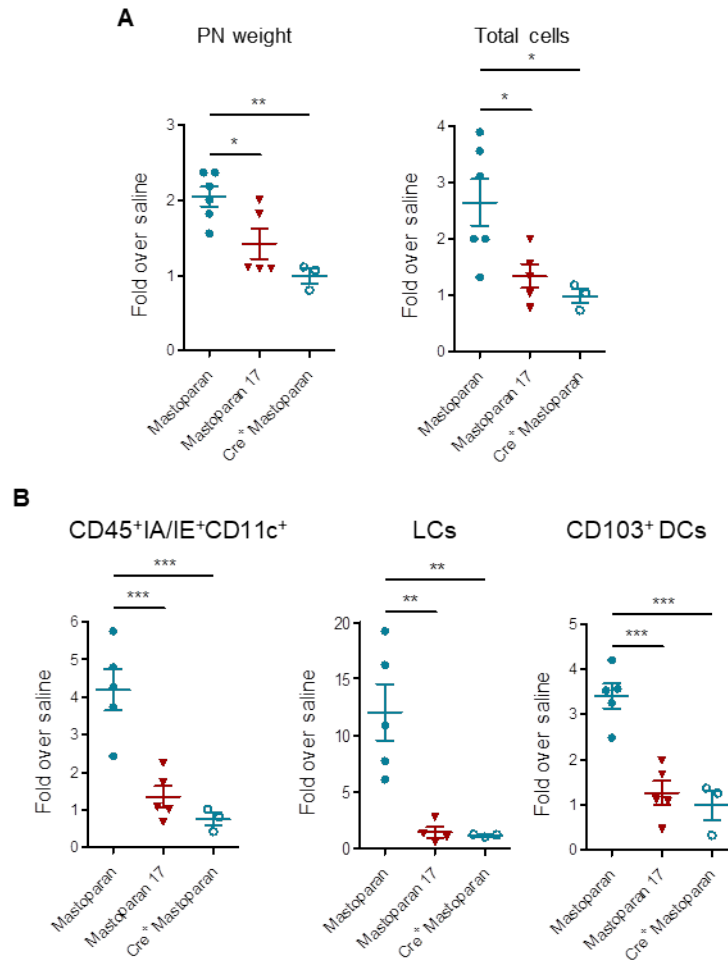


Figure 38: MCA mobilizes DCs to DLNs. (A) Weight of popliteal nodes (PNs) and total number of cells in the PN 24 hours post footpad injection of WT mice with saline, 10 μ g mastoparan or mastoparan 17, or MC-depleted mice with mastoparan (Cre⁺ Mastoparan group). (B) Numbers of CD11c⁺IA/IE⁺ antigen presenting cells, LCs and CD103⁺ DCs in PNs 24 hours post various treatments described above. Data are representative of two independent experiments.

Therefore, we speculated that mastoparan treatment could provide a powerful adjuvant effect during infection and augment bacterial antigen-specific antibody production.

3.3.11 Treatment with MCA boosts antibody responses and protects from reinfection

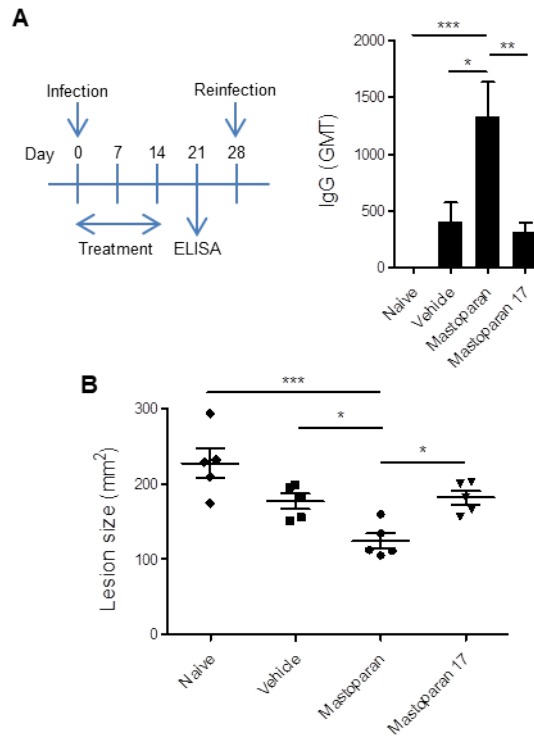


Figure 39: Mastoparan boosts adaptive immunity and controls reinfection. (A) Schematic showing experimental plan and graph depicting IgG geometric mean titer (GMT) against whole *S. aureus* cells in sera collected on day 21 post infection from mice infected with *S. aureus* and treated with vehicle, mastoparan or mastoparan 17 for two weeks or in sera of uninfected (naive) mice (n = 5). (B) Lesion size 24 hours post reinfection with 10^8 *S. aureus* of mouse groups described above (n = 5). Note that the lesion sizes were larger since the bacteria were not coated with microbeads (see Methods).

To test the hypothesis that mastoparan treatment might improve adaptive immunity, dermonecrotic infections were topically treated with vehicle, mastoparan or mastoparan 17 for two weeks as described before and sera from each group of mice were collected on day 21 and assayed for *S. aureus*-specific total IgG. Indeed, IgG titers were

significantly higher in mastoparan-treated group compared to mice treated with vehicle or mastoparan 17 (Figure 39A). Note that the antimicrobial effect of mastoparan which accelerated bacterial clearance and therefore reduced the source of immunogens did not cancel out its adjuvant effect. To determine if increased antibody response is associated with protection from reinfection, we infected the dorso-rostral area of mice with *S. aureus* on day 28 (one week after complete resolution of initial infections in all mice) and measured the lesion size after 24 hours. We observed that lesions upon reinfection in mice previously infected and treated with mastoparan were significantly smaller than that in mice previously infected and treated with vehicle or mastoparan 17 or that in previously uninfected (naive) mice (Figure 39B). These data demonstrate that along with expediting resolution of infection, the MCA is capable of boosting adaptive immunity which provides protection against reinfection.

3.4 Discussion

A cell type not often considered during infection is the mast cell (MC). MCs have mostly been associated with propagating chronic inflammatory disorders such as IgE mediated asthma, arthritis, and Crohn's disease (144, 145). This negative reputation is due mostly to their capacity to release large amounts of proinflammatory mediators. Over twenty years ago, we demonstrated the critical role of MCs in modulating bacterial clearance in the lungs and peritoneal cavities of mice through recruitment of neutrophils (53). Since then, evidences have emerged from various laboratories implicating MCs as critical modulators of defense against wide variety of bacterial and viral infections at different body sites (96, 97). Conventional MC knockout models involve mutations in or upstream of *c-kit* which have been shown to display confounding abnormalities such as neutrophilia or neutropenia (146, 147). Therefore, in this study we further verified MCs' role in neutrophil recruitment and control of skin infections by employing inducible CTMC depletion system (*Mcpt5-Cre⁺ iDTR⁺* mice) which does not affect levels of other immune cells (119).

Since MCs can be activated exogenously by natural or synthetic MCAs, we reasoned that administering small amounts of MCAs locally, at sites of infection, could boost bacterial clearance through enhanced neutrophil recruitment without evoking any systemic side effects. Unlike other sentinel immunocytes, MCs prestore granules loaded with chemoattractants and other proinflammatory mediators and are therefore ideal

cellular targets for rapid triggering of the immune system. Furthermore, MCs recruits immunocytes of both innate and adaptive pathways, therefore a coordination between them could be achievable. Topical application of MCAs was found to be highly effective in reducing *S. aureus* skin infections and in resolving the resulting lesions. That this effect was via neutrophil recruitment was deduced from the observations that bacterial clearance was closely associated with neutrophil influx into the infection site and the effect was abolished if neutrophils were depleted. Since the MRGPRX2 receptor is expressed primarily on CTMCs and not on other immune cells, the actions of MCAs can be assumed to target only this subset of MCs. Indeed, the protective actions of the MCA were critically dependent on CTMCs since the MCA had limited efficacy in recruiting neutrophils or resolving infections in CTMC-depleted mice. Therefore, the inflammation that MCAs evoke are likely to be more controlled, as opposed to TLR ligands or other PAMPs which can activate PRRs on various immune and nonimmune cells. Another important property of MRGPRX2 receptor on MCs is that unlike FcεRI, it is resistant to desensitization (106) upon activation by peptide MCAs and therefore, it is likely to remain responsive allowing for successive MCA treatments.

Since MCs can recruit heterogeneous dendritic cell population and release panoply of growth factors, some of which can promote wound healing processes (99, 136, 148), there was also a possibility that these factors might contribute to the beneficial effects of MCAs. This study identified a novel role of CTMCs in restoring wound-

healing CD301b⁺ DDC population which disappeared from skin upon infection. The CD301b⁺ DDC is also a key transporter of antigens to skin-draining lymph nodes (137, 138). Therefore, the low abundance of CD301b⁺ DDC we observed post infection was presumably due to their continuous migration to lymph nodes upon exposure to bacterial antigens, which continued until the bacterial burden became low. We also did not detect any increase in CD301b⁺ cells within the dead cell population in the infected skin (data not shown), supporting that the disappearance of these cells were due to their migration and not cell death. This wound-healing role of MCs does not appear to occur in the absence of infection as dermal CD301b⁺ cell frequency does not alter during sterile wounding (136). Several recent studies have also shown MCs as dispensable in sterile wound healing (149, 150).

Like many natural cationic peptides, mastoparan had previously been reported in several *in vitro* studies to have direct antibacterial activity. The bactericidal action of this peptide was attributed partly to its net positive charge which facilitated penetration and disruption of the negatively charged bacterial surface membranes (131, 151). Surprisingly when we examined a mutant derivative of mastoparan, MP-6I, which had lost its ability to activate MCs but still retained its antibacterial activity, for its capacity to resolve *S. aureus* infections, we found very little activity. Furthermore, when we examined the ability of mastoparan to resolve dermonecrotic infections in MC-depleted mice where the immune stimulating activity of mastoparan should not occur; we found

no significant therapeutic benefit. Taken together, the protective actions of mastoparan *in vivo* are primarily attributable to its innate immunostimulatory activity rather than to any antibacterial actions. This is consistent with recent findings that many host defense peptides with antimicrobial properties based on *in vitro* studies, have limited activity *in vivo*. Their positive charge causes many soluble host proteins to adsorb to these peptides and interfere with their ability to intercalate with bacterial membrane (152-154), presumably without impeding their ability to activate MCs.

While our studies here have primarily dwelled on the use of MCs in boosting innate immune responses, our current study demonstrates that MCA treatment of skin can also enhance DC recruitment and protective antibody response during infection, indicating that MCs can be targeted to induce both innate and adaptive immunity to pathogens simultaneously, which would be the most advantageous means to develop host-directed therapy.

The notion of employing MCAs as therapeutics must be balanced with concerns over these MCAs getting into the circulation to cause systemic MC degranulation leading to anaphylaxis. However, these concerns could be unwarranted when we consider that two peptide antibiotics, polymyxin B and colistin, are actually strong MCAs that have been approved for systemic use since 1964(155-159). The lack of anaphylaxis when using these agents may be because MC responses to non IgE MCAs are distinct in both speed and mediator contents than those typically elicited by IgE and

allergen (108). Indeed, our studies involving topical MCAs failed to reveal any harmful side effects either at the site of application or systemically, even after multiple applications. Additionally, although the MCAs were found to elevate IgG and IgA responses, very little IgE was found to be evoked by MCAs (104).

This work reveals for the first time that purposeful activation of mast cells (MCs) in the skin can not only accelerate bacterial clearance mechanisms but also enhance cutaneous healing mechanisms as well as adaptive immune responses, which are protective against future infections. By employing a peptide that targets a receptor found almost exclusively on CTMCs, we can specifically target this subset of cells for activation without evoking any off-target effects. Since the MCAs are directed at host cells, there is less likelihood that bacterial pathogens will develop resistance to this mode of treatment. Furthermore, since the MCAs are boosting the general innate immune response, it will be effective regardless of the identity of the pathogen. Since the mode of action of MCA is distinct from that of conventional antibiotics, they can readily be applied as adjuncts to current standard of care antibiotics, possibly resulting in a synergistic outcome.

4. Conclusion

Our study shows that understanding immune cell functions and their interactions with pathogens at peripheral barrier sites and secondary immune-checkpoints, such as the lymph nodes, can identify novel immunotherapeutic approaches against infections. These approaches involve subverting pathogen exploitation of immune cell functions as well as boosting innate capacities of particular immune cells, as demonstrated in the previous two chapters, respectively.

4.1 Cooption of innate immune cells in promoting infection

Yersinia pestis is the causative agent of the Black Death, a high-mortality epidemic which accounted for the death of at least one-third of Europe's population in the space of 6 years in the 14th century and which has continued to plague mankind since then (31). Even in this 21st century, outbreaks of *Y. pestis* infections in countries such as Madagascar continue to result in hundreds of fatalities (160). To date, early events of *Y. pestis* infection leading to its spread in the body have been poorly understood, primarily due to rapid progression of the disease in animal models. Using mice and an infectious route that faithfully mimics the natural course of *Y. pestis* infection and a *Y. pestis* strain that progress slowly *in vivo*, we discovered that following intradermal inoculation, colonization of the primary DLN is a pivotal beachhead in the pathogenic process and host cell death plays a critical part in it. The model for the role of cell death in *Y. pestis* dissemination within buboes is in the schema in Figure 40.

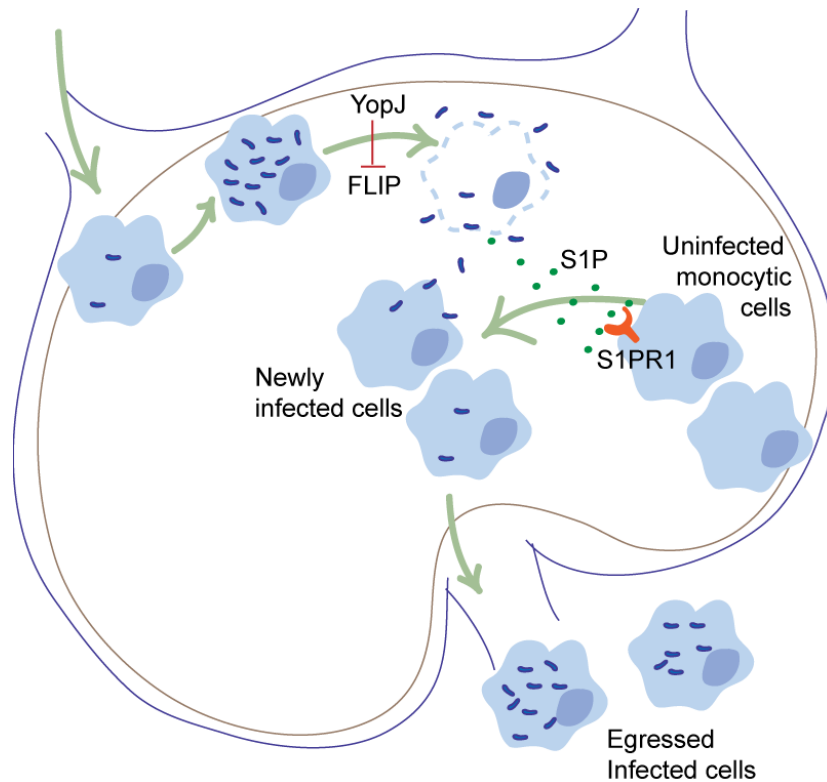


Figure 40: Mechanism of *Y. pestis* dissemination within buboes

Conversion of lymph nodes into pathognomonic buboes is the key hallmark of bubonic plague, however, it has long been considered merely as a pathological feature. Our study demonstrates the functional utility of the buboes in disease progression is that they are the byproduct of bacterial co-option of immune cell trafficking; and cell death serves as a switch between intracellular and extracellular stages of the bacteria. We reveal that the aggregates of commandeered cells in buboes provide a hub for bacterial multiplication and spread. In this regard, the buboes appear to resemble pathogenic mycobacteria-induced granulomas, which are distinct macrophage-rich structures that promote both growth and spread of intracellular bacteria (25).

Understanding the underlying basis for the formation of such bacteria-driven cellular structures may reveal novel therapeutic strategies directed at blocking dissemination of various bacterial pathogens.

Our study also highlights the role of programmed cell death in bacterial dissemination which has previously been underappreciated. While immune cell death is closely associated with inflammation and therefore considered as a host response, recent studies have revealed that various types of programmed cell death are often associated but not necessary for inflammatory responses against pathogens (161-163). These new findings question the theory that cell death is merely a collateral for inflammation; and why the signaling pathways for cell death, inflammation and cell death collide remains an enigma. This study suggests that lytic cell death can be beneficial for intracellular pathogens, especially in situations when the pathogen takes advantage of the massive inflammatory responses. Although extensive necrosis of buboes is routinely observed during postmortems of *Y. pestis* infected subjects and in animal models of bubonic plague (31, 32, 164), its association with *Y. pestis* virulence has gone largely unnoticed. Our findings highlight that the causality in host-pathogen interactions can be elusive and requires careful evaluation as what might have been misconstrued as the 'effect' can turn out to be the 'cause' and vice versa.

Although it has been known for many decades that *Y. pestis* reside and even multiply in macrophages (35, 36) by resisting lysosomal killing (37), the significance of

this activity has not been fully deciphered. This could partly be attributable to the differences between the infectious states of flea-regurgitated bacteria and lab-cultured bacteria. Since the *Yersinia* T3SS effector proteins express only at 37°C upon contact with mammalian host cells, it is a common practice to grow bacteria at 37°C which allows abundant production of these proteins as well as studying their effects *in vitro* (47, 165). However, since natural expression of these proteins is minimal at 26°C in flea midgut and only activates upon inoculation into mammal skin via flea bites, pre-activation of these factors may not mimic their natural role in pathogenesis. For instance, pre-activation of the effector proteins with antiphagocytic capacity (such as YopH) results in rapid injection of the antiphagocytic factors as soon as the bacteria come in contact of the host cells and as a result the host cells fail to phagocytose bacteria. Therefore, it has been proposed that *Yersinia* employs these antiphagocytic factors to avoid phagocytosis and subsequent killing by macrophages. This predisposition has led to overlooking the role of intracellular bacteria in pathogenesis even though *Yersinia pestis* also employ several highly efficient effector proteins to facilitate their invasion into host cells (41). An alternative hypothesis, therefore, could be that the antiphagocytic factors do not get produced largely until the bacteria enter the host cells, the intracellular bacteria then inject the factors through phagosomal or other vacuolar membranes to prevent phagocytosis of additional bacteria, providing a niche for intracellular replication of the bacteria which have already entered the host cells. Subsequent delayed lytic death of

host cells would allow release of newly replicated intracellular bacteria, facilitating further infection, as we observed in this study by employing bacterial culture that better replicates the infectious state of bacteria during transmission via fleabites. Therefore, employing models of infection that closely mimic the natural route of bacterial progression in the body can help better inform us on pathogenic tactics.

4.2 Cooption of innate immune cells in combating infection

With the rapid emergence of multiresistant bacteria and the lack of new antibiotics in the pipeline (166, 167), there is a dire need for alternative antibacterial therapy. Due to their critical role against pathogen invasion at barrier sites, innate immunocytes could potentially be targeted for novel therapeutic approaches; however, non-specific activation may lead to unregulated outcomes. As described in the third chapter, we identified distinct immunoregulatory functions of mast cells during early and late stages of *Staphylococcus aureus* skin infection, which are critical for infection control and tissue repair, respectively. We envisioned and eventually demonstrated that activation of local mast cells via a mast cell-specific receptor could be employed as a safe immunotherapeutic approach. Topical treatment with mastoparan, a peptide mast cell activator, resulted in enhanced clearance of *Staphylococcus aureus* from infected mouse

skins. The mechanism of action is depicted in Figure 41.

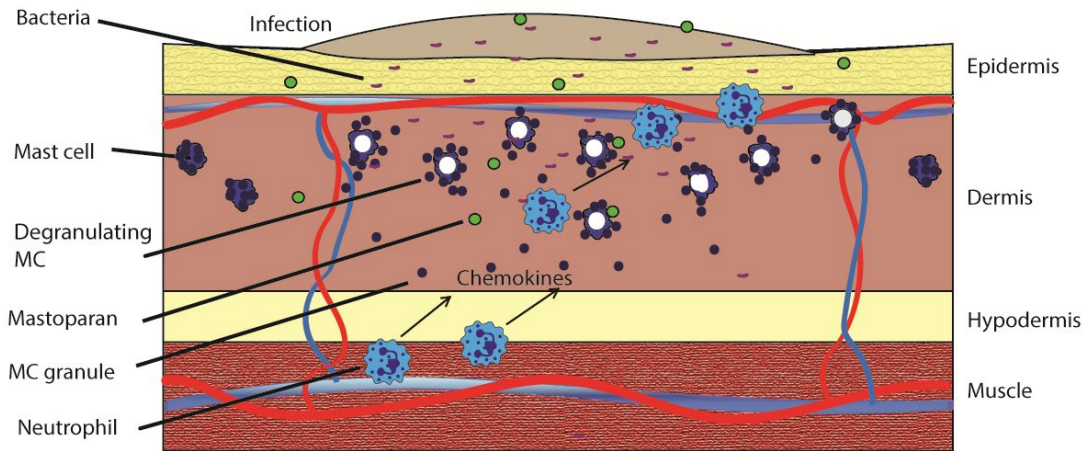


Figure 41: Mechanism for mastoparan's therapeutic effect

We demonstrate that mastoparan functions by activating connective tissue mast cells (CTMCs) via the MRGPRX2 receptor. Peripheral CTMC activation, in turn, enhances recruitment of bacteria-clearing neutrophils. In addition to neutrophil recruitment, mast cell activation also promotes repair of infectious wounds and improves adaptive immunity via mediating mobilizations of various dendritic cells.

Our work supports the notion that targeting immunoregulatory cells such as mast cells might have several benefits over targeting immune-effector cells such as neutrophils. First, the regulatory capacities of mast cells (168) may prevent unwanted inflammatory events. Second, unlike effector immune cells such as neutrophils, mast cells do not die after activation and their granules regenerate over time, allowing for multiple activations. Third, activation of mast cells appears to modulate both innate and

adaptive immunity to pathogens, which may provide long-term benefits in addition to immediate therapeutic effects (93). Our approach also highlights the importance of receptor specificity in host-directed therapy. Mastoparan functions via a receptor exclusive to mast cells, therefore, nonspecific activation of other immune cells would be minimal. Identifying receptors that are unique to distinct immune cell types and novel ligands that binds to those cell type-specific receptors could be a safer and more effective approach in host-directed therapy.

4.3 Concluding remarks

In summary, our studies revealed a previously unknown pathogenic mechanism for intracellular bacteria relies on manipulating hosts' programmed cell death pathways. This study also identifies the mast cell as a candidate for therapeutic intervention to bacterial infections, whose potential in host-directed innate defense has not previously been explored. With this work, we contribute to the understanding of the role of innate immune cells during bacterial infections which will likely open new strategies for therapeutics against infections.

References

1. Medzhitov R. Recognition of microorganisms and activation of the immune response. *Nature*. 2007;449(7164):819-26.
2. Turvey SE, and Broide DH. Innate immunity. *J Allergy Clin Immunol*. 2010;125(2 Suppl 2):S24-32.
3. Jinushi M. The role of innate immune signals in antitumor immunity. *Oncoimmunology*. 2012;1(2):189-94.
4. MacLeod AS, and Mansbridge JN. The Innate Immune System in Acute and Chronic Wounds. *Adv Wound Care (New Rochelle)*. 2016;5(2):65-78.
5. Peiser L, Mukhopadhyay S, and Gordon S. Scavenger receptors in innate immunity. *Curr Opin Immunol*. 2002;14(1):123-8.
6. Schafer C, Ascui G, Ribeiro CH, Lopez M, Prados-Rosales R, Gonzalez PA, Bueno SM, Riedel CA, Baena A, Kalergis AM, et al. Innate immune cells for immunotherapy of autoimmune and cancer disorders. *Int Rev Immunol*. 2017;36(6):315-37.
7. Haley PJ. The lymphoid system: a review of species differences. *J Toxicol Pathol*. 2017;30(2):111-23.
8. Kastenmuller W, Torabi-Parizi P, Subramanian N, Lammermann T, and Germain RN. A spatially-organized multicellular innate immune response in lymph nodes limits systemic pathogen spread. *Cell*. 2012;150(6):1235-48.
9. Kuka M, and Iannacone M. The role of lymph node sinus macrophages in host defense. *Ann N Y Acad Sci*. 2014;1319(38-46).
10. Savina A, and Amigorena S. Phagocytosis and antigen presentation in dendritic cells. *Immunol Rev*. 2007;219(143-56).
11. Rabinovitch M. Professional and non-professional phagocytes: an introduction. *Trends Cell Biol*. 1995;5(3):85-7.
12. Hughes CE, Benson RA, Bedaj M, and Maffia P. Antigen-Presenting Cells and Antigen Presentation in Tertiary Lymphoid Organs. *Front Immunol*. 2016;7(481).

13. Brinkmann V, Reichard U, Goosmann C, Fauler B, Uhlemann Y, Weiss DS, Weinrauch Y, and Zychlinsky A. Neutrophil extracellular traps kill bacteria. *Science*. 2004;303(5663):1532-5.
14. Lacy P, and Stow JL. Cytokine release from innate immune cells: association with diverse membrane trafficking pathways. *Blood*. 2011;118(1):9-18.
15. Diamond G, Beckloff N, Weinberg A, and Kisich KO. The roles of antimicrobial peptides in innate host defense. *Curr Pharm Des*. 2009;15(21):2377-92.
16. Franchi L, Eigenbrod T, Munoz-Planillo R, and Nunez G. The inflammasome: a caspase-1-activation platform that regulates immune responses and disease pathogenesis. *Nat Immunol*. 2009;10(3):241-7.
17. Miao EA, and Rajan JV. Salmonella and Caspase-1: A complex Interplay of Detection and Evasion. *Front Microbiol*. 2011;2(85).
18. Minnich SA, and Rohde HN. A rationale for repression and/or loss of motility by pathogenic *Yersinia* in the mammalian host. *Adv Exp Med Biol*. 2007;603(298-310).
19. Vladimer GI, Weng D, Paquette SW, Vanaja SK, Rathinam VA, Aune MH, Conlon JE, Burbage JJ, Proulx MK, Liu Q, et al. The NLRP12 inflammasome recognizes *Yersinia pestis*. *Immunity*. 2012;37(1):96-107.
20. Shannon JG, Hasenkrug AM, Dorward DW, Nair V, Carmody AB, and Hinnebusch BJ. *Yersinia pestis* subverts the dermal neutrophil response in a mouse model of bubonic plague. *MBio*. 2013;4(5):e00170-13.
21. Vagima Y, Zauberman A, Levy Y, Gur D, Tidhar A, Aftalion M, Shafferman A, and Mamroud E. Circumventing *Y. pestis* Virulence by Early Recruitment of Neutrophils to the Lungs during Pneumonic Plague. *PLoS Pathog*. 2015;11(5):e1004893.
22. Choi HW, Brooking-Dixon R, Neupane S, Lee CJ, Miao EA, Staats HF, and Abraham SN. *Salmonella typhimurium* impedes innate immunity with a mast-cell-suppressing protein tyrosine phosphatase, SptP. *Immunity*. 2013;39(6):1108-20.

23. Andersson K, Magnusson KE, Majeed M, Stendahl O, and Fallman M. Yersinia pseudotuberculosis-induced calcium signaling in neutrophils is blocked by the virulence effector YopH. *Infect Immun.* 1999;67(5):2567-74.
24. Fukuto HS, Svetlanov A, Palmer LE, Karzai AW, and Bliska JB. Global gene expression profiling of Yersinia pestis replicating inside macrophages reveals the roles of a putative stress-induced operon in regulating type III secretion and intracellular cell division. *Infect Immun.* 2010;78(9):3700-15.
25. Davis JM, and Ramakrishnan L. The role of the granuloma in expansion and dissemination of early tuberculous infection. *Cell.* 2009;136(1):37-49.
26. Winter SE, Thiennimitr P, Winter MG, Butler BP, Huseby DL, Crawford RW, Russell JM, Bevins CL, Adams LG, Tsolis RM, et al. Gut inflammation provides a respiratory electron acceptor for Salmonella. *Nature.* 2010;467(7314):426-9.
27. Mellman I, Coukos G, and Dranoff G. Cancer immunotherapy comes of age. *Nature.* 2011;480(7378):480-9.
28. Alangari AA, Al-Zamil F, Al-Mazrou A, Al-Muhsen S, Boisson-Dupuis S, Awadallah S, Kambal A, and Casanova JL. Treatment of disseminated mycobacterial infection with high-dose IFN-gamma in a patient with IL-12Rbeta1 deficiency. *Clinical & developmental immunology.* 2011;2011(691956).
29. Matthews SJ, and McCoy C. Peginterferon alfa-2a: a review of approved and investigational uses. *Clin Ther.* 2004;26(7):991-1025.
30. Hengge UR, and Cusini M. Topical immunomodulators for the treatment of external genital warts, cutaneous warts and molluscum contagiosum. *The British journal of dermatology.* 2003;149 Suppl 66(15-9).
31. Perry RD, and Fetherston JD. Yersinia pestis--etiologic agent of plague. *Clin Microbiol Rev.* 1997;10(1):35-66.
32. Sebbane F, Gardner D, Long D, Gowen BB, and Hinnebusch BJ. Kinetics of disease progression and host response in a rat model of bubonic plague. *Am J Pathol.* 2005;166(5):1427-39.
33. Zhou D, Han Y, and Yang R. Molecular and physiological insights into plague transmission, virulence and etiology. *Microbes Infect.* 2006;8(1):273-84.

34. Cavanaugh DC, and Randall R. The role of multiplication of *Pasteurella pestis* in mononuclear phagocytes in the pathogenesis of flea-borne plague. *J Immunol.* 1959;83(348-63).
35. Janssen WA, and Surgalla MJ. Plague bacillus: survival within host phagocytes. *Science.* 1969;163(3870):950-2.
36. Straley SC, and Harmon PA. *Yersinia pestis* grows within phagolysosomes in mouse peritoneal macrophages. *Infect Immun.* 1984;45(3):655-9.
37. Pujol C, Klein KA, Romanov GA, Palmer LE, Ciota C, Zhao Z, and Bliska JB. *Yersinia pestis* can reside in autophagosomes and avoid xenophagy in murine macrophages by preventing vacuole acidification. *Infect Immun.* 2009;77(6):2251-61.
38. Brubaker B. In: Dworkin M, Falkow S, Rosenberg E, Schleifer K-H, and Stackebrandt E eds. *The Prokaryotes: Volume 6: Proteobacteria: Gamma Subclass.* New York, NY: Springer New York; 2006:399-442.
39. Gonzalez RJ, Lane MC, Wagner NJ, Weening EH, and Miller VL. Dissemination of a highly virulent pathogen: tracking the early events that define infection. *PLoS Pathog.* 2015;11(1):e1004587.
40. Fallman M, and Gustavsson A. Cellular mechanisms of bacterial internalization counteracted by *Yersinia*. *Int Rev Cytol.* 2005;246(135-88).
41. Ke Y, Chen Z, and Yang R. *Yersinia pestis*: mechanisms of entry into and resistance to the host cell. *Front Cell Infect Microbiol.* 2013;3(106).
42. Cornelis GR. The *Yersinia* Ysc-Yop 'type III' weaponry. *Nat Rev Mol Cell Biol.* 2002;3(10):742-52.
43. Plano GV, Schesser K, and Nilles ML. Type III Secretion Systems. *Bacterial Protein Toxins.* 2003;Chapter 7(95).
44. Hinnebusch BJ. The evolution of flea-borne transmission in *Yersinia pestis*. *Curr Issues Mol Biol.* 2005;7(2):197-212.

45. St John AL, Ang WX, Huang MN, Kunder CA, Chan EW, Gunn MD, and Abraham SN. SIP-Dependent trafficking of intracellular yersinia pestis through lymph nodes establishes Buboes and systemic infection. *Immunity*. 2014;41(3):440-50.
46. Zauberman A, Cohen S, Mamroud E, Flashner Y, Tidhar A, Ber R, Elhanany E, Shafferman A, and Velan B. Interaction of Yersinia pestis with macrophages: limitations in YopJ-dependent apoptosis. *Infect Immun*. 2006;74(6):3239-50.
47. Weng D, Marty-Roix R, Ganesan S, Proulx MK, Vladimer GI, Kaiser WJ, Mocarski ES, Pouliot K, Chan FK, Kelliher MA, et al. Caspase-8 and RIP kinases regulate bacteria-induced innate immune responses and cell death. *Proc Natl Acad Sci U S A*. 2014;111(20):7391-6.
48. Planet PJ. Life After USA300: The Rise and Fall of a Superbug. *J Infect Dis*. 2017;215(suppl_1):S71-S7.
49. Hancock RE, Nijnik A, and Philpott DJ. Modulating immunity as a therapy for bacterial infections. *Nat Rev Microbiol*. 2012;10(4):243-54.
50. Czaplewski L, Bax R, Clokie M, Dawson M, Fairhead H, Fischetti VA, Foster S, Gilmore BF, Hancock RE, Harper D, et al. Alternatives to antibiotics-a pipeline portfolio review. *Lancet Infect Dis*. 2016;16(2):239-51.
51. Malaviya R, Ross, EA, MacGregor, JI, Ikeda, T, Little, JR, Jakschik, BA, Abraham, SN. Mast cell phagocytosis of Fim-H-expressing enterobacteria. *Journal of Immunology*. 1994;152(4):1907-14.
52. Malaviya R, and Georges A. Regulation of mast cell-mediated innate immunity during early response to bacterial infection. *Clinical reviews in allergy & immunology*. 2002;22(2):189-204.
53. Malaviya R, Ikeda T, Ross E, and Abraham SN. Mast cell modulation of neutrophil influx and bacterial clearance at sites of infection through TNF-alpha. *Nature*. 1996;381(6577):77-80.
54. Rigby KM, and DeLeo FR. Neutrophils in innate host defense against Staphylococcus aureus infections. *Seminars in immunopathology*. 2012;34(2):237-59.

55. Thakurdas SM, Melicoff E, Sansores-Garcia L, Moreira DC, Petrova Y, Stevens RL, and Adachi R. The mast cell-restricted tryptase mMCP-6 has a critical immunoprotective role in bacterial infections. *The Journal of biological chemistry*. 2007;282(29):20809-15.
56. Theoharides TC, Kempuraj D, Tagen M, Conti P, and Kalogeromitros D. Differential release of mast cell mediators and the pathogenesis of inflammation. *Immunological reviews*. 2007;217(65-78).
57. Junt T, Scandella E, and Ludewig B. Form follows function: lymphoid tissue microarchitecture in antimicrobial immune defence. *Nat Rev Immunol*. 2008;8(10):764-75.
58. Bar-Haim E, Gat O, Markel G, Cohen H, Shafferman A, and Velan B. Interrelationship between dendritic cell trafficking and *Francisella tularensis* dissemination following airway infection. *PLoS Pathog*. 2008;4(11):e1000211.
59. St John AL, and Abraham SN. Salmonella disrupts lymph node architecture by TLR4-mediated suppression of homeostatic chemokines. *Nat Med*. 2009;15(11):1259-65.
60. Jorgensen I, Rayamajhi M, and Miao EA. Programmed cell death as a defence against infection. *Nat Rev Immunol*. 2017;17(3):151-64.
61. Monack DM, Mecsas J, Ghorri N, and Falkow S. *Yersinia* signals macrophages to undergo apoptosis and YopJ is necessary for this cell death. *Proc Natl Acad Sci U S A*. 1997;94(19):10385-90.
62. Paquette N, Conlon J, Sweet C, Rus F, Wilson L, Pereira A, Rosadini CV, Goutagny N, Weber AN, Lane WS, et al. Serine/threonine acetylation of TGFbeta-activated kinase (TAK1) by *Yersinia pestis* YopJ inhibits innate immune signaling. *Proc Natl Acad Sci U S A*. 2012;109(31):12710-5.
63. Zheng Y, Lilo S, Brodsky IE, Zhang Y, Medzhitov R, Marcu KB, and Bliska JB. A *Yersinia* effector with enhanced inhibitory activity on the NF-kappaB pathway activates the NLRP3/ASC/caspase-1 inflammasome in macrophages. *PLoS Pathog*. 2011;7(4):e1002026.

64. Vanden Berghe T, Linkermann A, Jouan-Lanhouet S, Walczak H, and Vandenabeele P. Regulated necrosis: the expanding network of non-apoptotic cell death pathways. *Nat Rev Mol Cell Biol.* 2014;15(2):135-47.
65. Grootjans S, Vanden Berghe T, and Vandenabeele P. Initiation and execution mechanisms of necroptosis: an overview. *Cell Death Differ.* 2017.
66. Newton K, Dugger DL, Wickliffe KE, Kapoor N, de Almagro MC, Vucic D, Komuves L, Ferrando RE, French DM, Webster J, et al. Activity of protein kinase RIPK3 determines whether cells die by necroptosis or apoptosis. *Science.* 2014;343(6177):1357-60.
67. Oberst A, Dillon CP, Weinlich R, McCormick LL, Fitzgerald P, Pop C, Hakem R, Salvesen GS, and Green DR. Catalytic activity of the caspase-8-FLIP(L) complex inhibits RIPK3-dependent necrosis. *Nature.* 2011;471(7338):363-7.
68. Li J, McQuade T, Siemer AB, Napetschnig J, Moriwaki K, Hsiao YS, Damko E, Moquin D, Walz T, McDermott A, et al. The RIP1/RIP3 necrosome forms a functional amyloid signaling complex required for programmed necrosis. *Cell.* 2012;150(2):339-50.
69. Wallach D, Kang TB, Dillon CP, and Green DR. Programmed necrosis in inflammation: Toward identification of the effector molecules. *Science.* 2016;352(6281):aaf2154.
70. Brubaker RR, Beesley ED, and Surgalla MJ. *Pasteurella pestis*: Role of Pesticin I and Iron in Experimental Plague. *Science.* 1965;149(3682):422-4.
71. Zhang X, Goncalves R, and Mosser DM. The isolation and characterization of murine macrophages. *Curr Protoc Immunol.* 2008;Chapter 14(Unit 14 1).
72. Degtarev A, Maki JL, and Yuan J. Activity and specificity of necrostatin-1, small-molecule inhibitor of RIP1 kinase. *Cell Death Differ.* 2013;20(2):366.
73. Justus CR, Leffler N, Ruiz-Echevarria M, and Yang LV. In vitro cell migration and invasion assays. *J Vis Exp.* 2014(88).
74. Wang RF, and Kushner SR. Construction of versatile low-copy-number vectors for cloning, sequencing and gene expression in *Escherichia coli*. *Gene.* 1991;100(195-9).

75. Kelliher MA, Grimm S, Ishida Y, Kuo F, Stanger BZ, and Leder P. The death domain kinase RIP mediates the TNF-induced NF-kappaB signal. *Immunity*. 1998;8(3):297-303.
76. Degterev A, Hitomi J, Germscheid M, Ch'en IL, Korkina O, Teng X, Abbott D, Cuny GD, Yuan C, Wagner G, et al. Identification of RIP1 kinase as a specific cellular target of necrostatins. *Nat Chem Biol*. 2008;4(5):313-21.
77. Vandenabeele P, Galluzzi L, Vanden Berghe T, and Kroemer G. Molecular mechanisms of necroptosis: an ordered cellular explosion. *Nat Rev Mol Cell Biol*. 2010;11(10):700-14.
78. Wang H, Sun L, Su L, Rizo J, Liu L, Wang LF, Wang FS, and Wang X. Mixed lineage kinase domain-like protein MLKL causes necrotic membrane disruption upon phosphorylation by RIP3. *Mol Cell*. 2014;54(1):133-46.
79. Tenev T, Bianchi K, Darding M, Broemer M, Langlais C, Wallberg F, Zachariou A, Lopez J, MacFarlane M, Cain K, et al. The Ripoptosome, a signaling platform that assembles in response to genotoxic stress and loss of IAPs. *Mol Cell*. 2011;43(3):432-48.
80. Majkut J, Sgobba M, Holohan C, Crawford N, Logan AE, Kerr E, Higgins CA, Redmond KL, Riley JS, Stasik I, et al. Differential affinity of FLIP and procaspase 8 for FADD's DED binding surfaces regulates DISC assembly. *Nat Commun*. 2014;5(3350).
81. Crawford N, Stasik I, Holohan C, Majkut J, McGrath M, Johnston PG, Chessari G, Ward GA, Waugh DJ, Fennell DA, et al. SAHA overcomes FLIP-mediated inhibition of SMAC mimetic-induced apoptosis in mesothelioma. *Cell Death Dis*. 2013;4(e733).
82. Gude DR, Alvarez SE, Paugh SW, Mitra P, Yu J, Griffiths R, Barbour SE, Milstien S, and Spiegel S. Apoptosis induces expression of sphingosine kinase 1 to release sphingosine-1-phosphate as a "come-and-get-me" signal. *FASEB J*. 2008;22(8):2629-38.
83. Medina CB, and Ravichandran KS. Do not let death do us part: 'find-me' signals in communication between dying cells and the phagocytes. *Cell Death Differ*. 2016;23(6):979-89.

84. Schwab SR, and Cyster JG. Finding a way out: lymphocyte egress from lymphoid organs. *Nat Immunol.* 2007;8(12):1295-301.
85. Fang V, Chaluvadi VS, Ramos-Perez WD, Mendoza A, Baeyens A, Rivera R, Chun J, Cammer M, and Schwab SR. Gradients of the signaling lipid S1P in lymph nodes position natural killer cells and regulate their interferon-gamma response. *Nat Immunol.* 2017;18(1):15-25.
86. Kawamori T, Kaneshiro T, Okumura M, Maalouf S, Uflacker A, Bielawski J, Hannun YA, and Obeid LM. Role for sphingosine kinase 1 in colon carcinogenesis. *FASEB J.* 2009;23(2):405-14.
87. Chen X, He WT, Hu L, Li J, Fang Y, Wang X, Xu X, Wang Z, Huang K, and Han J. Pyroptosis is driven by non-selective gasdermin-D pore and its morphology is different from MLKL channel-mediated necroptosis. *Cell Res.* 2016;26(9):1007-20.
88. Micheau O, Lens S, Gaide O, Alevizopoulos K, and Tschopp J. NF-kappaB signals induce the expression of c-FLIP. *Mol Cell Biol.* 2001;21(16):5299-305.
89. Mamroud E, Tidhar A, Levy Y, Bar-Haim E, Halperin G, Flashner Y, Cohen S, Shafferman A, and Zauberman A. Dordrecht: Springer Netherlands; 2010:45-55.
90. Peterson LW, Philip NH, DeLaney A, Wynosky-Dolfi MA, Asklof K, Gray F, Choa R, Bjanes E, Buza EL, Hu B, et al. RIPK1-dependent apoptosis bypasses pathogen blockade of innate signaling to promote immune defense. *J Exp Med.* 2017;214(11):3171-82.
91. Skurnik M, Peippo A, and Ervela E. Characterization of the O-antigen gene clusters of *Yersinia pseudotuberculosis* and the cryptic O-antigen gene cluster of *Yersinia pestis* shows that the plague bacillus is most closely related to and has evolved from *Y. pseudotuberculosis* serotype O:1b. *Mol Microbiol.* 2000;37(2):316-30.
92. Harris PA, Berger SB, Jeong JU, Nagilla R, Bandyopadhyay D, Campobasso N, Capriotti CA, Cox JA, Dare L, Dong X, et al. Discovery of a First-in-Class Receptor Interacting Protein 1 (RIP1) Kinase Specific Clinical Candidate (GSK2982772) for the Treatment of Inflammatory Diseases. *J Med Chem.* 2017;60(4):1247-61.

93. Abraham SN, and St John AL. Mast cell-orchestrated immunity to pathogens. *Nature reviews Immunology*. 2010;10(6):440-52.
94. Marshall JS. Mast-cell responses to pathogens. *Nature reviews Immunology*. 2004;4(10):787-99.
95. St John AL, Rathore AP, Yap H, Ng ML, Metcalfe DD, Vasudevan SG, and Abraham SN. Immune surveillance by mast cells during dengue infection promotes natural killer (NK) and NKT-cell recruitment and viral clearance. *Proceedings of the National Academy of Sciences of the United States of America*. 2011;108(22):9190-5.
96. Gendrin C, Vornhagen J, Ngo L, Whidbey C, Boldenow E, Santana-Ufret V, Clauson M, Burnside K, Galloway DP, Waldorf KA, et al. Mast cell degranulation by a hemolytic lipid toxin decreases GBS colonization and infection. *Sci Adv*. 2015;1(6):e1400225.
97. Sieberhaar F, Syska W, Weller K, Magerl M, Zuberbier T, Metz M, and Maurer M. Control of *Pseudomonas aeruginosa* skin infections in mice is mast cell-dependent. *Am J Pathol*. 2007;170(6):1910-6.
98. Echtenacher B, Mannel DN, and Hultner L. Critical protective role of mast cells in a model of acute septic peritonitis. *Nature*. 1996;381(6577):75-7.
99. Shelburne CP, Nakano H, St John AL, Chan C, McLachlan JB, Gunn MD, Staats HF, and Abraham SN. Mast cells augment adaptive immunity by orchestrating dendritic cell trafficking through infected tissues. *Cell Host Microbe*. 2009;6(4):331-42.
100. Heib V, Becker M, Warger T, Rechtsteiner G, Tertilt C, Klein M, Bopp T, Taube C, Schild H, Schmitt E, et al. Mast cells are crucial for early inflammation, migration of Langerhans cells, and CTL responses following topical application of TLR7 ligand in mice. *Blood*. 2007;110(3):946-53.
101. Jawdat DM, Rowden G, and Marshall JS. Mast cells have a pivotal role in TNF-independent lymph node hypertrophy and the mobilization of Langerhans cells in response to bacterial peptidoglycan. *J Immunol*. 2006;177(3):1755-62.

102. McLachlan JB, Hart JP, Pizzo SV, Shelburne CP, Staats HF, Gunn MD, and Abraham SN. Mast cell-derived tumor necrosis factor induces hypertrophy of draining lymph nodes during infection. *Nature immunology*. 2003;4(12):1199-205.
103. Kunder CA, St John AL, Li G, Leong KW, Berwin B, Staats HF, and Abraham SN. Mast cell-derived particles deliver peripheral signals to remote lymph nodes. *J Exp Med*. 2009;206(11):2455-67.
104. McLachlan JB, Shelburne CP, Hart JP, Pizzo SV, Goyal R, Brooking-Dixon R, Staats HF, and Abraham SN. Mast cell activators: a new class of highly effective vaccine adjuvants. *Nat Med*. 2008;14(5):536-41.
105. Tatemoto K, Nozaki Y, Tsuda R, Konno S, Tomura K, Furuno M, Ogasawara H, Edamura K, Takagi H, Iwamura H, et al. Immunoglobulin E-independent activation of mast cell is mediated by Mrg receptors. *Biochemical and biophysical research communications*. 2006;349(4):1322-8.
106. Subramanian H, Gupta K, Guo Q, Price R, and Ali H. Mas-related gene X2 (MrgX2) is a novel G protein-coupled receptor for the antimicrobial peptide LL-37 in human mast cells: resistance to receptor phosphorylation, desensitization, and internalization. *The Journal of biological chemistry*. 2011;286(52):44739-49.
107. McNeil BD, Pundir P, Meeker S, Han L, Udem BJ, Kulka M, and Dong X. Identification of a mast-cell-specific receptor crucial for pseudo-allergic drug reactions. *Nature*. 2015;519(7542):237-41.
108. Gaudenzio N, Sibilano R, Marichal T, Starkl P, Reber LL, Cenac N, McNeil BD, Dong X, Hernandez JD, Sagi-Eisenberg R, et al. Different activation signals induce distinct mast cell degranulation strategies. *J Clin Invest*. 2016;126(10):3981-98.
109. Daum RS. Clinical practice. Skin and soft-tissue infections caused by methicillin-resistant *Staphylococcus aureus*. *The New England journal of medicine*. 2007;357(4):380-90.
110. McCaig LF, McDonald LC, Mandal S, and Jernigan DB. *Staphylococcus aureus*-associated skin and soft tissue infections in ambulatory care. *Emerging infectious diseases*. 2006;12(11):1715-23.

111. Moran GJ, Krishnadasan A, Gorwitz RJ, Fosheim GE, McDougal LK, Carey RB, Talan DA, and Group EMINS. Methicillin-resistant *S. aureus* infections among patients in the emergency department. *The New England journal of medicine*. 2006;355(7):666-74.
112. Bunce C, Wheeler L, Reed G, Musser J, and Barg N. Murine model of cutaneous infection with gram-positive cocci. *Infect Immun*. 1992;60(7):2636-40.
113. Montgomery CP, Daniels M, Zhao F, Alegre ML, Chong AS, and Daum RS. Protective immunity against recurrent *Staphylococcus aureus* skin infection requires antibody and interleukin-17A. *Infect Immun*. 2014;82(5):2125-34.
114. Hirai Y, Yasuhara T, Yoshida H, Nakajima T, Fujino M, and Kitada C. A new mast cell degranulating peptide "mastoparan" in the venom of *Vespula lewisii*. *Chemical & pharmaceutical bulletin*. 1979;27(8):1942-4.
115. Higashijima T, Burnier J, and Ross EM. Regulation of Gi and Go by mastoparan, related amphiphilic peptides, and hydrophobic amines. Mechanism and structural determinants of activity. *The Journal of biological chemistry*. 1990;265(24):14176-86.
116. Peranteau WH, Zhang L, Muvarak N, Badillo AT, Radu A, Zoltick PW, and Liechty KW. IL-10 overexpression decreases inflammatory mediators and promotes regenerative healing in an adult model of scar formation. *J Invest Dermatol*. 2008;128(7):1852-60.
117. Caesar CE, Esbjorner EK, Lincoln P, and Norden B. Membrane interactions of cell-penetrating peptides probed by tryptophan fluorescence and dichroism techniques: correlations of structure to cellular uptake. *Biochemistry*. 2006;45(24):7682-92.
118. Souza BM, Cabrera MP, Gomes PC, Dias NB, Stabeli RG, Leite NB, Neto JR, and Palma MS. Structure-activity relationship of mastoparan analogs: Effects of the number and positioning of Lys residues on secondary structure, interaction with membrane-mimetic systems and biological activity. *Peptides*. 2015;72(164-74).
119. Dudeck A, Dudeck J, Scholten J, Petzold A, Surianarayanan S, Kohler A, Peschke K, Vohringer D, Waskow C, Krieg T, et al. Mast cells are key promoters of contact allergy that mediate the adjuvant effects of haptens. *Immunity*. 2011;34(6):973-84.

120. Subramanian H, Kashem SW, Collington SJ, Qu H, Lambris JD, and Ali H. PMX-53 as a dual CD88 antagonist and an agonist for Mas-related gene 2 (MrgX2) in human mast cells. *Mol Pharmacol*. 2011;79(6):1005-13.
121. Kamohara M, Matsuo A, Takasaki J, Kohda M, Matsumoto M, Matsumoto S, Soga T, Hiyama H, Kobori M, and Katou M. Identification of MrgX2 as a human G-protein-coupled receptor for proadrenomedullin N-terminal peptides. *Biochemical and biophysical research communications*. 2005;330(4):1146-52.
122. Kobilka BK. G protein coupled receptor structure and activation. *Biochimica et biophysica acta*. 2007;1768(4):794-807.
123. Subramanian H, Gupta K, Lee D, Bayir AK, Ahn H, and Ali H. beta-Defensins activate human mast cells via Mas-related gene X2. *J Immunol*. 2013;191(1):345-52.
124. Kadamur G, and Ross EM. Mammalian phospholipase C. *Annu Rev Physiol*. 2013;75(127-54).
125. Maus UA, Waelsch K, Kuziel WA, Delbeck T, Mack M, Blackwell TS, Christman JW, Schlondorff D, Seeger W, and Lohmeyer J. Monocytes are potent facilitators of alveolar neutrophil emigration during lung inflammation: role of the CCL2-CCR2 axis. *J Immunol*. 2003;170(6):3273-8.
126. Gomez-Cambronero J, Horn J, Paul CC, and Baumann MA. Granulocyte-macrophage colony-stimulating factor is a chemoattractant cytokine for human neutrophils: involvement of the ribosomal p70 S6 kinase signaling pathway. *J Immunol*. 2003;171(12):6846-55.
127. Yuo A, Kitagawa S, Kasahara T, Matsushima K, Saito M, and Takaku F. Stimulation and priming of human neutrophils by interleukin-8: cooperation with tumor necrosis factor and colony-stimulating factors. *Blood*. 1991;78(10):2708-14.
128. Huber AR, Kunkel SL, Todd RF, 3rd, and Weiss SJ. Regulation of transendothelial neutrophil migration by endogenous interleukin-8. *Science*. 1991;254(5028):99-102.
129. Weisbart RH, Golde DW, Clark SC, Wong GG, and Gasson JC. Human granulocyte-macrophage colony-stimulating factor is a neutrophil activator. *Nature*. 1985;314(6009):361-3.

130. de Oliveira S, Rosowski EE, and Huttenlocher A. Neutrophil migration in infection and wound repair: going forward in reverse. *Nature reviews Immunology*. 2016;16(6):378-91.
131. Katsu T, Kuroko M, Morikawa T, Sanchika K, Yamanaka H, Shinoda S, and Fujita Y. Interaction of wasp venom mastoparan with biomembranes. *Biochimica et biophysica acta*. 1990;1027(2):185-90.
132. Vaara M. Agents that increase the permeability of the outer membrane. *Microbiol Rev*. 1992;56(3):395-411.
133. Zasloff M. Antimicrobial peptides of multicellular organisms. *Nature*. 2002;415(6870):389-95.
134. Edwards R, and Harding KG. Bacteria and wound healing. *Curr Opin Infect Dis*. 2004;17(2):91-6.
135. Singer AJ, and McClain SA. Persistent wound infection delays epidermal maturation and increases scarring in thermal burns. *Wound repair and regeneration : official publication of the Wound Healing Society [and] the European Tissue Repair Society*. 2002;10(6):372-7.
136. Yang B, Suwanpradid J, Sanchez-Lagunes R, Choi HW, Hoang P, Wang D, Abraham SN, and MacLeod AS. IL-27 Facilitates Skin Wound Healing through Induction of Epidermal Proliferation and Host Defense. *J Invest Dermatol*. 2017;137(5):1166-75.
137. Kumamoto Y, Denda-Nagai K, Aida S, Higashi N, and Irimura T. MGL2 Dermal dendritic cells are sufficient to initiate contact hypersensitivity in vivo. *PloS one*. 2009;4(5):e5619.
138. Kumamoto Y, Linehan M, Weinstein JS, Laidlaw BJ, Craft JE, and Iwasaki A. CD301b(+) dermal dendritic cells drive T helper 2 cell-mediated immunity. *Immunity*. 2013;39(4):733-43.
139. Dudeck J, Ghouse SM, Lehmann CH, Hoppe A, Schubert N, Nedospasov SA, Dudziak D, and Dudeck A. Mast-Cell-Derived TNF Amplifies CD8(+) Dendritic Cell Functionality and CD8(+) T Cell Priming. *Cell Rep*. 2015;13(2):399-411.

140. Charmoy M, Brunner-Agten S, Aebischer D, Auderset F, Launois P, Milon G, Proudfoot AE, and Tacchini-Cottier F. Neutrophil-derived CCL3 is essential for the rapid recruitment of dendritic cells to the site of *Leishmania major* inoculation in resistant mice. *PLoS Pathog.* 2010;6(2):e1000755.
141. Osterholzer JJ, Curtis JL, Polak T, Ames T, Chen GH, McDonald R, Huffnagle GB, and Toews GB. CCR2 mediates conventional dendritic cell recruitment and the formation of bronchovascular mononuclear cell infiltrates in the lungs of mice infected with *Cryptococcus neoformans*. *J Immunol.* 2008;181(1):610-20.
142. Lin CL, Suri RM, Rahdon RA, Austyn JM, and Roake JA. Dendritic cell chemotaxis and transendothelial migration are induced by distinct chemokines and are regulated on maturation. *Eur J Immunol.* 1998;28(12):4114-22.
143. Henri S, Guilliams M, Poulin LF, Tamoutounour S, Ardouin L, Dalod M, and Malissen B. Disentangling the complexity of the skin dendritic cell network. *Immunol Cell Biol.* 2010;88(4):366-75.
144. Galli SJ. New concepts about the mast cell. *The New England journal of medicine.* 1993;328(4):257-65.
145. Humbert M, Menz G, Ying S, Corrigan CJ, Robinson DS, Durham SR, and Kay AB. The immunopathology of extrinsic (atopic) and intrinsic (non-atopic) asthma: more similarities than differences. *Immunology today.* 1999;20(11):528-33.
146. Chervenick PA, and Boggs DR. Decreased neutrophils and megakaryocytes in anemic mice of genotype W/W. *J Cell Physiol.* 1969;73(1):25-30.
147. Nigrovic PA, Gray DH, Jones T, Hallgren J, Kuo FC, Chaletzky B, Gurish M, Mathis D, Benoist C, and Lee DM. Genetic inversion in mast cell-deficient (*Wsh*) mice interrupts *corin* and manifests as hematopoietic and cardiac aberrancy. *Am J Pathol.* 2008;173(6):1693-701.
148. Artuc M, Steckelings UM, and Henz BM. Mast cell-fibroblast interactions: human mast cells as source and inducers of fibroblast and epithelial growth factors. *J Invest Dermatol.* 2002;118(3):391-5.
149. Antsiferova M, Martin C, Huber M, Feyerabend TB, Forster A, Hartmann K, Rodewald HR, Hohl D, and Werner S. Mast cells are dispensable for normal and

- activin-promoted wound healing and skin carcinogenesis. *J Immunol.* 2013;191(12):6147-55.
150. Nauta AC, Grova M, Montoro DT, Zimmermann A, Tsai M, Gurtner GC, Galli SJ, and Longaker MT. Evidence that mast cells are not required for healing of splinted cutaneous excisional wounds in mice. *PloS one.* 2013;8(3):e59167.
151. Li ML, Liao RW, Qiu JW, Wang ZJ, and Wu TM. Antimicrobial activity of synthetic all-D mastoparan M. *International journal of antimicrobial agents.* 2000;13(3):203-8.
152. Bowdish DM, Davidson DJ, Lau YE, Lee K, Scott MG, and Hancock RE. Impact of LL-37 on anti-infective immunity. *J Leukoc Biol.* 2005;77(4):451-9.
153. Maisetta G, Di Luca M, Esin S, Florio W, Brancatisano FL, Bottai D, Campa M, and Batoni G. Evaluation of the inhibitory effects of human serum components on bactericidal activity of human beta defensin 3. *Peptides.* 2008;29(1):1-6.
154. Svenson J, Brandsdal BO, Stensen W, and Svendsen JS. Albumin binding of short cationic antimicrobial micropeptides and its influence on the in vitro bactericidal effect. *J Med Chem.* 2007;50(14):3334-9.
155. Bushby SR, and Green AF. The release of histamine by polymyxin B and polymyxin E. *British journal of pharmacology and chemotherapy.* 1955;10(2):215-9.
156. Ellis HV, 3rd, Johnson AR, and Moran NC. Selective release of histamine from rat mast cells by several drugs. *The Journal of pharmacology and experimental therapeutics.* 1970;175(3):627-31.
157. Parratt JR, and West GB. Release of 5-hydroxytryptamine and histamine from tissues of the rat. *The Journal of physiology.* 1957;137(2):179-92.
158. Voitenko VG, Bayramashvili DI, Zebrev AI, and Zinchenko AA. Relationship between structure and histamine releasing action of polymyxin B and its analogues. *Agents and actions.* 1990;30(1-2):153-6.
159. FDA. 1964.
160. Roberts L. Echoes of Ebola as plague hits Madagascar. *Science.* 2017;358(6362):430-1.

161. Kitur K, Wachtel S, Brown A, Wickersham M, Paulino F, Penaloza HF, Soong G, Bueno S, Parker D, and Prince A. Necroptosis Promotes Staphylococcus aureus Clearance by Inhibiting Excessive Inflammatory Signaling. *Cell Rep.* 2016;16(8):2219-30.
162. Najjar M, Saleh D, Zelic M, Nogusa S, Shah S, Tai A, Finger JN, Polykratis A, Gough PJ, Bertin J, et al. RIPK1 and RIPK3 Kinases Promote Cell-Death-Independent Inflammation by Toll-like Receptor 4. *Immunity.* 2016;45(1):46-59.
163. Daniels BP, Snyder AG, Olsen TM, Orozco S, Oguin TH, 3rd, Tait SWG, Martinez J, Gale M, Jr., Loo YM, and Oberst A. RIPK3 Restricts Viral Pathogenesis via Cell Death-Independent Neuroinflammation. *Cell.* 2017;169(2):301-13 e11.
164. Flexner S. The pathology of bubonic plague. *Am J Med Sci.* 1901;122(396-416).
165. Straley SC, and Bowmer WS. Virulence genes regulated at the transcriptional level by Ca²⁺ in Yersinia pestis include structural genes for outer membrane proteins. *Infect Immun.* 1986;51(2):445-54.
166. Payne DJ, Gwynn MN, Holmes DJ, and Pompliano DL. Drugs for bad bugs: confronting the challenges of antibacterial discovery. *Nat Rev Drug Discov.* 2007;6(1):29-40.
167. Silver LL. Challenges of antibacterial discovery. *Clinical microbiology reviews.* 2011;24(1):71-109.
168. Chan CY, St John AL, and Abraham SN. Mast cell interleukin-10 drives localized tolerance in chronic bladder infection. *Immunity.* 2013;38(2):349-59.

Biography

Mohammad 'Arif' Arifuzzaman was born in Dhaka, the capital of Bangladesh. He obtained his Bachelor of Science degree from University of Dhaka. Then he obtained his Master of Science in Biochemistry and Molecular Biology from the same university where he joined Dr. Firdausi Qadri's laboratory at the International Centre for Diarrhoeal Disease Research, studying the adaptive immune responses in human to enteric pathogens. Before joining Duke, Arif joined Dr. Edward Ryans's lab in the Massachusetts General Hospital at the Harvard University where he worked as a research fellow, studying the efficacy of various adjuvants to improve vaccines against enteric pathogens. These early research experiences exposed Arif to the field of immunology and microbiology. Then, he joined the graduate program of Molecular Genetics and Microbiology at Duke University; and began his thesis under the guidance of Dr. Soman Abraham. He is a gold medalist for outstanding achievements during his master's studies and received Duke Chancellor Award for incoming PhD students. His relevant publications are listed below:

Arifuzzaman M, Ang W X G, Choi H W, Nilles M L, St. John A L, Abraham S N.

Necroptosis of infiltrated macrophages drives *Yersinia pestis* dispersal within buboes. *JCI Insight*. 2018 Sep 20;3(18). pii: 122188. PMID: 30232285

Arifuzzaman M, Mobley YR, Choi HW, Bist P, Salinas CA, Brown ZD, Chen SL, Staats HF, Abraham SN. MRGPR-mediated activation of local mast cells clears cutaneous bacterial infection and protects against reinfection. *Science Advances* (in press)

Arifuzzaman M, Choi HW, Wu J, McLeod AS, Abraham SN. CD301b⁺ dermal dendritic cells control bacterial skin infection and promote resolution via distinct mechanisms (*manuscript in preparation*)

Arifuzzaman M, St. John AL, Abraham SN. Multifactorial tactics employed by *Yersinia pestis* to spread in the body (*review in preparation*)